Neuroplastic Refinement Explains Enhanced Visuomotor Decision-Making in Action Video Game Players

by

Kyle Joseph Cahill

Under the Direction of Mukesh Dhamala, PhD

Dissertation Submitted in Partial Fulfillment of the Requirements for the Degree of

Doctor of Philosophy

in the College of Arts and Sciences

Georgia State University

2025

ABSTRACT

Action video games (AVGs) offer a powerful experimental paradigm for investigating how sustained cognitive demands reshape the brain's structural and functional organization. Long-term AVG players—referred to in this dissertation as gamers—engage in high-stakes, fast-paced environments that require rapid transformation of visuomotor information into action selection and adaptive decision-making under uncertainty. Prior research has identified several cognitive enhancements in gamers, including faster response times and improved visuomotor coordination; however, it has lacked mechanistic insight into how the brain from prolonged engagement while playing AVGs orchestrates neuroplastic refinements that give rise to these advantages.

This dissertation presents a multi-faceted investigation of neuroplasticity in gamers, across three complementary studies. First, a targeted network analysis revealed enhanced structural and functional connectivity in the dorsal visual streams of gamers. The functional enhancements, both undirected and directed functional connectivity measures, correlated with faster response times. Second, a structurally constrained framework assessed how anatomical connectivity constrains functional and directed interactions. Gamers exhibited connectivity patterns consistent with a shift from feedback-driven object-in-place, iterative corrections to a more anticipatory, feedforward strategy, facilitating streamlined visuomotor transformation, scene integration, attentional control, and adaptive action selection compared with non-gamers. Third, a novel principal component analysis (PCA) method revealed that gamers exhibited a stronger convergence of top-down cognitive clarity, learned value-to-action transformation, and bottom-up motor readiness, factors that were each associated with improved response times.

Across these three studies, findings support a proposed framework underlying the observed neuroplastic refinements: Cognitive Resource Reallocation (CRR). While prior research has discussed resource reallocation, this dissertation is the first to formally define CRR as a dynamic neurophysiological process embedded in physically lawful neural dynamics. It describes how functional and metabolic resources are redistributed in response to cognitive strain to support behaviorally relevant processes more effectively. CRR provides a unifying theoretical lens to explain how long-term gameplay leads to the targeted refinement of neural circuits that enable efficient visuomotor decision-making. More broadly, this work positions action video games as an ecologically valid paradigm for studying adaptive neuroplasticity, with implications for cognitive training, rehabilitation, and performance enhancement.

INDEX WORDS: Action video games, Decision-making, Visuomotor, Cognitive resource reallocation, Functional connectivity, Principal component analysis

Neuroplastic Refinement Explains Enhanced Visuomotor Decision-Making in Action Video Game Players

by

Kyle Cahill

Committee Chair: Mukesh Dhamala PhD

Committee: Vadym Apalkov PhD

Brian Thoms PhD

Electronic Version Approved:

Office of Graduate Services

College of Arts and Sciences

Georgia State University

July 2025

DEDICATION

To my mother, Gail DeGeorge, whose unwavering support and encouragement have shaped every step of my path. Your love and faith in me made this journey possible.

To my father, Shawn Cahill, who instilled in me the value of learning and education principles that have guided me throughout this work. Through both of you, I've learned to treat others with care, respect, and a commitment to uplift those around me.

To my brother Matthew, family, and dear friends, thank you for always having my back and walking this journey beside me.

This is for you.

ACKNOWLEDGEMENTS

I would first like to express my deepest gratitude to my advisor, Dr. Mukesh Dhamala, for his guidance, mentorship, and support throughout this journey. I also sincerely thank my committee members, Dr. Vadym Apalkov and Dr. Brian Thoms, for their thoughtful feedback and for generously dedicating their time to support my research.

This dissertation would not have been possible without the foundational work of Dr. Timothy Jordan, who led the initial study on which this project is built. From participant recruitment to experimental design, his contributions laid the groundwork for everything that followed. I am also deeply grateful to Dr. Bhim Adhikari for his guidance and for providing the preprocessing pipeline used in our fMRI analysis, and to Chandrama Mukherjee for her work on the FreeSurfer analysis, which provided valuable insights into gray matter organization for this study.

To Dr. Murad Sarsour, thank you for your consistent support and clear guidance as graduate program director when I needed it most. To Dr. Sebastien Lepine, thank you for your leadership as the department chair and for generously supporting my trip to OHBM 2023, helping make that experience possible.

To my family, thank you for your unwavering support, love, and belief in me. I am especially grateful to my mother, Gail DeGeorge, and father, Shawn Cahill, whose encouragement and values shaped my educational journey and made this achievement possible. I am deeply thankful to Dr. Margarita Rodriguez, whose guidance and perspective have been instrumental throughout my life and academic pursuits. Finally, to my peers, collaborators, colleagues, and friends, thank you for walking this road with me. I wouldn't be the person I am today without you by my side. I am especially thankful to the professors and mentors who have guided me throughout my

academic journey. Your insight, encouragement, and belief in my potential have shaped me into the scientist I am today.

TABLE OF CONTENTS

LIST OF TABLES

LIST OF FIGURES

LIST OF ABBREVIATIONS

AFNI	Analysis of Functional NeuroImages
AVG	Action Video Game
CRA	Cognitive Resource Allocation
CRR	Cognitive Resource Reallocation
CRT	Cognitive Resource Theory
dFC	Directed Functional Connectivity
FC	Functional Connectivity
FDR	False Discovery Rate
FEP	Free Energy Principle
FSL	FMRIB Software Library
GC	Granger Causality
PCA	Principal Component Analysis
rcPCA	Region-Based Cumulative PCA
ROI	Region of Interest
RT	Response Time
SC	Structural Connectivity
SC-dFC	Structurally Constrained dFC
SC-FC	Structurally Constrained FC
SFC	Structure–Function Coupling
SdFC	Structure–Directed Functional Coupling

TE	Echo Time
TGC	Time-Domain Granger Causality
TI	Inversion Time
TR	Repetition Time

1 INTRODUCTION

Video games have emerged as one of the most widely consumed and cognitively engaging forms of interactive media in the world, with more than 3.2 billion players globally in 2023 (Media & Entertainment: Video Games Sector, 2024). Among these, action video games (AVGs), characterized by their fast-paced, perceptually demanding, and motor-intensive gameplay, offer a unique platform for studying how sustained environmental challenges shape brain function. Long-term AVG players referred to throughout this dissertation as 'gamers' are placed in dynamic, goal-oriented environments that demand rapid decision-making, attentional switching, visuospatial tracking, and complex motor coordination. Long-term exposure to such cognitive demands has been linked to measurable improvements in visuomotor performance and cognitive flexibility (Basak *et al*., 2008; Green & Bavelier, 2012; Glass *et al.,* 2013; Howard *et al.,* 2023; Lynch *et al.,* 2010).

These cognitive benefits have been shown to translate beyond the virtual environment, supporting improved performance in real-world domains such as surgical precision (Rosser *et al*., 2007), driving safety (Howard *et al*., 2023), military training (Orvis *et al*., 2010), and even literacy improvement in individuals with dyslexia (Bertoni *et al*., 2024). AVGs have also gained traction as cognitive training tools, with a notable clinical example being *EndeavorRx*, the first FDA-approved prescription digital therapeutic designed to help reduce attentional deficits in children with ADHD (Oh *et al.,* 2024). Complementing behavioral studies, a growing number of neuroimaging investigations have linked AVG play to changes in brain structure and function. Reported adaptations include increases in gray matter volume (Kühn & Gallinat, 2014), cortical thickness (Kühn, Lorenz, *et al*., 2014), and white matter coherence (Cahill *et al*., 2024; Lewandowska *et al*., 2022) as well as shifts in functional and directed connectivity within

attention, visual, and motor circuits(Brilliant *et al*., 2019; T. Jordan & M. Dhamala, 2022; Palaus *et al.*, 2017). These neural findings provide compelling evidence for experience-driven neuroplasticity in systems supporting perceptual decision-making and goal-directed behavior.

Yet despite this promising body of work, many unanswered questions remain. Prior studies often rely on either structural or functional data in isolation, lack direct cognitive testing to measure transfer effects, or report descriptive rather than mechanistic findings (Brilliant *et al*., 2019; Bediou *et al.,* 2023). Few have integrated multimodal neuroimaging (e.g., SC, FC, dFC) within a unified framework, especially in healthy, non-addicted populations, or tested whether observed network differences systematically align with behavior. This has left a gap in the literature regarding how localized neural changes give rise to coordinated, system-level dynamics that support cognitive performance.

To bridge this gap, this dissertation introduces a guiding theoretical model, Cognitive Resource Reallocation (CRR). CRR is defined as the dynamic redistribution of metabolic and functional neural resources toward behaviorally relevant, anatomically plausible neural circuits and away from redundant or inefficient processes. The CRR framework is supported by prior research demonstrating that environmental pressure can drive neuroplastic adaptation in task-relevant networks (Barbot *et al*., 2021; Buhusi & Meck, 2009; Taylor *et al.,* 2023). This reallocation occurs when task demands result in strained baseline support, producing cognitive friction during sustained engagement motivated by goal-directed or reward-seeking behaviors. In response, the brain reallocates energy over time to support task efficiency by upregulating task-relevant circuits and downregulating those that are inefficient or redundant, resulting in functional optimization.

In the context of AVG play, the "task" is not simply pressing buttons or responding to screen flashes. It is a prolonged, socially meaningful pursuit of performance under pressure—tracking fast-moving targets, managing risk, coordinating timing, and adapting strategy. Success in this environment depends not just on raw reaction time but on how quickly and precisely the brain can predict, select, and execute contextually appropriate actions. CRR posits that long-term AVG exposure encourages the brain to allocate its resources toward anticipatory, feedforward mechanisms that reduce visuomotor surprise, defined as the mismatch between expected and actual visual or motor feedback during decision-making.

In doing so, neural systems over time reorganize to reduce internal conflict and streamline action selection under uncertainty. This process gradually results in more optimized visuomotor pathways whereby visual input is more efficiently transformed into motor output, with reduced internal conflict and faster resolution of uncertainty. Conversely, non-gamers may rely more on compensatory or feedback-heavy processing, devoting more resources to early visual regions and less efficient action selection circuits. This aligns conceptually with the goal of attaining a more energetically efficient, low-surprise state, reducing cognitive friction associated with prediction error, and thus more closely aligning with the free-energy minimizing regime proposed by Dr. Karl Friston's Free Energy Principle (Friston, 2010; Friston & Kiebel, 2009).

While this dissertation does not directly quantify visuomotor surprise, it tests whether neural signatures are consistent with CRR predictions, including enhanced structural and functional connectivity in task-relevant circuits, reduced reliance on compensatory or non-task-relevant networks, and greater behavioral efficiency in these circuits, reflected in faster response times without accuracy loss.

The central hypothesis for this dissertation is that under repeated high-demand conditions, such as those found in action video games, the brain gradually reallocates its finite energetic resources to reinforce task-relevant circuits. This adaptive neuroplastic refinement enhances decision-making efficiency by reducing uncertainty and improving task performance. In tasks like our moving dots paradigm, where the outcome is uncertain (e.g., a 50/50 probability), it is suspected that gamers anticipate both possibilities more readily. This enhanced capacity to manage multiple potential outcomes reflects greater cognitive flexibility (Glass *et al.*, 2013) and attentional control (Bavelier & Green, 2019; Bavelier & Green, 2025), features consistently observed in gamers. Such adaptations would be reflected in connectivity patterns that facilitate feedforward, goal-directed action selection in response to task instructions (*i.e.,* perform as accurately and quickly as possible), while also integrating scene-specific, contextual cues, such as relative motion, that help resolve uncertainty more efficiently.

If confirmed, the findings of this project would offer a necessary and sufficient explanation for the improved speed–accuracy tradeoffs observed in gamers. This adaptation likely results from the repeated need to make rapid, high-stakes decisions during gameplay. The results would also support CRR as a mechanistic account of the cognitive advantages seen in gamers and help identify candidate pathways undergoing neuroplastic refinement. These pathways may serve as targets for cognitive training strategies and interventions aimed at improving visuomotor decision-making through action video game–based training or therapy.

To empirically evaluate CRR, this dissertation integrates three complementary methodological approaches, each designed to capture distinct aspects of brain network organization utilizing both structural and functional connectivity.

Chapter 3 focuses on a specific task-relevant regional network, the dorsal and ventral visual streams. Using predefined anatomical regions of interest (ROIs), this analysis tests whether gamers show enhanced visuomotor integration and faster decision-making, as predicted by stream-specific neuroplastic adaptation. Building on this targeted analysis, Chapter 4 expands the scope to the whole brain using a tractography constrained connectivity framework. By restricting analysis to biologically viable white matter pathways, this approach improves both interpretability and statistical power, enabling a focused investigation of functional connectivity (FC) and dynamic functional connectivity (dFC) across broader neural systems. Chapter 5 introduces a data-driven principal component analysis (PCA) framework designed to identify high-information ROIs across modalities. This technique reduces the multiple comparisons burden and enhances sensitivity to structured intersubject variability, allowing for the detection of meaningful patterns of neural reorganization that align with enhanced visuomotor decision making.

Each approach is optimized for a specific tradeoff between network specificity (Chapter 3), whole-brain anatomical plausibility (Chapter 4), and whole-brain statistical efficiency (Chapter 5). Together, these modes of analysis test whether adaptive reallocation patterns consistent with CRR emerge across structural and functional data and whether they reliably align with improved visuomotor decision-making observed in gamers.

In summary, this dissertation investigates how long-term action video game play shapes brain network architecture and cognitive performance. Through multimodal neuroimaging, connectivity analysis, and a unifying theoretical model, it offers a structured, mechanistic account of how experience-driven plasticity supports enhanced visuomotor decision-making. By introducing CRR as a generalizable principle of experience-driven neuroplastic adaptation and validating it across multiple modalities, this work contributes both novel methods and foundational theory to the emerging science of cognitive optimization.

2 MATERIALS AND METHODS

2.1 Materials and Data Acquisition

2.1.1 Participant Data and Demographics

A total of 47 right-handed participants were recruited for this study, comprising 28 gamers (24 male, 4 female) and 19 non-gamers (7 male, 12 female). The groups were age-matched (gamers: 20.6 ± 2.4 years; non-gamers: 19.9 ± 2.6 years). Participants were classified as gamers if they reported playing action video games for 5 or more hours per week over the past two years. Game genres included First-Person Shooter (FPS), Real-Time Strategy (RTS), Multiplayer Online Battle Arena (MOBA), and Battle Royale (BR), in alignment with industry demographics and prior categorization standards (Green & Bavelier, 2003, 2007, 2015; Gao *et al*., 2018; Stewart *et al.,* 2020). Non-gamers reported playing less than 30 minutes per week on average during the same time frame.

To confirm eligibility and assign participants to the appropriate group, a questionnaire was administered assessing video game genre and play frequency over the past two years. All participants passed the Ishihara Test for Color Deficiency and completed informed consent and health screening forms before data collection. The study was approved by the Institutional Review Boards of Georgia State University and the Georgia Institute of Technology, both located in Atlanta, Georgia. Cohort classification, task design, and additional recruitment procedures followed those originally reported in Jordan (2021).

2.1.1.1 Study-Specific Participant Pool

While the same general participant cohort was used across all analyses, final sample sizes varied slightly across imaging modalities due to modality-specific quality control procedures.

Subjects were excluded on a per-modality basis if their data did not meet predefined quality criteria (e.g., motion artifacts in fMRI, low signal-to-noise in DWI reconstructions). Specific sample sizes for each analysis are reported in the relevant methods subsections.

2.1.1.1.1 Brain Network Analysis: The Visual Streams

One gamer from the structural connectivity analysis, due to incomplete tractography data, and one non-gamer from the functional connectivity analysis, due to incomplete fMRI data. Two additional subjects' data (one gamer and one non-gamer) were excluded from the brain-behavior regressions due to incomplete response time data. The effective number of participants for the functional connectivity analysis was 46 total participants (28 gamers and 18 non-gamers), with 44 total participants (27 gamers and 17 non-gamers) for brain-behavior regression between functional connectivity measures with response time. The effective number of participants for the structural connectivity analysis was 46 total participants (27 gamers and 19 non-gamers), with 44 total participants (26 gamers and 18 non-gamers) for brain-behavior regression between structural connectivity measures with response time.

2.1.1.1.2 Whole Brain Analysis: Tractography Constrained Functional and Directed Connectivity

After initial recruitment of 47 participants (28 gamers, 19 non-gamers), a subset of subjects was excluded based on modality-specific data quality thresholds. One participant was excluded from the SC-FC and SC-TGC analyses due to unusable structural connectivity data. Three participants were excluded from FC analysis due to excessive head motion, ensuring reliable functional connectivity estimation. For the brain–behavior regressions, two additional subjects were excluded due to missing response time data. This resulted in a final analytic sample of n = 42 for SC-FC and SC-TGC connectivity analyses and n = 40 for brain–behavior

regression models. While this modest reduction in sample size slightly reduced statistical power, it ensured that all included data met rigorous quality control standards, thereby enhancing the reliability of observed effects.

2.1.1.1.3 Whole Brain Analysis: PCA-Based ROI Selection

After preprocessing and quality control, the final sample size varied slightly by modality. Functional and directed functional connectivity (FC and dFC) analyses included 43 participants (25 gamers and 18 non-gamers), while brain–behavior correlations using FC and dFC included 41 participants (24 gamers and 17 non-gamers). Structural connectivity (SC) analyses included 46 participants (27 gamers and 19 non-gamers), with 44 participants (26 gamers and 18 non-gamers) used in SC brain–behavior analyses. Finally, SC–FC and SC–dFC coupling analyses included 42 participants (24 gamers and 18 non-gamers), and the corresponding brain–behavior coupling analyses included 40 participants (23 gamers and 17 non-gamers).

2.1.2 MRI Scanning Protocols

Whole-brain structural and functional MR imaging was conducted on a 3T Siemens Magnetom Prisma MRI scanner (Siemens, Atlanta, GA, USA) at the joint Georgia State University and Georgia Institute of Technology Center for Advanced Brain Imaging, Atlanta, GA, USA. High-resolution anatomical images were acquired using a T1-MEMPRAGE scan sequence for voxel-based morphometry and anatomical reference. The acquisition parameters were as follows: TR = 2530 ms, TE1-4 = 1.69–7.27 ms, TI = 1260 ms, flip angle = 7°, and voxel size = 1 mm × 1 mm × 1 mm.

Diffusion-weighted imaging (DWI) data were collected using a multi-shell diffusion scheme with b-values of 300, 650, 1000, and 2000 s/mm², corresponding to 4, 17, 39, and 68 diffusion-encoding directions, respectively. One non-diffusion-weighted (b = 0) volume was also

included. The acquisition was performed using a single-shot echo-planar imaging (EPI) sequence with anterior-to-posterior (AP) phase encoding. Each diffusion volume consisted of 60 axial slices acquired with a 2 mm isotropic resolution (slice thickness = 2 mm, in-plane resolution = 2 × 2 mm), and the field of view (ReadoutFOV) was 220 mm. The diffusion data acquisition was approximately 6.5 minutes. Acquisition parameters for the diffusion imaging included TR = 2750 ms and TE = 79 ms. Functional imaging was performed using a T2-weighted gradient echo-planar imaging (EPI)* sequence during the behavioral tasks. Four functional runs were acquired with the following parameters: TR = 535 ms, TE = 30 ms, flip angle = 46°, and voxel size = 3.8 mm × 3.8 mm × 4 mm. The field of view was 240 mm, and 32 slices were collected in an interleaved order with a slice thickness of 4 mm. A total of 3440 brain images were acquired during task performance.

2.2 Analytical Methods and Experiment Design

2.2.1 Experiment Design and Behavioral Results

The experimental task used in this study was a modified version of the moving dots left–right discrimination paradigm originally developed and implemented as described by Jordan (2021) to investigate sensorimotor decision-making performance in gamers and non-gamers. The same design was employed here to ensure consistency in behavioral demands and fMRI task structure, enabling direct comparison and methodological continuity.

This task engages a sequence of subprocesses that collectively define visuomotor decision-making, as outlined by Jordan (2021) and Jordan & Dhamala (2022b). The process begins with a visual stimulus that initiates sensory evidence accumulation, where input is processed and integrated; this is followed by a perceptual judgment based on sensory evidence;

and finally, a motor response is selected and executed based on this perceptual judgment. Attentional selection and control modulate this process at every stage of the decision.

Each task block began with a cue screen indicating the color participants should attend, followed by the presentation of two overlapping sets of 600 MDs (one in the cued color and one distractor set). Participants had 3 seconds to indicate whether the cued color dots were moving left, right, or not at all. Motion direction and color pairings were randomized across trials, with difficulty manipulated via color contrast (easy, medium, hard) and motion speed (five levels, including a no-motion condition). Each block contained three task trials (totaling 15 seconds), followed by a 15-second rest period. A total of 60 task blocks were presented across four fMRI runs, with all combinations of difficulty and speed occurring multiple times per subject. Stimulus presentation was controlled using PsychoPy (Peirce *et al*., 2019), and participant responses were collected using an MR-compatible button box.

Behavioral performance measures included response accuracy and response time. Gamers responded significantly faster and slightly more accurately than non-gamers particularly under low-difficulty and moderate-speed conditions. In the general condition, gamers responded significantly faster than non-gamers (930 ± 430 ms vs. 1120 ± 490 ms, $p = 2.05 \times 10^{-70}$), with an average response time advantage of 190 ms. They also exhibited significantly higher task accuracy ($95.3\% \pm 3.9\%$ vs. $93.0\% \pm 5.6\%$, $p = 0.0008$), reflecting a 2.2% improvement in overall performance accuracy.

2.2.2 Brain Network Analysis, Visual Streams

2.2.2.1 Regions of Interest

In our investigation, we examined the structural and functional organization of the dorsal and ventral visual streams using fourteen regions of interest (ROIs) defined in a prior study from the Neurosynth functional meta-analysis platform (https://neurosynth.org/). The ROIs were derived based on relevant search terms, including "primary visual," "ventral visual," "visual stream," and "dorsal visual" as described by (Wong *et al*., 2021). The identified ROIs encompassed two regions situated within the primary visual cortex (V1), specifically the bilateral Calcarine (Calc) areas. VS (visual stream) denotes the primary connections from the Calcarine region to the bilateral superior and inferior occipital gyri. Additionally, we identified four ROIs within the ventral visual stream (VVS), which included the bilateral fusiform gyrus (FG) and inferior temporal gyrus (ITG).

Moreover, four ROIs were identified in the dorsal visual stream (DVS), encompassing the bilateral inferior parietal lobule (IPL) and superior parietal lobule (SPL). The nomenclature used in this classification was based on the Eickhoff-Zilles macro labels from N27 and was implemented in AFNI as described by Wong *et al.* (2021). We constructed a BrainNet Viewer (Xia M) representation of the general organization, subsystems, and the 14 ROIs along with the 12 connections composing the visual streams shown in Figure 2.1.

The construction of the ROIs for the structural tractography was carried out with a 12 mm radius to ensure the analysis accounted for anatomical variability and adequately encompassed the white matter tracts connecting the visual streams, thus mitigating the risk of missing important connections. We employed the MNI coordinate system and constructed the ROIs using the FSLeyes visualization tool within the FSL (FMRIB Software Library) (Jenkinson *et al*., 2012;

Woolrich *et al*., 2009) environment. The functional connectivity analysis utilized 6 mm radius ROIs using the same MNI coordinates.

Table 2.1 Anatomically defined regions of interest (ROIs) used in visual stream tractography. Each ROI is represented by its central MNI coordinate and categorized as belonging to the dorsal visual stream (DVS), ventral visual stream (VVS), or shared visual system (VS).

Region of Interest (ROI)	MNI coordinates (x, y, z)	Subsystem
Left Superior Occipital Gyrus (L SOG)	-26, -73, 23	DVS, VS
Left Inferior Parietal Lobule (L IPL)	-24, -52, 52	DVS
Left Superior Parietal Lobule (L SPL)	-30, -46, 66	DVS
Right Superior Occipital Gyrus (R SOG)	23, -91, 26	DVS, VS
Right Inferior Parietal Lobule (R IPL)	24, -48, 42	DVS
Right Superior Parietal Lobule (R SPL)	20, -68, 62	DVS
Left Inferior Occipital Gyrus (L IOG)	-42, -64, -12	VVS, VS
Left Inferior Temporal Gyrus (L ITG)	-44, -50, -15	VVS
Left Fusiform Gyrus (L FG)	-34, -48, -16	VVS
Right Inferior Occipital Gyrus (R IOG)	40, -64, -12	VVS, VS
Right Inferior Temporal Gyrus (R ITG)	48, -60, -12	VVS
Right Fusiform Gyrus (R FG)	40, -52, -16	VVS
Left Calcarine (L Calc)	-8, -86, 6	VS
Right Calcarine (R Calc)	8, 86, 6	VS

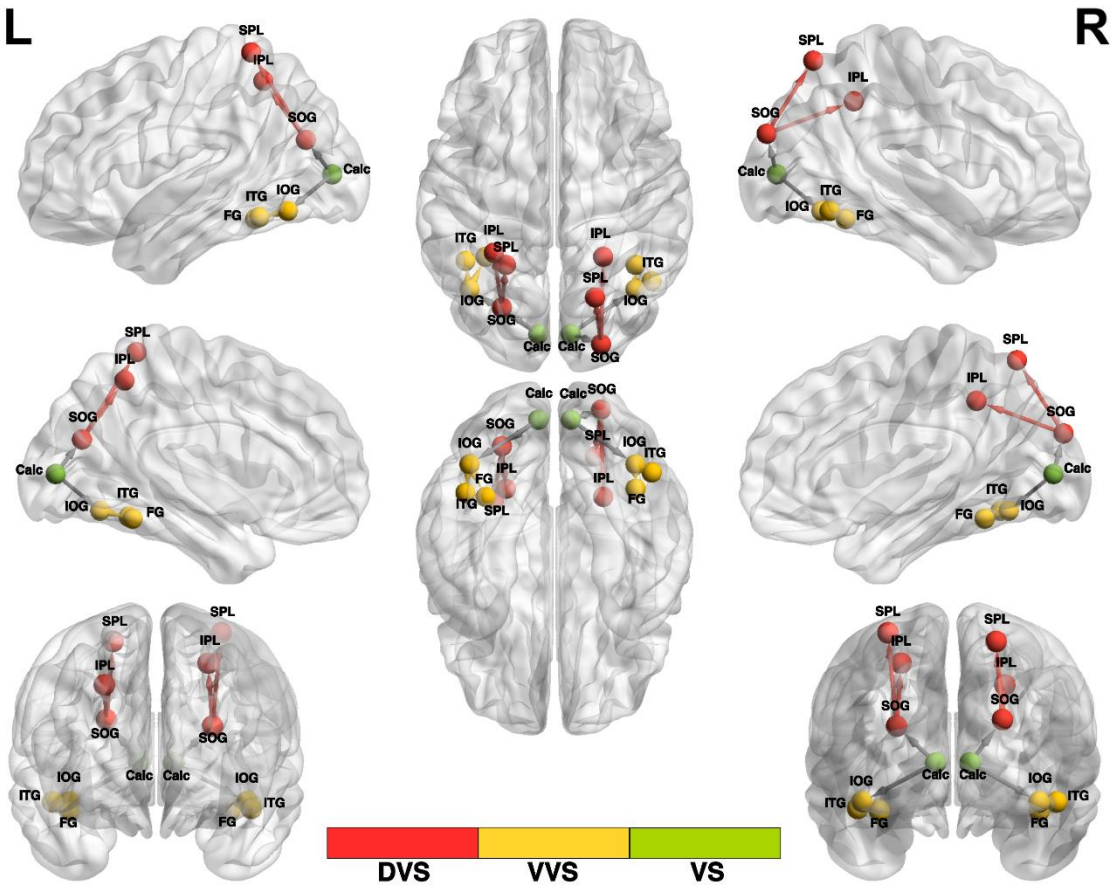

Figure 2.1 Meta-analysis derived ROIs: Visual Streams BrainNet Viewer (Xia M) representation of the locations of the 14 spherical ROIs and 12 connections considered that constitute the subsystems of the two visual streams. (Left to Right): The dorsal visual stream (DVS) extends from SOG to IPL and from SOG to SPL, shown in red; the ventral visual stream (VVS) extends from IOG to FG and from IOG to ITG, shown in yellow; and the visual stream (VS) denotes the primary connections from the Calcarine region, namely Calcarine to IOG and Calcarine to SOG.

2.2.2.2 Grey Matter Morphometry

2.2.2.2.1 FreeSurfer Preprocessing

Anatomical data preprocessing and morphometric parameter estimation were conducted by Chandrama Mukherjee (PhD student, Neurophysics Lab, GSU) under the supervision of Dr. Mukesh Dhamala. The full *recon-all* pipeline in FreeSurfer (version 7.4.1; https://surfer.nmr.mgh.harvard.edu) was used for cortical surface reconstruction and subcortical segmentation (Dale *et al*., 1999). Motion artifacts were corrected using intensity normalization and rigid-body alignment (Ségonne *et al*., 2004). Each subject's brain was transformed into Talairach space and segmented according to the Desikan-Killiany atlas (Desikan *et al*., 2006). Additional methodological details are available in prior work (Dale *et al*., 1999; Fischl *et al*., 2002; Fischl, 2012). All outputs—T1 volumes, skull-stripped brains, and pial surfaces—underwent rigorous visual inspection to ensure anatomical accuracy and data quality.

2.2.2.2.2 Data Extraction and Preparation

Cortical thickness (CT) values and intracranial volume (ICV) were assessed using the FreeSurfer utilities *mri_surf2surf*, *mris_anatomical_stats*, and *aparcstats2table* (Fischl, 2012). Each brain was parcellated into 70 cortical regions (35 per hemisphere) according to the Desikan-Killiany atlas (Desikan *et al*., 2006). Quality control was rigorously performed by visually inspecting raw structural images, skull-stripped volumes, and reconstructed pial surfaces within FreeSurfer's visual tools (e.g., Freeview). Criteria for quality control included accurate skull stripping without visible dura, consistent cortical ribbon delineation, and correct anatomical segmentation. Manual interventions such as control point edits, brain mask adjustments, and pial

surface regeneration commands (*recon-all -autorecon-pial -subjid subjectID*) were used to correct identified segmentation and normalization errors

2.2.2.2.3 Statistical Analysis

Statistical analysis was performed using IBM SPSS Statistics (version 29.0; IBM Corp., Armonk, NY, USA). A multivariate analysis of covariance (MANCOVA) was conducted to assess group differences in cortical thickness across the 70 regions, with group (gamer vs. non-gamer) as the independent variable and total intracranial volume (ICV) entered as a covariate. Main effects and interactions were evaluated with statistical significance set at $p \leq 0.05$. Effect sizes were reported using F-statistics and partial eta squared (ηp^2).

A parallel MANCOVA was conducted to evaluate regional cortical volume differences using the same model. However, no statistically significant group-wide volumetric differences were observed. The inclusion of ICV as a covariate ensured that variations in head size were accounted for in both analyses.

2.2.2.3 White Matter Tractography

2.2.2.3.1 DSI-Studio Preprocessing

DSI Studio version 2022.08.0 is a non-commercial software program that was utilized in this study for diffusion MR image analysis and provided functions including deterministic fiber tracking and 3D visualization (Yeh *et al*., 2013). We used a multi-shell diffusion scheme with b-values of 300, 650, 1000, and 2000 s/mm². The acquisition parameters consisted of an in-plane resolution of 2 mm and a slice thickness of 2 mm. The accuracy of b-table orientation was examined by comparing fiber orientations with those of a population-averaged template (Yeh

FC, 2018). Diffusion-weighted images were preprocessed using the EDDY tool implemented via DSI Studio, which corrected for eddy current–induced distortions and motion artifacts. The diffusion data were reconstructed in the MNI space using q-space diffeomorphic reconstruction (Yeh *et al*., 2010) to obtain the spin distribution function (Yeh & Tseng, 2011). A diffusion sampling length ratio of 1.25 was used. The resulting diffeomorphic reconstruction output had an isotopic resolution of 2 mm.

2.2.2.3.2 Tractography Protocols & Structural Connectivity Analysis

Seeds were randomly placed throughout the ROIs until reaching a cutoff of 50,000,000 seeds. Additionally, two pairwise spherical ROIs were also defined as ending regions. In the case between the L SOG and the L IPL, for example, the ending regions were placed at (52,74,37) and (51,64,51). An angular threshold of 60 degrees was set as the maximum allowed angular deviation between steps. The step size was randomly selected from 0.5 voxels to 1.5 voxels. Tracks with lengths shorter than 10 mm or longer than 100 mm were excluded from further analysis. The process continued until mapping each subsystem of the dorsal and ventral visual streams (DVS, VVS, VS), with an exhaustive exploration of all pairwise links in each section denoted in Table 2.2. For full reproducibility, the parameter ID used in DSI Studio to configure the settings described above is provided: 0AD7233C9A99193Fba3Fdb2041bC84280F0FA02ec. This ID allows others to load the exact parameters used in our analysis, ensuring that tractography and derived metrics can be replicated using identical configurations. Adjustments to the parameters for maximum length and angular threshold were made based on the connection being mapped, as detailed in Table 2.2.

Table 2.2 Minimum and maximum streamline angular thresholds for visual stream connections

Subsystem	Connection	Min length (mm)	Max length (mm)	Angular Threshold (deg)
DVS	L SOG L IPL	10	100	60
	L SOG L SPL	10	300	70
	R SOG R IPL	10	100	75
	R SOG R SPL	10	150	70
VVS	L IOG L ITG	10	20	50
	L IOG L FG	10	35	50
	R IOG R ITG	10	20	50
	R IOG R FG	10	35	50
VS	L Calc L IOG	10	70	65
	L Calc L SOG	5	20	50
	R Calc R IOG	10	80	65
	R Calc R SOG	10	30	50

For tracking eligibility, a quantitative anisotropy threshold of 0.01 was universally applied in all connections, except for the connection between R SOG and R IPL. In this case, a lower quantitative anisotropy threshold of 0.005 was necessary to prevent the inadvertent exclusion of subjects with valid fibers from the analysis. Consequently, voxels with a qualitative anisotropy value exceeding the specified threshold were deemed anisotropic and suitable for inclusion in the fiber tracking process. The fiber pathways between the L SOG and L IPL are shown in a representative participant in Figure 2.2, where the axis is color-coded to distinguish the orientation of the fibers. The X-axis is coded for red from right to left, the Y-axis is coded for green from anterior to posterior, and the Z-axis is coded for blue from superior to inferior.

Structural connectivity measures the anatomical organization of the brain using white matter fiber tracts (Babaeeghazvini *et al.*, 2021). Although relatively stable on shorter time scales (seconds to minutes), it can exhibit plastic experience-dependent changes at longer periods (hours to days) (Sporns, 2013). Fractional Anisotropy (FA), based on diffusivity, is calculated as the

normalized fraction of the diffusion tensor's magnitude (Soares *et al*., 2013). Fractional anisotropy (FA) is a useful measure and is often a standard in structural connectivity analysis (Sammer *et al*., 2022; Soares *et al*., 2013). Quantitative anisotropy (QA) is known to be less susceptible to partial volume effects due to crossing fibers and free water in the brain than FA, resulting in a better resolution and improved tractography(Ahn & Lee, 2011; Yeh *et al*., 2010).

QA is a model-free measure derived from the Fourier transform relation between MR signals and diffusion displacement and is nonparametrically calculated from peak orientations on a spin distribution function (Yeh *et al*., 2013). QA is known to be less susceptible to partial volume effects due to crossing fibers and free water in the brain than FA, resulting in a better resolution and improved tractography (Ahn & Lee, 2011; Yeh *et al*., 2010). Both FA and QA were utilized as primary measures of enhanced structural connectivity and were extracted for each pair of ROIs composing the two visual streams, and we investigated the brain-behavior relation of these two structural connectivity measures with the participants' response times.

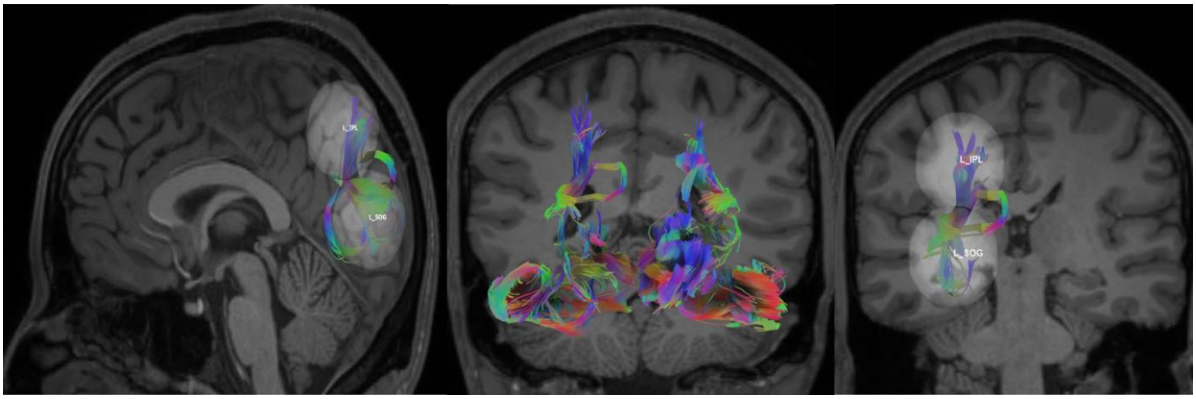

Figure 2.2 Tractography Fiber Tracks, Visual Streams. The fibers are colored-coded using the RGB model to represent their orientation, where "red" indicates fibers along the X-axis (i.e., left-right), "green" indicates fibers along the Y-axis (i.e., anterior-posterior), and "blue" indicates fibers along the Z-axis (i.e., inferior-superior).

Mixed colors, such as "yellow," represent fibers with combined orientations (e.g., red and green). (Left to Right): Sagittal, reconstruction of white matter fiber tracts modelling pathways between L SOG and L IPL; Coronal, reconstruction of white matter tracts modelling the pathways that constitute the entire dorsal and ventral streams; Coronal, reconstruction of white matter tracts modelling the pathways between the L SOG and L IPL.

2.2.2.4 Undirected and Directed Functional Connectivity

Functional connectivity (FC), i.e., pairwise Pearson correlation coefficients in neuroimaging, measures temporal correlations of the Blood Oxygen Level Dependent BOLD signal time series in spatially distant brain regions.(Bastos & Schoffelen, 2016; Friston, 1994; Rosch & Mostofsky, 2019) Thus, two regions are considered functionally connected if there is a statistical relationship between the measures of recorded BOLD activity (Eickhoff & Müller, 2015). FC was computed using 6 mm spherical ROIs. For the directed connectivity analysis, the appropriate model order for time-domain Granger causality (TGC) was determined by minimizing the spectral difference between the Granger-generated time series and the original

signal. After evaluating model orders ranging from two to twenty, a model order of six was selected, as it yielded the lowest spectral discrepancy for the visual stream analysis. TGC matrices were then computed for each participant using the same ROIs and the model order, using the bivariate autoregressive model outlined by Dhamala *et al.* (2008, 2018).

To investigate the relationship between brain connectivity and behavior, undirected FC and TGC values were obtained for each participant per connection. Spearman's rank correlation coefficient was used to assess the correlation between FC and response time (RT) as well as between TGC and RT.

2.2.2.5 Statistical Analysis

Statistical comparison of connectivity measures between ROIs across gamers and non-gamers was carried out using the Wilcoxon rank-sum test (also known as the Mann-Whitney U test). This non-parametric test was chosen because it does not assume normality of the connectivity measure's distribution, making it suitable for comparing the two groups without requiring any assumptions about the underlying distribution of the data. For multiple comparison corrections in this analysis, we employed the Holm-Bonferroni method. This method was selected for its ability to enhance statistical power and sensitivity to individual significant comparisons while effectively controlling for Type I errors (Giacalone *et al*., 2018; Holm, 1979). We applied a $p < 0.05$ significance threshold, within each main section (DVS, VVS, VS), to ensure statistical significance while simultaneously controlling for the family-wise error rate in the dorsal and ventral streams, Holm-Bonferroni corrected indicated by p^*, providing a robust framework for identifying meaningful differences in connectivity measures.

2.2.3 Whole Brain Analysis: Tractography Constrained Functional and Directed Connectivity

2.2.3.1 Whole Brain Tractography Protocols

Following data acquisition, the diffusion data were reconstructed in the MNI space using q-space diffeomorphic reconstruction (QSDR)(Yeh & Tseng, 2011) to compute the spin distribution function (Yeh *et al*., 2010) in DSI Studio (Version Hou, 2024). A diffusion sampling length ratio of 1.25 was applied, with the output resolution in diffeomorphic reconstruction set to 2 mm isotropic. Diffusion-weighted images were preprocessed using the EDDY tool implemented via DSI Studio, which corrected for eddy current–induced distortions and motion artifacts.

For fiber tractography, a deterministic fiber tracking algorithm (Yeh *et al.,* 2013) was used, incorporating augmented tracking strategies (Yeh, 2020) to improve reproducibility. The quantitative anisotropy (QA) threshold was set to 0.12, and the angular threshold was set to 60 degrees. The step size was 1.00 mm, and tracks shorter than 10 mm or longer than 400 mm were discarded. A total of 5 million tracts were calculated for each participant. Shape analysis was conducted to derive shape metrics for the tractography(Yeh, 2020).

For full reproducibility, the parameter ID used in DSI Studio to configure these settings is 8FC2F53D9A99193Fba3Fb803Fcb2041bC843404B4Cca01cbaCDCC4C3Ec. This ID allows others to load the exact settings and parameters used in the analysis, ensuring that the tractography and other measures can be reproduced using the same configurations.

2.2.3.2 fMRI Pre-Processing Pipeline

The preprocessing pipeline for functional MRI data that was acquired as described in Section 2.1.2. combined with tools from AFNI (Cox, 1996; Cox & Hyde, 1997) and FSL(Jenkinson *et al*., 2012; Smith *et al.,* 2004; Woolrich *et al*., 2009) to ensure high-quality data for subsequent analysis (Adhikari *et al*., 2018; B. M. Adhikari *et al*., 2018; Adhikari *et al.,* 2019) The process began with denoising the fMRI data to reduce noise from physiological artifacts such as head motion and scanner drift, using AFNI's *dwidenoise* command. This step resulted in denoised datasets for each run of the fMRI data. Following this, motion correction was performed using AFNI's *3dvolreg*, which registers each volume of the fMRI data to a reference volume within the session. After motion correction, the data were aligned to the MNI space using FSL's FLIRT tool, ensuring that all data were in a common standard space for group-level comparisons.

To remove any motion-related artifacts, outlier detection was carried out using AFNI's 3dToutcount, which computes the fraction of outlier voxels in each volume. A censoring procedure was then applied, excluding volumes where the fraction of outlier voxels exceeded a predefined threshold of 0.1. Despiking was performed with AFNI's *3dDespike*, which removed brief, spurious signal fluctuations, or "spikes," from the data. Following despiking, slice timing correction was applied using *3dTshift* to ensure temporal alignment across slices in each volume.

Time series were then extracted from predefined brain regions derived from the Automated Anatomical Labeling 3 (AAL3) parcellation using AFNI's *3dROIstats*, which computes the average signal within each ROI. These time series were saved as text files for further analysis. The signal-to-noise ratio for each run was computed using AFNI's 3dTstat to

calculate the mean signal and 3dTproject to compute the standard deviation of the noise. Additionally, global correlation averages were computed to assess overall data quality.

The degree of spatial blurring in the data was estimated using FSL's *3dFWHMx*, which calculates the full width at half maximum (FWHM) of the data's spatial blurring. Following this, a mask was created using AFNI's 3dmask_tool to identify valid brain regions with usable data across all volumes. The data were then registered to the MNI template (ENIGMA Template) using AFNI's *@auto_tlrc*, which applies a transformation matrix to warp each subject's data into standard space for group-level analysis.

To further improve data quality, Principal Component Analysis (PCA) was applied using AFNI's *3dpc* to remove non-neuronal signals, such as global signal fluctuations and motion-related noise. PCA regressors were generated from ventricular and brain regions and were used in subsequent regression analysis to remove unwanted variance from the data. Finally, the processed datasets were reviewed for quality control, and any remaining temporary files were removed to prepare the data for further analysis.

After the AFNI and FSL preprocessing steps, additional processing was performed in MATLAB to further refine the data for task-based analysis. This included outlier correction, where extreme values in the time series that exceeded 5 standard deviations were identified and corrected. Detrending was applied to remove any linear trends from the data using MATLAB's detrend function, ensuring that any slow drifts in the signal did not affect subsequent analyses.

The time series data were then parsed by behavioral condition and time block, creating condition-specific time series data for each subject. This allowed for a detailed analysis of brain activity that aligned with experimental conditions. The preprocessed time series data for each ROI in the AAL3 atlas were stored in structured files and saved for subsequent analysis.

2.2.3.3 Atlas Selection & AAL3 Parcellation

For the functional and structural connectivity analysis, the Automated Anatomical Labeling 3 (AAL3) atlas was selected due to its widespread use and strong effect sizes in capturing brain structure-function relationships, especially when compared to other well-known atlases (Revell *et al.,* 2022). The AAL3 atlas includes 166 parcellations, with critical task-relevant regions such as the orbitofrontal cortex, cerebellum, and thalamic nuclei, which are particularly relevant for video game studies investigating neural processes underlying cognitive functions like visuomotor decision-making.

Thus, the AAL3 atlas was deemed highly suitable for whole-brain analysis in this study (Rolls *et al.,* 2020). For better visual clarity and interpretability, we organized the regions of the AAL3 atlas intoclear subdivisions Orbitofrontal, Occipital, Limbic System, Frontal, Temporal, Thalamus, Parietal, Basal Ganglia, Cerebellum, and Brain Stem shown in Figure 2.3a based on their known anatomical locations, while preserving individual regions in our analysis as displayed in Table 2.3 As the brain slices progress in Figure 2.3b, the organization of these regions becomes more apparent, revealing how these anatomical structures are spatially arranged. This clear organizational structure aids in interpreting the results of our analysis.

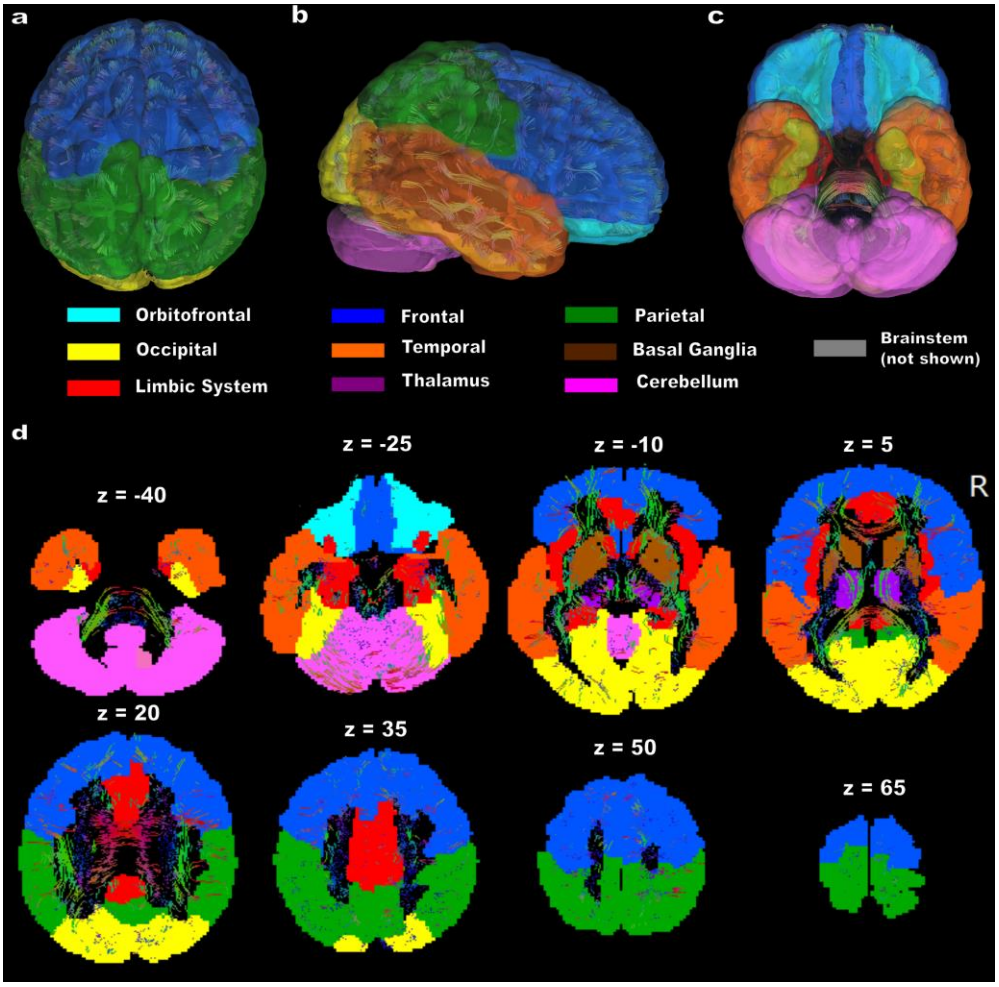

Figure 2.3 AAL3 Atlas Parcellation Categories for Connectivity Analysis. Visualization of the AAL3 atlas with anatomically grouped parcellations used in the connectivity analysis. (a) superior view, (b) right lateral view, (c) inferior view. (d) Axial slices illustrate the parcellation structure along the Z-axis. Colors correspond to distinct anatomical groups. The brainstem (gray) is not shown but is included in the analysis.

Table 2.3 AAL 3 Region Parcellation Categories by Anatomical Categories

No.	AAL 3 Region	Category	No.	AAL 3 Region	Category
1	Precentral_L	Frontal	84	Temporal_Pole_Sup_R	Temporal
2	Precentral_R	Frontal	85	Temporal_Mid_L	Temporal
3	Frontal_Sup_2_L	Frontal	86	Temporal_Mid_R	Temporal
4	Frontal_Sup_2_R	Frontal	87	Temporal_Pole_Mid_L	Temporal
5	Frontal_Mid_2_L	Frontal	88	Temporal_Pole_Mid_R	Temporal
6	Frontal_Mid_2_R	Frontal	89	Temporal_Inf_L	Temporal
7	Frontal_Inf_Oper_L	Frontal	90	Temporal_Inf_R	Temporal
8	Frontal_Inf_Oper_R	Frontal	91	Cerebellum_Crus1_L	Cerebellum
9	Frontal_Inf_Tri_L	Frontal	92	Cerebellum_Crus1_R	Cerebellum
10	Frontal_Inf_Tri_R	Frontal	93	Cerebellum_Crus2_L	Cerebellum
11	Frontal_Inf_Orb_2_L	Frontal	94	Cerebellum_Crus2_R	Cerebellum
12	Frontal_Inf_Orb_2_R	Frontal	95	Cerebellum_3_L	Cerebellum

13	Rolandic_Oper_L	Frontal	96	Cerebellum_3_R	Cerebellum
14	Rolandic_Oper_R	Frontal	97	Cerebellum_4_5_L	Cerebellum
15	Supp_Motor_Area_L	Frontal	98	Cerebellum_4_5_R	Cerebellum
16	Supp_Motor_Area_R	Frontal	99	Cerebellum_6_L	Cerebellum
17	Olfactory_L	Frontal	100	Cerebellum_6_R	Cerebellum
18	Olfactory_R	Frontal	101	Cerebellum_7b_L	Cerebellum
19	Frontal_Sup_Medial_L	Frontal	102	Cerebellum_7b_R	Cerebellum
20	Frontal_Sup_Medial_R	Frontal	103	Cerebellum_8_L	Cerebellum
21	Frontal_Med_Orb_L	Frontal	104	Cerebellum_8_R	Cerebellum
22	Frontal_Med_Orb_R	Frontal	105	Cerebellum_9_L	Cerebellum
23	Rectus_L	Frontal	106	Cerebellum_9_R	Cerebellum
24	Rectus_R	Frontal	107	Cerebellum_10_L	Cerebellum
25	OFCmed_L	Orbitofrontal	108	Cerebellum_10_R	Cerebellum
26	OFCmed_R	Orbitofrontal	109	Vermis_1_2	Cerebellum

27	OFCant_L	Orbitofrontal	110	Vermis_3	Cerebellum
28	OFCant_R	Orbitofrontal	111	Vermis_4_5	Cerebellum
29	OFCpost_L	Orbitofrontal	112	Vermis_6	Cerebellum
30	OFCpost_R	Orbitofrontal	113	Vermis_7	Cerebellum
31	OFClat_L	Orbitofrontal	114	Vermis_8	Cerebellum
32	OFClat_R	Orbitofrontal	115	Vermis_9	Cerebellum
33	Insula_L	Limbic	116	Vermis_10	Cerebellum
34	Insula_R	Limbic	117	Thal_AV_L	Thalamus
35	Cingulate_Mid_L	Limbic	118	Thal_AV_R	Thalamus
36	Cingulate_Mid_R	Limbic	119	Thal_LP_L	Thalamus
37	Cingulate_Post_L	Limbic	120	Thal_LP_R	Thalamus
38	Cingulate_Post_R	Limbic	121	Thal_VA_L	Thalamus
39	Hippocampus_L	Limbic	122	Thal_VA_R	Thalamus
40	Hippocampus_R	Limbic	123	Thal_VL_L	Thalamus
41	ParaHippocampal_L	Limbic	124	Thal_VL_R	Thalamus
42	ParaHippocampal_R	Limbic	125	Thal_VPL_L	Thalamus
43	Amygdala_L	Limbic	126	Thal_VPL_R	Thalamus
44	Amygdala_R	Limbic	127	Thal_IL_L	Thalamus

45	Calcarine_L	Occipital	128	Thal_IL_R	Thalamus
46	Calcarine_R	Occipital	129	Thal_Re_L	Thalamus
47	Cuneus_L	Occipital	130	Thal_Re_R	Thalamus
48	Cuneus_R	Occipital	131	Thal_MDm_L	Thalamus
49	Lingual_L	Occipital	132	Thal_MDm_R	Thalamus
50	Lingual_R	Occipital	133	Thal_MDl_L	Thalamus
51	Occipital_Sup_L	Occipital	134	Thal_MDl_R	Thalamus
52	Occipital_Sup_R	Occipital	135	Thal_LGN_L	Thalamus
53	Occipital_Mid_L	Occipital	136	Thal_LGN_R	Thalamus
54	Occipital_Mid_R	Occipital	137	Thal_MGN_L	Thalamus
55	Occipital_Inf_L	Occipital	138	Thal_MGN_R	Thalamus
56	Occipital_Inf_R	Occipital	139	Thal_PuI_L	Thalamus
57	Fusiform_L	Occipital	140	Thal_PuI_R	Thalamus
58	Fusiform_R	Occipital	141	Thal_PuM_L	Thalamus
59	Postcentral_L	Parietal	142	Thal_PuM_R	Thalamus
60	Postcentral_R	Parietal	143	Thal_PuA_L	Thalamus
61	Parietal_Sup_L	Parietal	144	Thal_PuA_R	Thalamus
62	Parietal_Sup_R	Parietal	145	Thal_PuL_L	Thalamus
63	Parietal_Inf_L	Parietal	146	Thal_PuL_R	Thalamus

64	Parietal_Inf_R	Parietal	147	ACC_sub_L	Limbic
65	SupraMarginal_L	Parietal	148	ACC_sub_R	Limbic
66	SupraMarginal_R	Parietal	149	ACC_pre_L	Limbic
67	Angular_L	Parietal	150	ACC_pre_R	Limbic
68	Angular_R	Parietal	151	ACC_sup_L	Limbic
69	Precuneus_L	Parietal	152	ACC_sup_R	Limbic
70	Precuneus_R	Parietal	153	N_Acc_L	Limbic
71	Paracentral_Lobule_L	Parietal	154	N_Acc_R	Limbic
72	Paracentral_Lobule_R	Parietal	155	VTA_L	Limbic
73	Caudate_L	Basal Ganglia	156	VTA_R	Limbic
74	Caudate_R	Basal Ganglia	157	SN_pc_L	Limbic
75	Putamen_L	Basal Ganglia	158	SN_pc_R	Limbic
76	Putamen_R	Basal Ganglia	159	SN_pr_L	Limbic
77	Pallidum_L	Basal Ganglia	160	SN_pr_R	Limbic
78	Pallidum_R	Basal Ganglia	161	Red_N_L	Brainstem
79	Heschl_L	Temporal	162	Red_N_R	Brainstem
80	Heschl_R	Temporal	163	LC_L	Brainstem
81	Temporal_Sup_L	Temporal	164	LC_R	Brainstem

82	Temporal_Sup_R	Temporal	165	Raphe_D	Brainstem
83	Temporal_Pole_Sup_L	Temporal	166	Raphe_M	Brainstem

2.2.3.4 Connectivity and Graph Theoretic Analysis

2.2.3.4.1 Computation of SC-FC Connectivity

Structurally constrained-functional connectivity (SC-FC) was computed by combining structural and functional connectivity matrices. Functional connectivity (FC) was calculated using Pearson's correlation coefficient between the time series of brain regions defined by the AAL3 atlas. Participant-level FC matrices were generated using time series data extracted from each parcellated region.

For the structural connectivity (SC) analysis, diffusion-weighted imaging (DWI) data were processed to derive a structural connectivity matrix based on deterministic tractography as described in Section 2.2.3. To constrain the FC data by SC, a QA threshold of 0.12 was applied to the structural connectivity matrix (using the same threshold as the original tractography analysis). This threshold was used to binarize the QA connectivity matrix, effectively excluding weak or insignificant connections. Once this binarized mask was created for each subject, it was applied to the functional connectivity matrix. This approach ensured that only the functional connections between regions with significant structural connectivity were retained for further analysis.

Once the SC-FC data was obtained for each subject, Fisher's Z transformation was applied to the Pearson's correlation coefficients to ensure valid and unbiased statistical comparisons, as Pearson's correlation is non-linear and not normally distributed. Mean differences between groups

were then computed on the Z-transformed data. The Mann-Whitney U rank sum test ($p < 0.05$) was used to determine significance, as it is a non-parametric method that allows for confident identification of significant differences, regardless of the underlying data distribution, minimizing the risk of false positives while maintaining sensitivity to true effects (McKnight & Najab, (2010)). To ensure the test assumptions were met, we verified that the degree of skewness in our data was comparable between groups. After significance testing, our data was transformed back into correlation coefficients for interpretability.

2.2.3.4.2 SC-FC Graph-Theoretic Analysis

For the undirected graph-theoretic network analysis, we applied a 95% threshold to binarize the SC-FC data, retaining the top 95% of the strongest connections. This approach was chosen to capture as much of the structural network as possible while ensuring that only valid, non-spurious connections were included.

Binarizing the network simplifies the analysis by focusing on the presence or absence of connections rather than their strength. Many recent studies discard link weights, as binary networks are, in most cases, simpler to characterize and have a more easily defined null model for statistical comparison (Rubinov & Sporns, 2010), making them more reliable for exploratory data analysis. This approach was particularly suited for examining whole-brain networks, allowing us to explore brain-wide network dynamics across many regions.

We considered both global and local graph-theoretic measures in our analysis, which were calculated using the Brain Connectivity Toolbox (BCT) (Rubinov & Sporns, 2010). Node degree and local efficiency were calculated for each AAL3 region in both gamers and non-gamers. Local efficiency reflects regional integration, measuring how effectively information is exchanged among a node's immediate neighbors if the node itself is removed. Node degree, a

local measure of centrality, reflects how many direct connections a region has to others in the network, indicating its level of participation in the SC-FC architecture. Local efficiency quantifies how effectively information is exchanged among a region's immediate neighbors if the region itself were removed, providing a measure of local network integration. These metrics were used to assess the regional properties of network nodes and to identify connectivity patterns associated with group differences.

2.2.3.4.3 Computation of SC-dFC Connectivity

Structurally constrained-directed functional connectivity (SC-dFC) was computed by combining structural and directed functional connectivity for each participant using the same ROIs of the AAL3 atlas. The dFC was calculated using time-domain Granger Causality (TGC) using the bivariate autoregressive model outlined by Dhamala *et al.* (2008, 2018). The evaluation of TGC was conducted in the frequency band in the range between f_1= 0.05 Hz to f_2 = 0.9 Hz, with a sampling rate of 1.87 Hz (TR^{-1}).

The appropriate model order for the TGC analysis was determined by minimizing the spectral difference between the Granger-generated time series and the original signal, while maintaining sensitivity to trial-specific dynamics governed by the trial duration and the repetition time (TR). To preserve this sensitivity, the model order was constrained such that it did not exceed the number of time points within a trial. The maximum allowable model order, denoted $\mathrm{mo}_{\max}$, is given by

$$\mathrm{mo}_{\max} = \frac{\mathrm{T}_{\mathrm{trial}}}{\mathrm{TR}}, \quad \text{where } \mathrm{T}_{\mathrm{trial}} \text{ is the inter-trial interval.}$$

Under this constraint, a model order of 5 was selected, as it best minimized the spectral discrepancy in the whole-brain analysis while preserving sensitivity to task-related GC

fluctuations. TGC matrices were computed between the AAL3 region time series using this model order, which served as the directed functional connectivity (dFC).

For structural connectivity (SC) analysis, diffusion-weighted imaging data were processed to derive a structural connectivity matrix using deterministic tractography. This involved q-space diffeomorphic reconstruction (QSDR) and a deterministic fiber tracking algorithm to estimate the number and strength of structural connections between each pair of brain regions.

To constrain the dFC data, a quantitative anisotropy (QA) threshold of 0.12 was applied to the SC matrix, consistent with the threshold used in the original tractography analysis. This threshold was used to binarize the QA-based connectivity matrix, excluding weak or insignificant connections. The resulting binary mask was then applied to each participant's dFC matrix, allowing only directed functional connections between structurally connected regions to be retained for further analysis.

Importantly, applying the SC mask to the dFC data yields a measure of effective connectivity, which captures the directional and causal influence one brain region exerts on another, constrained by the underlying anatomical substrate (Bajaj *et al*., 2016). Group differences were assessed using the Mann–Whitney U rank-sum test ($p < 0.05$).

2.2.3.4.4 SC-dFC Graph-Theoretic Analysis

FC is inherently symmetric, meaning that a valid connection between two nodes (A, B) implies that the same connection, with the same magnitude, exists for (B, A). In contrast, dFC is inherently asymmetric, meaning that a connection from source A to target B does not imply the same or a similar connection from B to A. This asymmetry results in dFC networks exhibiting greater variability and a sparser structure compared to FC networks.

To address this sparsity, we applied a 10% threshold to dFC, retaining only the top 10% of the strongest and most reliable directed interactions. This threshold minimized the influence of invalid or spurious connections, while preserving as many effective connections as possible. By doing so, we ensured that the global density of the SC-dFC network remained comparable to that of the SC-FC network within the same subject. This thresholding strategy aligned with our goal of maintaining as many meaningful connections as possible to accurately characterize the SC-dFC network while excluding invalid and spurious connections.

We considered both global and local graph-theoretic measures in our analysis, which were also calculated using BCT (Rubinov & Sporns, 2010). Node degree and local efficiency were calculated for each AAL3 region in both gamers and non-gamers.

2.2.3.4.5 Assessing Behavioral Relevance

To assess the behavioral relevance of brain connectivity measures and functional network properties, we used Spearman correlation to examine the association between each brain connectivity measure (SC-FC or SC-dFC) and response time (RT) in the behavioral task. The correlations were calculated for both group-level comparisons and within-group analyses.

For group comparisons, we tested for significant differences using the Mann-Whitney U rank-sum test with significance defined as $p < 0.05$ and $|r| \geq 0.2$. If a significant difference was observed, we plotted the corresponding brain-behavior correlation graph for the entire group, as well as separate graphs for each group (gamers and non-gamers) to explore within-group relationships. A positive correlation is associated with a brain measure that tracks slower response times, while a negative correlation is associated with faster response times.

This approach allowed us to identify brain regions and connectivity patterns that were significantly associated with response time differences across groups, as well as the extent to which these relationships persisted within each group.

2.2.4 Whole-Brain Analysis: rcPCA-Based ROI Selection

This section describes the analytical procedures used for data-driven, whole-brain connectivity analysis, applying a novel PCA-based ROI filtering framework across structural, functional, and directed connectivity modalities. Unless otherwise noted, data collection protocols, preprocessing steps, and atlas selection were consistent with those described in earlier sections of this dissertation.

2.2.4.1 MRI Data Acquisition

MRI acquisition parameters were identical to those detailed in Section 2.1.2, including all structural (T1 and DWI) and functional (task-based fMRI) imaging sequences. This consistency ensures comparability across modalities and chapters.

2.2.4.2 Data Collection, Scanning, and Tractography Protocols

Tractography and preprocessing procedures were consistent with those used in Chapter 4 and are detailed in Section 2.2.3.1. No changes were made to diffusion processing, streamline filtering, or tract length thresholds for the whole-brain PCA pipeline**.**

2.2.4.3 fMRI Preprocessing Pipeline

Functional preprocessing followed the same pipeline outlined in Section 2.2.3.2, including motion correction, spatial normalization, and nuisance regression. Retaining this pipeline across constrained and unconstrained analyses ensured methodological consistency.

2.2.4.4 Atlas Selection and AAL3 Parcellation

As in Chapter 4, all analyses in this chapter used the AAL3 atlas for parcellation. The rationale for this selection is discussed in Section 2.2.3.3. Maintaining the same atlas across all whole-brain analyses allowed for clear cross-modal interpretation of PCA-filtered results.

2.2.4.5 Functional Connectivity and Structure-Function Coupling

After preprocessing, functional connectivity (FC) was computed using pairwise Pearson correlations across the full set of parcellated time series obtained from the AAL3 atlas. Directed functional connectivity (dFC) was estimated using pairwise time-domain Granger causality, following the procedure described in Section 2.2.3.5.1.

To assess the degree of alignment between anatomical structure and functional signaling, structure–function coupling (SFC) metrics were computed by correlating SC matrices with both FC and dFC (Fotiadis *et al*., 2024). All matrices were aligned using the AAL3 parcellation to ensure consistency across modalities. For SFC, the coupling was computed by extracting, for each ROI pair, the corresponding values from the SC and FC matrices, then calculating the Pearson correlation across participants. This yielded region-wise SFC values reflecting the strength of association between anatomical connectivity and functional co-activation.

A similar procedure was used to compute structure–directed functional coupling (SdFC), where each participant's SC matrix was compared to their sender-mode Granger causality (dFC) matrix. Since SC is symmetric and undirected, the analysis held the row index constant to assess, for each region, the correlation between its structural substrate and its outbound directed functional influences. This yielded region-wise SdFC values that quantify how well a region's anatomical connections support its role as a functional sender.

Although both intra-regional and pairwise SdFC coupling values were initially computed, the analysis was ultimately restricted to intra-regional sender-mode values—denoted SdFC(sender). This constraint enabled a focused examination of region-specific structure–function alignment and established a foundation for future work extending beyond sender-mode dynamics.

2.2.4.6 rcPCA-Based ROI Selection

To identify the most informative ROIs across structural and functional connectivity domains, a novel data-driven principal component analysis (PCA) framework was developed for dimensionality reduction. This region-based cumulative PCA (rcPCA) method decomposes subject-level connectivity matrices into orthogonal principal components and derives regional contribution scores by quantifying each ROI's influence on the structured variance of the dataset. All analyses were implemented in MATLAB using custom scripts developed for this study.

This approach adapts standard PCA protocols and interpretation strategies widely used in neuroimaging, emphasizing high-loading features within each component to enable principled ROI selection and structured dimensionality reduction without sacrificing interpretability. To prioritize meaningful contributors and minimize noise, we capped contribution accumulation at the top 20 ROIs per component. This cap avoids rank dilution from low-weight contributors, enhances interpretability, and emphasizes regions that consistently explain variance across components.

For undirected connectivity data such as FC, diagonal elements from each participant's 166 × 166 ROI-wise matrix and reshaped the resulting 3D array into a two-dimensional matrix of

size n × E, where n is the number of subjects and E is the number of unique off-diagonal connections between ROIs. This matrix reshaping was handled by the script undirected_pca_analysis.m. This script then calls a custom function *run_pca.m* that uses MATLAB's built-in *pca()* function, which performs singular value decomposition (Wall, 2002) on a mean-centered data matrix of size n × E. This function returns the component loadings, subject scores, and variance explained by each principal component. ROI-level contributions were used to interpret latent components, while subject-level scores served as PCA-derived features for potential classifier enrichment.

Finally, the ROI contributions were identified for each component by summing the absolute values of the PCA loadings associated with each region. For connectivity-wise decompositions (*e.g.,* FC), loadings were reshaped into full ROI × ROI matrices with NaNs along the diagonal to exclude self-connections. The sum of absolute values across each row yielded a scalar contribution score per region, reflecting how strongly a given ROI influenced the variance captured by that component. For ROI-wise decompositions (*e.g.,* structure–function coupling), each coefficient directly corresponded to a region, and the absolute values were taken as contribution scores. ROIs were ranked in descending order for each component and saved for downstream analysis.

The script *undirected_pca_roi_contributions.m* was used to compute each region's cumulative contribution to the explained variance. This script sets the number of top pca rois, the cumulative explained variance percentage, and calls the custom function *pca_roi_contributions.m,* which calculates the cumulative contribution of each roi to the user's desired explained variance threshold, which we set to 80% using a weighted sum set by the weights of each PC.

By capturing 80% of the total variance across components, we retain the dominant patterns in the data that are most likely to reflect a structured signal rather than noise, while discarding components that account for only a small portion of the variance, which may be less interpretable and more sensitive to measurement error. This threshold also stabilizes the ranking of contributing ROIs across modalities and ensures that our contribution scores are derived from a meaningful, high-variance subspace rather than dominated by noisy low-variance dimensions.

This procedure was carried out not only for FC, but also for all 13 categorically distinct SC measures, organized in Table 2.3, as well as for all 13 SFC and 13 SdFC (sender) coupling matrices, using the same run_pca.m script and ROI contribution framework. Additional technical descriptions of these diffusion MRI measures are available in the DSI Studio documentation provided by Dr. Fang-Cheng Yeh (Yeh, n.d.-a; Yeh, n.d.-b). Each analysis followed the same pipeline: data reshaping, PCA decomposition, ROI-wise contribution scoring, and cumulative variance weighting, providing a unified approach to data-driven region selection across modalities.

Table 2.3 Structural connectivity (SC) measures and definitions reflecting standard interpretations of diffusion and tractography measures from DSI Studio

SC Measure	Description
Axial Diffusivity (AD)	Diffusion along the primary fiber axis; reflects axonal integrity.
Count	Raw number of tractography streamlines between regions.
Fractional Anisotropy (FA)	Degree of directional water diffusion; higher values indicate organized fiber structure, broadly linked to myelination.
Isotropy (ISO)	Uniformity of diffusion in all directions
Mean Diffusivity (MD)	Average diffusion in all directions; reflects overall water mobility.
Mean Length	Average length of streamlines between ROIs
None-Restricted Diffusion Imaging (NRDI)	Measures extracellular diffusion; sensitive to edema or extracellular space.
Normalized Count (Ncount)	Streamline count adjusted for ROI size and distance.
Normalized Count (Inverse-Length Weighted) (Ncount2)	Streamline count weighted by inverse length; emphasizes shorter, potentially more reliable tracts.
Normalized Quantitative Anisotropy (NQA)	Tracks the anisotropy of the principal fiber direction, normalized to background noise.
Quantitative Anisotropy) QA	Signal intensity along the principal fiber orientation; related to tract integrity.
Radial Diffusivity (RD)	Diffusion perpendicular to the main axis; associated with myelin integrity.
Restricted Diffusion Imaging (RDI)	Estimates intracellular diffusion; linked to axonal density

For directed connectivity data, such as Granger-causal (dFC) matrices, a parallel pipeline was developed using the scripts *directed_pca_analysis.m* and *run_dpca.m.* Since directed matrices represent asymmetric interactions between regions from sender to receiver, we performed rcPCA separately for the sender, receiver, and total connectivity modes. Directed connectivity matrices are square (N × N), where each element represents the strength of influence from a sender region to a receiver region. A companion script to

pca_roi_contributions.m, titled *directed_roi_contributions_dpca.m*, was created to compute cumulative contributions in sender, receiver, and total modes. For each region, cumulative sender influence was calculated by holding the row index constant and summing across columns, whereas cumulative receiver influence was computed by holding the column index constant and summing across rows. Total contributions were computed by summing each region's sender and receiver values, followed by normalization. These direction-specific contributions were then used to rank ROIs according to their influence in the structured variance of the directed connectivity data.

All outputs, including PCA loadings, explained variance, region rankings, and component-wise visualizations, were saved for each participant group and connectivity modality. In addition, the top ROIs, their corresponding AAL3 region labels, and all cumulative ROI contribution scores were saved to support downstream interpretation and reproducibility. After confirming the internal validity of our approach by comparing PCA-derived region rankings to raw variance rankings within each connectivity measure, these results were used in downstream analyses to identify high-variance ROIs for group comparisons and behavioral correlation testing.

Overall, this PCA-based ROI selection framework offered a principled and scalable strategy for prioritizing informative brain regions in high-dimensional neuroimaging data. By reducing noise and redundancy while preserving structured variability, the method improves sensitivity to behaviorally relevant effects and significantly lowers the burden of multiple comparisons.

2.2.4.7 Validation of rcPCA-Derived Region Rankings

To evaluate the internal consistency and robustness of rcPCA, a multi-pronged validation was developed to test the derived regional rankings compared to the raw variance using a

combination of rank correlation, permutation testing, and hypergeometric overlap statistics using a significance threshold of $p < 0.001$. This procedure was implemented in the script *validate_pca_variance.m* and carried out separately for each modality, including FC, dFC, SC, SFC, and SdFC(sender).

First, the regions were ranked according to their raw pre-PCA variance. This ranking was then compared to PCA-derived rankings using Spearman's rank correlation across a range of top-k values, from 2 up to 166, reflecting the full resolution of the AAL3 parcellation. These tests provided converging evidence that the region-based cumulative PCA (rcPCA) method reliably identifies regions based on structured variance patterns, supporting the method's selectivity and stability across modalities. The choice of k = 20 offered a practical compromise, large enough to capture meaningful connectivity patterns while remaining selective enough to highlight informative ROIs.

In the Spearman analysis, we calculated rank correlation coefficients between the top-k PCA-derived ROIs and the top-k raw-variance ROIs at each k. This approach was chosen for its robustness to non-normal distributions and its sensitivity to monotonic relationships. The correlation coefficient was calculated as

$$\rho = \frac{cov(\text{ ranks }_{raw}, \text{ranks}_{PCA})}{\sigma_{\text{ranks,raw}}\, \sigma_{\text{ranks,PCA}}},$$

where ranks $_{\text{raw}}$ are the ranks of the raw data, $r$anks $_{\text{PCA}}$ are the ranks of regions based on the cumulative PCA-derived variance contributions, cov is the covariance between two ranked vectors and σ is the standard deviation of ranks. The correlation was computed in MATLAB using the *corr()* function with the 'Type', 'Spearman' option, which is given by

$$[\rho_{\text{k}}, p_k] = \text{corr}(rank_{raw}\_k,\ ran\text{k}_{\text{PCA}}\_\text{k}, 'Type', 'Spearman').$$

To assess whether the number of overlapping ROIs between the top-k PCA-selected and raw variance-selected regions could be attributed to chance, we used the cumulative distribution function of the hypergeometric distribution. This distribution models the probability of x or more successes (i.e., overlapping ROIs) when drawing two sets of size k from a population of N=166 ROIs without replacement. The probability of observing at least x overlaps under the null hypothesis of random selection is given by the standard expression for hypergeometric p-value

$$p_{\text{hyper}}(x) = 1 - \sum_{i=0}^{x-1} \frac{\binom{k}{i}\binom{N-k}{k-i}}{\binom{N}{k}}$$

where N is the total number of ROIs (166), k is the number of top-ranked ROIs selected in each set, and x is the observed number of overlapping ROIs between the PCA-based and raw variance-based rankings. This computation was implemented in MATLAB using the built-in hygecdf function and is given by (p_hyper = 1 - hygecdf(x - 1, N, k, k)).

Finally, a null distribution of random overlap values was generated by permuting the raw variance ROI rankings 10,000 times. For each value of k, the top-k ROIs were selected from each permutation, and their overlap with the PCA-selected top-k ROIs, denoted as x, was recorded. The empirical p-value was then computed as the proportion of permutations in which the number of overlapping ROIs was greater than or equal to x, relative to the total number of permutations

$$p_{\text{perm}} = \frac{\#\text{ of null overlaps } \geq x}{\text{num\_permutations}}$$

and the equivalent MATLAB statement used for this calculation is given by (perm_pvals(i) = mean(rand_overlaps >= overlap_counts(i))). This allowed us to assess whether the observed overlap between PCA-selected and raw variance-based regions exceeded what would be expected by chance.

All results, including overlap counts, p-values (Spearman, hypergeometric, and permutation), and rank correlations, were logged and plotted across k-values. Summary figures included correlation curves and significance levels as a function of k, bar plots comparing top-k PCA- and raw-variance ROI values, and permutation histograms and hypergeometric threshold overlays for observed overlap

Across all modalities, hypergeometric and permutation tests yielded exceptionally low p-values, often well below the $p < 0.001$ threshold. At higher values of k, both tests frequently reached the limits of machine precision. In such cases, MATLAB returned literal zero values due to numerical underflow, requiring the imposition of a floor at p = 1e-15. This indicated that the observed overlaps were so unlikely under the null distribution that their probabilities could not be accurately represented in double-precision floating-point arithmetic.

This provides compelling evidence that the overlap between PCA-derived and raw-variance ROI rankings was highly unlikely to occur by chance. They further validate the selectivity, robustness, and internal consistency of the proposed method.

Notably, using cumulative contributions across all ROIs before selecting the top 20 restored the Spearman rank significance that was lost in the dFC receiver, SC, SFC, and SdFC modalities when only the top 20 ROIs per component were used during accumulation.

These validation results confirmed that PCA-selected ROIs consistently overlapped with high-variance regions across modalities, supporting the interpretability, reproducibility, and robustness of the rcPCA selection method. For final visualizations, we used ‘n’ in place of ‘k’ to denote the number of top-ranked ROIs, as it provided a clear and intuitive shorthand in contexts where there was no conflicting N variable.

Furthermore, full convergence of PCA-derived ROI rankings with raw variance rankings, across all validation metrics, was observed within the range of k=100-150. This included Spearman correlations approaching unity, permutation-based p-values below machine-level significance ($p < 1e\text{-}15$), and hypergeometric overlaps exceeding chance across all thresholds. Isotropy was the last measure to show full convergence, but did so by k = 90, making the k = 100-150 range a conservative benchmark for achieving maximal rank agreement. This defines a convergence ceiling for PCA-based variance decomposition in whole-brain neuroimaging data for the AAL3 atlas. The observed convergence window likely reflects the resolution of the AAL3 atlas's 166 ROIs. While this range defines full convergence for this specific parcellation, the maximum k required for machine-level agreement is expected to scale proportionally with atlas dimensionality.

Another observation was that the permutation-based p-values exhibited a characteristic rebound at high k values (e.g., $k \geq 160$), as the overlap between random samples and observed sets approached the full ROI space. This behavior reflects the design of permutation tests, which become less discriminative as sampling exhausts the comparison space. This plateau confirms that p-value inflation near the maximum ROI count is an expected property of null model behavior due to sampling saturation.

Together, these results confirm that the PCA-based ROI selection framework reliably identifies regions that meaningfully contribute to structured variance across modalities. The strong convergence across multiple statistical tests affirms that top-ranked ROIs are not artifacts of random variation, but rather reflect well-founded, mathematically principled selection criteria. In short, the method behaved exactly as intended, yielding high-variance-contributing, interpretable ROI candidates for downstream analysis.

2.2.4.8 Group Comparisons and Brain–Behavior Relationships (rcPCA-Derived ROIs)

To investigate group-level differences and the behavioral relevance of connectivity across modalities, we used the top 20 PCA-derived ROIs from each modality-specific decomposition as filters. We applied this procedure to FC, dFC (sender, receiver, and total modes), SC, SFC, and SdFC(sender). For each modality, we extracted submatrices containing any connection that involved a top-ranked ROI. These filtered matrices were then analyzed to compare gamers and non-gamers and to examine correlations between brain connectivity and response time.

False discovery rate (FDR) correction was applied independently within each connectivity modality to account for multiple comparisons during group comparisons. Two standard approaches were considered: the Storey-Tibshirani (ST) method(Storey & Tibshirani, 2003) (which estimates the proportion of true null hypotheses, π_0) and the Benjamini–Hochberg (BH) procedure(Benjamini & Hochberg, 1995) (which ranks p-values and applies a fixed step-up threshold). The choice between them was guided by both observed performance and the underlying assumptions of each method.

The ST method was deemed valid for FC data only. In all FC comparisons, the estimated q-values remained consistently less than or equal to the corresponding uncorrected p-values, indicating that the proportion of true nulls could be reliably estimated and that the method behaved as expected. These results suggest that Storey's assumptions were met for FC, likely due to the dense, symmetric, and continuous nature of FC matrices, along with their relatively uniform distribution of connectivity values.

In contrast, the ST method was not reliable for the other modalities. In SC, dFC, and coupling metrics, q-values were frequently observed to fall below their corresponding p-values despite p-values being well above the uncorrected significance threshold, a pattern inconsistent

with valid FDR correction. This behavior indicated instability in π_0 estimation, likely due to skewed or zero-inflated distributions, sparse matrices, and directional asymmetries, which are conditions known to violate the assumptions behind Storey's estimator.

To ensure robust and conservative control of false discoveries in these cases, the BH procedure was applied instead. BH does not rely on π_0 estimation and is more stable under non-ideal conditions. It was, therefore, used for dFC, SC, SFC, SdFC(sender) coupling, and dFC variants, where structural constraints or directional signal flow introduced potential sources of bias. For brain-behavior correlations, we computed Spearman correlations between response time and connectivity values for all connections involving the top 20 PCA-derived ROIs per modality. These correlations were tested with a significance threshold of $\alpha = 0.05$, and results were further filtered using an effect size threshold of $|r| \geq 0.2$ to ensure robustness and interpretability.

3 BRAIN NETWORK ANALYSIS: THE VISUAL STREAMS

This chapter investigates how long-term action video game (AVG) play influences functional and structural connectivity within the brain's visual processing networks, focusing specifically on the dorsal ("where/how") and ventral ("what") streams. These two visual pathways support essential components of visual cognition, including spatial attention, object recognition, perceptual decision-making, and visuomotor integration (Mishkin *et al*., 1983; Goodale & Milner, 1992; Kravitz *et al*., 2011). Since AVGs involve complex cognitive, perceptual, and motor demands, these pathways represent ideal targets for studying neuroplastic adaptation in response to sustained visuomotor training.

Neuroplasticity refers to the brain's capacity to reorganize its structure and function in response to experience. In the context of video game play, repeated exposure to challenging tasks has been associated with improvements in attention, object tracking, visual search, distractor filtering, and sensorimotor decision-making (Green & Bavelier, 2003, 2007, 2015; Dye *et al*., 2009; Powers *et al*., 2013). These behavioral gains are accompanied by differences in brain structure and function, as observed through neuroimaging studies of visuospatial and motor systems (Basak *et al*., 2011; Brilliant *et al*., 2019; Kühn & Gallinat, 2014; Palaus *et al*., 2017).

However, few studies have collected both structural and functional MRI data from the same participants, and even fewer have linked these neural findings to individual differences in behavior. As a result, it remains unclear whether imaging-based biomarkers of connectivity can reliably predict behavioral outcomes or whether structural and functional measures provide complementary explanatory value.

To address this gap, we used a multimodal approach focused on anatomically defined regions within the dorsal and ventral streams. Specifically, functional connectivity (FC), directed functional connectivity using time-domain Granger causality (TGC), and structural connectivity based on diffusion MRI measures, including fractional anisotropy (FA) and quantitative anisotropy (QA). Our primary goal is to test whether gamers show enhanced connectivity within visual stream networks and whether these connectivity patterns relate to behavior during a visuomotor decision-making task.

The dorsal stream projects from early visual areas to the parietal cortex and supports spatial localization and motion tracking, while the ventral stream projects to temporal regions and supports object recognition (Goodale & Milner, 1992; Micheletti *et al*., 2021). These pathways are jointly involved in fast, accurate decision-making and are well-positioned to undergo plastic changes in response to the demands of AVG play. Using a region-based analysis grounded in anatomical specificity, we examine whether long-term gaming experience leads to strengthened communication between visual stream nodes and whether such patterns predict faster response times.

In addition to white matter connectivity, grey matter adaptations have also been reported in regions associated with visuospatial attention, memory, and motor planning. Studies have shown cortical thickening and increased grey matter volume in these areas among gamers (Kühn & Gallinat, 2014; Hyun *et al.,* 2013). To contextualize our investigation within this broader literature, we incorporate grey matter morphometric data provided by Chandrama Mukherjee (Georgia State University, under the supervision of Dr. Mukesh Dhamala). This additional

analysis offers insight into structural plasticity, since neuroplasticity occurs across both white and grey matter.

This chapter builds directly on prior work demonstrating that gamers exhibit significantly faster response times, approximately 190 milliseconds faster, without compromising accuracy, as detailed in Section 2.2.1. Based on this foundation, we test two key hypotheses. First, we predict that both functional and structural connectivity within the visual streams may undergo neuroplastic enhancement due to prolonged AVG play. Second, we hypothesize that these connectivity differences are behaviorally relevant and correlate with improved performance in visuomotor decision-making. Together, these findings would provide evidence that action video games shape brain network architecture in ways that enhance visual processing in contexts requiring rapid motor responses.

3.1 Results

3.1.1 Structural Effects

3.1.1.1 Grey Matter Differences Between Gamers and Non-Gamers

A significant group difference in cortical thickness was found using a one-way ANOVA, $F(2, 41) = 19.828$, $p = 0.049$, $\eta p^2 = 0.998$. The F-statistic reflects the ratio of variance between groups to variance within groups, and ηp^2 (partial eta squared) indicates the proportion of variance in cortical thickness explained by group membership. All reported p-values were Bonferroni-corrected for multiple comparisons across 70 regions of interest (ROIs) to reduce the risk of false positives. The most robust group differences between video game players (VGPs), *i.e.,* gamers, and non-video game players (NVGP), *i.e.,* non-gamers, were observed in the right inferior parietal lobule, precuneus, superior parietal lobule, and supramarginal gyrus, as shown in Figures 3.1 and

3.2. The results depict a significant difference in cortical thickness between video game players (VGP) and non-video game players (NVGP). The four regions, namely right inferior parietal, right precuneus, right superior parietal, and right supramarginal, had the strongest differences.

Table 3.1 Group differences in cortical thickness of right parietal ROIs based on one-way ANOVA (df = 1, 42), with Bonferroni-corrected *p*-values. Reported *F*-values indicate test strength; partial eta squared (ηp^2) values reflect effect sizes

Identified regions (Thickness)	***p***	η_p^2	***F(1,42)***
Right inferior parietal	0.006	0.169	8.521
Right precuneus	0.002	0.210	11.154
Right postcentral	0.055	0.085	3.902
Right superior parietal	0.021	0.121	5.779
Right supramarginal	0.010	0.148	7.293

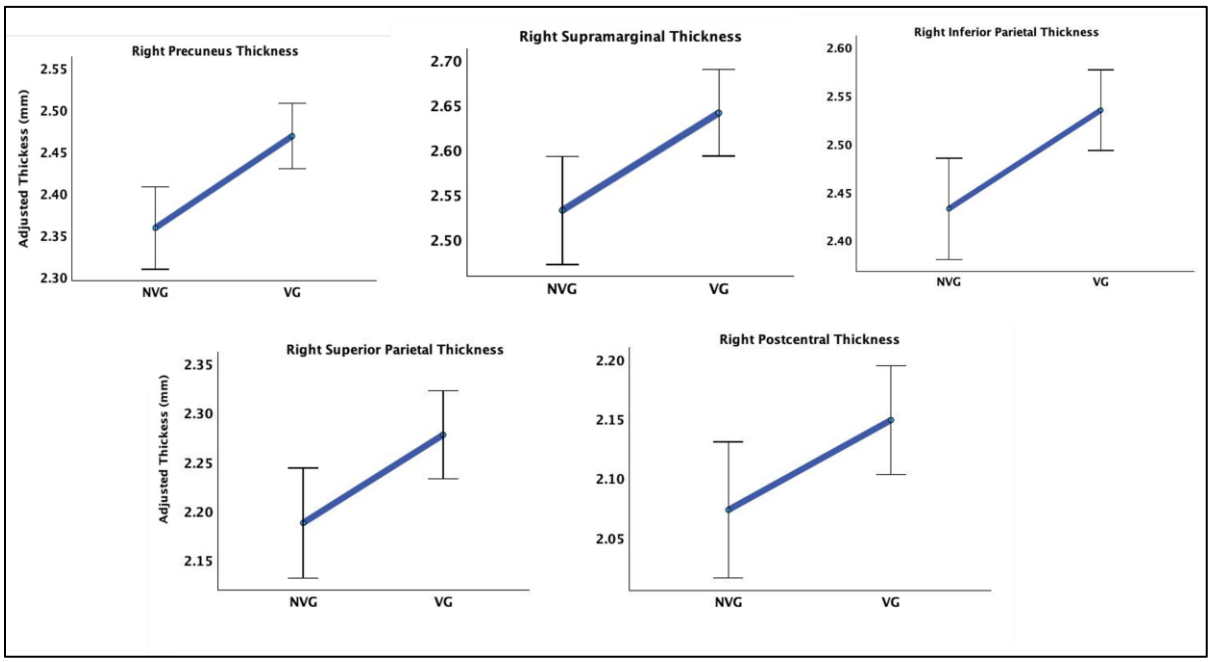

Figure 3.1 Gamers (VGP), exhibited significantly greater grey matter thickness than non-gamers (NVGP) in four right parietal regions: inferior parietal lobule, precuneus, superior parietal lobule, and supramarginal gyrus (Bonferroni-corrected $p < 0.05$). The right postcentral gyrus showed a borderline effect ($p = 0.055$, Bonferroni-corrected).

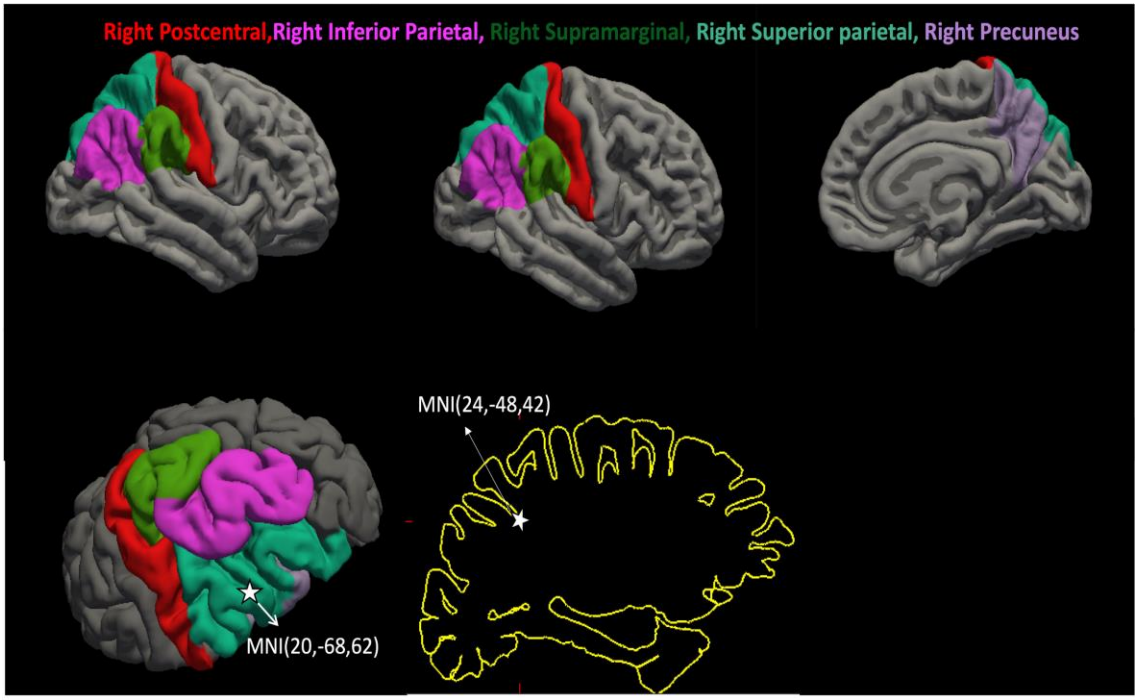

Figure 3.2 Grey Matter 3D Rendering of Group Differences. Non-Gamers (NVGP), and gamers (VGP), showed significant differences in grey matter thickness in parietal regions, specifically the right inferior parietal, right precuneus, right superior parietal, and right supramarginal areas.

3.1.1.2 White Matter Integrity

The statistical comparison of structural connectivity measures, specifically fractional anisotropy and quantitative anisotropy, between gamers and non-gamers utilized the Wilcoxon rank-sum test. Multiple comparisons were corrected using the Holm-Bonferroni method indicated by p^* (Holm, 1979). In this analysis, gamers exhibited elevated FA values between the L SOG and the L IPL ($p^* = 0.024$). Gamers also demonstrated elevated QA values between the same regions (L SOG and L IPL) with statistical significance ($p^* = 0.039$). In addition to the observed elevation in FA and QA values within the left dorsal stream, notably between L SOG and L IPL, our investigation revealed heightened QA values in the right dorsal stream as well. Specifically, gamers exhibited increased QA R SOG and the R SPL ($p^* = 0.036$), as well as between R SOG and the R IPL ($p = 0.047$). The increased QA between R SOG and R IPL did not survive multiple comparison corrections but remained significant at the individual level, warranting consideration for further study. To visually illustrate the significant differences in values between gamers and non-gamers, violin plots were constructed as shown in Figures 3.3-3.5. Structural connectivity measures, FA and QA, did not show a significant correlation with participants' response time.

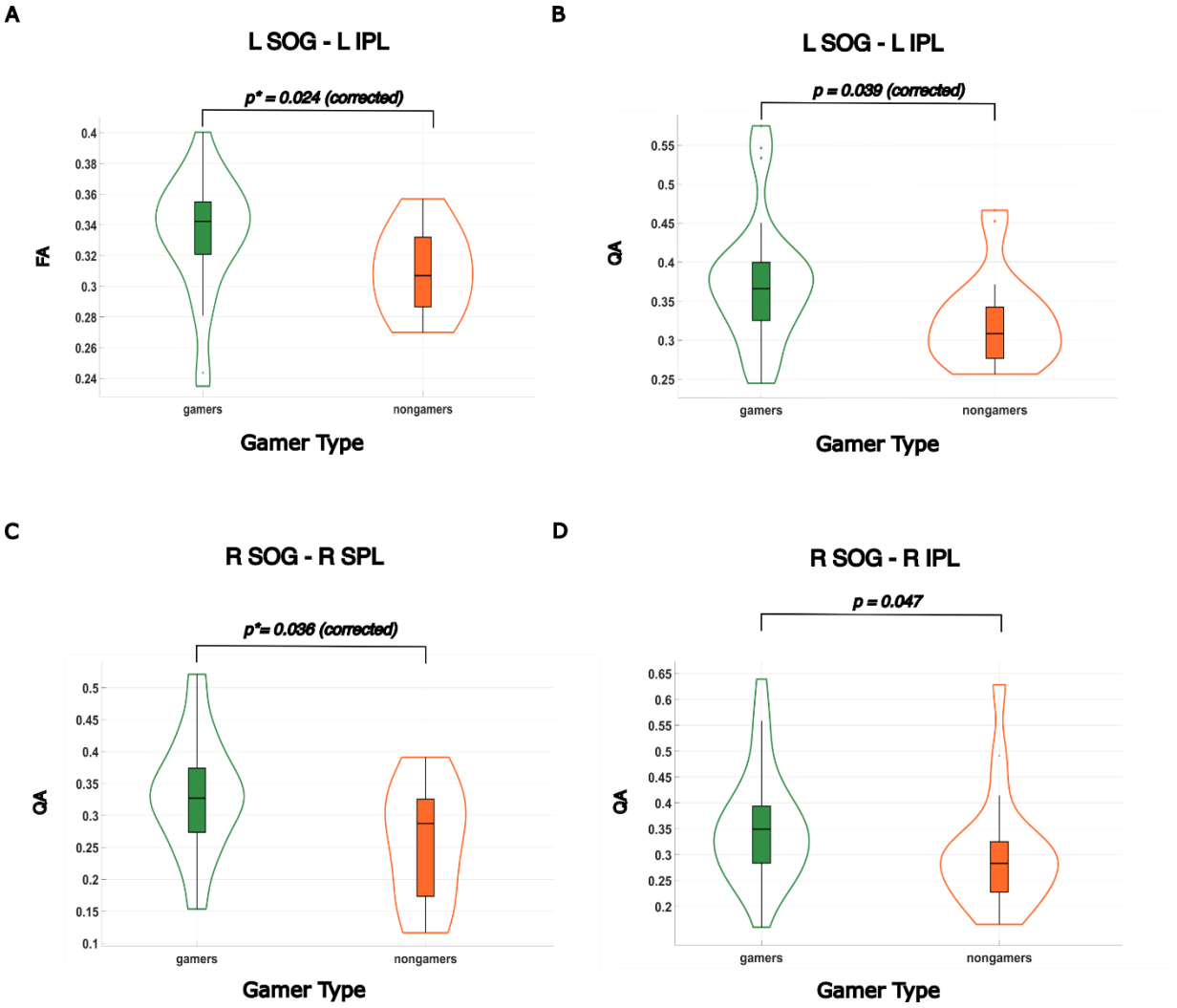

Figure 3.3 Structural Connectivity in the Dorsal Stream is Elevated in Gamers. (A) Gamers exhibited significantly higher fractional anisotropy (FA) between the left superior occipital gyrus (L SOG) and the left inferior parietal lobule (L IPL) ($p^* = 0.024$).
(B) Gamers showed significantly higher quantitative anisotropy (QA) between the L SOG and L IPL ($p^* = 0.039$). (C) Higher QA values were observed in gamers between the right superior occipital gyrus (R SOG) and the right superior parietal lobule (R SPL) ($p^* = 0.036$).
(D) A trend-level increase in QA was also observed between the R SOG and the right inferior parietal lobule (R IPL), though this did not survive Holm-Bonferroni correction ($p = 0.047$).

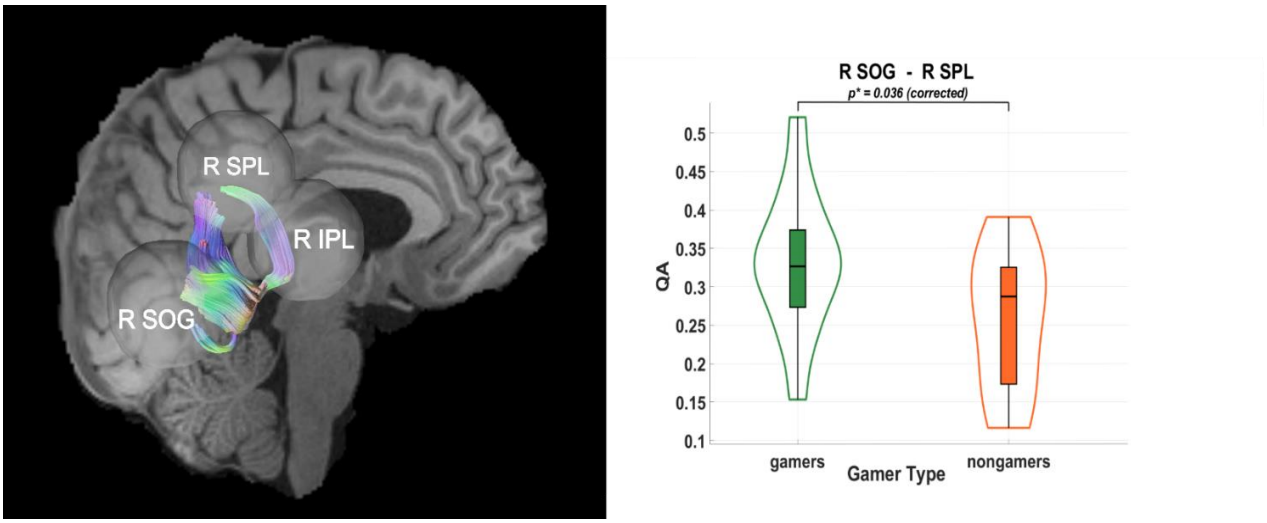

Figure 3.4. Right Dorsal Stream Connectivity Differences Between Groups. (Left) Tractography visualization in a representative subject showing white matter connections between the right superior occipital gyrus (R SOG), right superior parietal lobule (R SPL), and right inferior parietal lobule (R IPL). The X-axis is coded for red from right to left, the Y-axis is coded for green from anterior to posterior, and the Z-axis is coded for blue from superior to inferior. (Right) Group differences in quantitative anisotropy (QA) for the R SOG–R SPL connection, with significantly higher QA values observed in video game players (VGPs) compared to non-video game players (NVGPs) ($p^* = 0.036$).

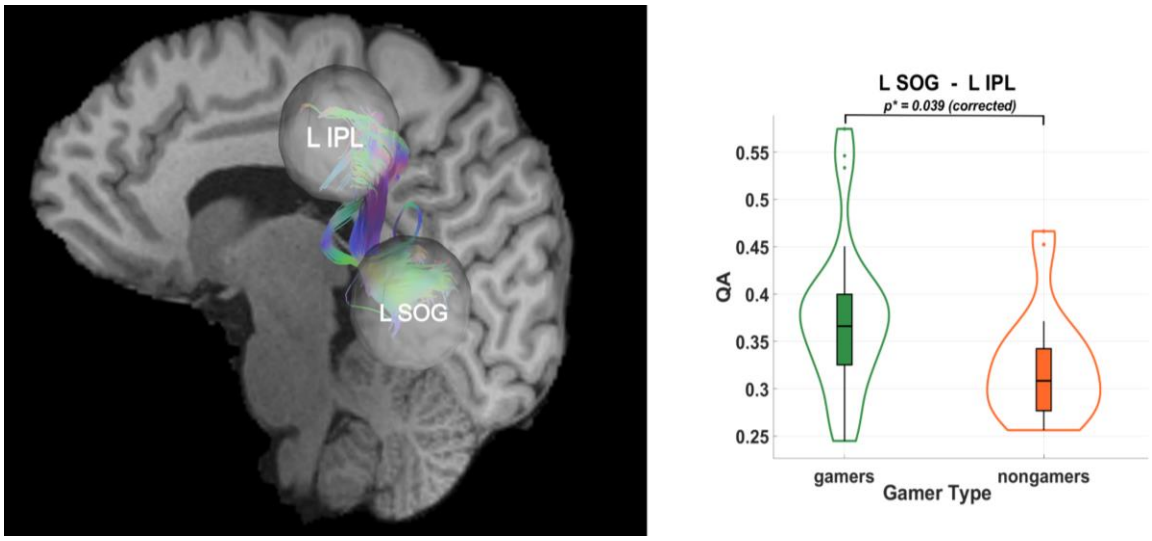

Figure 3.5 Tractography Visualization and Group Differences in Left SOG–IPL Connectivity. (Left) Tractography in a representative subject showing white matter connections between the left superior occipital gyrus (L SOG) and the left inferior parietal lobule (L IPL). Diffusion directions are color-coded: red for right–left (X-axis), green for anterior–posterior (Y-axis), and blue for superior–inferior (Z-axis). (Right) Group differences in quantitative anisotropy (QA) for the L SOG–L IPL connection, with significantly higher QA observed in gamers compared to non-gamers ($p^* = 0.039$).

3.1.2 Functional Connectivity

3.1.2.1 Undirected Functional Connectivity

Pairwise Pearson correlation was used to compute undirected functional connectivity (FC). Statistical comparison between video gamers and non-gamers was conducted using the Wilcoxon rank-sum test. Gamers exhibited significantly higher FC between the left superior occipital gyrus (L SOG) and the left superior parietal lobule (L SPL). This result survived Holm–Bonferroni correction for multiple comparisons across the four dorsal stream ROI connections and remained statistically significant ($p^* = 0.042$). A violin plot illustrating this group difference is shown in Figure 3.6A. FC values were also plotted against response time (RT), and Spearman correlation was computed to assess the brain–behavior relationship. As shown in Figure 3.6B, FC was moderately and significantly correlated with RT ($r = –0.41$, $p^* = 0.026$).

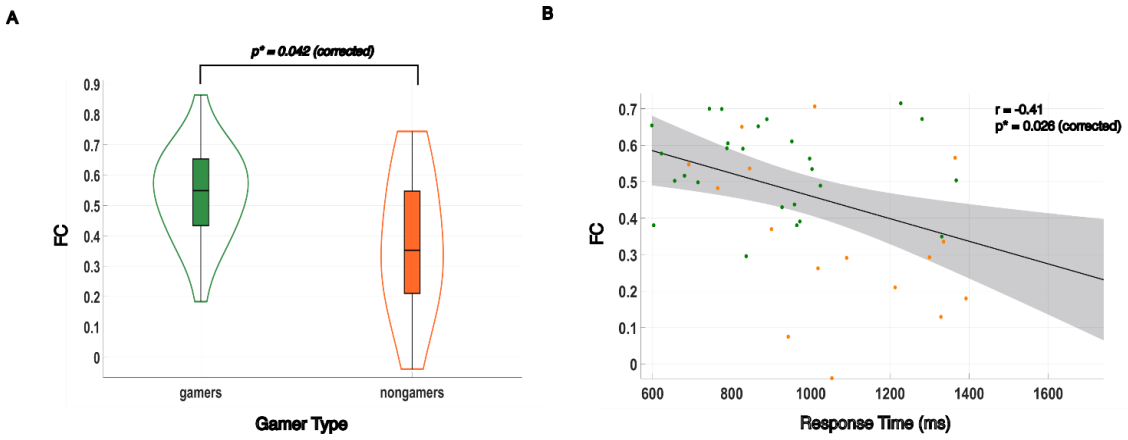

Figure 3.6. Left SOG–SPL Functional Connectivity. **(**A) Gamers exhibited significantly stronger undirected functional connectivity between the left superior occipital gyrus (SOG) and left superior parietal lobule (SPL) ($p^* = 0.042$, Holm–Bonferroni corrected). (B) A significant negative Spearman correlation was found between functional connectivity and response time ($r = –0.41$, $p^* = 0.026$). Green dots represent gamers; orange dots represent non-gamers.

3.1.2.2 Directed Functional Connectivity

Directed connectivity analysis was performed using pairwise Granger causality to assess directional influences along the visual streams. A range of model orders was tested by minimizing the total spectral difference between the Granger-generated time series and the original signal. The optimal model order for this dataset was determined to be six. Time-domain Granger causality (TGC) was then computed for all pairwise connections across participants. When comparing gamers to non-gamers, elevated TGC values were observed between the left superior occipital gyrus (L SOG) and the left superior parietal lobule (L SPL), with an uncorrected p-value of 0.044. This group difference is visually represented in Figure 3.7 using a violin plot. To explore brain–behavior relationships, TGC values were plotted against response time (RT), and a Spearman correlation was computed. As shown in Figure 3.7B, TGC exhibited a significant moderate negative correlation with RT ($r = –0.45$, $p^* = 0.01$), indicating that stronger directed connectivity between L SOG and L SPL is associated with faster responses.

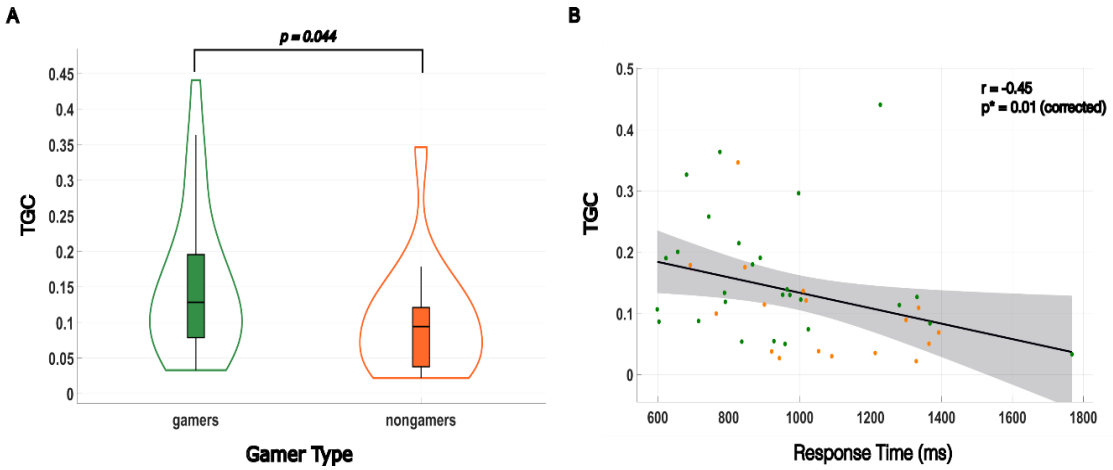

Figure 3.7. Directed Functional Connectivity L SOG → L SPL. (A) Gamers showed significantly higher TGC (time-lagged Granger causality) values between the left superior occipital gyrus (L SOG) and the left superior parietal lobule (L SPL) ($p = 0.044$, uncorrected). (B) A significant negative Spearman correlation was observed between TGC and response time ($r = –0.45$, $p = 0.01$), indicating that stronger directed connectivity predicted faster responses. Gamers are shown in green; non-gamers are shown in orange.

3.2 Discussion of Findings and Interpretation

This study investigated structural and functional connectivity differences between gamers and non-gamers within the dorsal and ventral visual streams. Structural analyses revealed increased white matter integrity in gamers, particularly within the dorsal stream. Elevated FA and QA values in connections involving the superior occipital gyrus and inferior parietal lobule suggest enhanced fiber tract organization, potentially indicating greater directional coherence between regions involved in visuospatial integration. However, these structural differences did not correlate with response time (RT).

Functional connectivity analyses revealed greater connectivity between key dorsal stream regions in gamers, especially between the left superior occipital gyrus and left superior parietal

lobule. Both FC and TGC values were moderately correlated with faster RT, suggesting that dynamic coordination within these visuomotor pathways contributes meaningfully to behavioral performance. Although TGC results did not survive correction for multiple comparisons, the directional information they provide offers important insight into altered information flow in gamers and warrants further investigation.

Additional analyses revealed increased cortical thickness in right parietal regions among gamers, including the IPL, SPL, precuneus, and supramarginal gyrus—areas associated with spatial attention, action planning, and visuomotor coordination. These findings align with previous work by (Kühn & Gallinat, 2014; Kühn, Gleich, *et al.,* 2014), which demonstrated that video game training can lead to increased gray matter volume in prefrontal and parietal cortices. However, while cortical thickening may reflect long-term use-dependent plasticity, it did not predict performance in this rapid decision-making task. Similarly, white matter integrity, as measured by FA and QA, was not significantly associated with RT. This dissociation suggests that although structural properties such as gray and white matter may reflect the brain's capacity for neural signal transmission, real-time performance may depend more directly on dynamic functional coordination.

The absence of a correlation between FA and QA in visual streams with RT further supports the notion that functional integration plays a critical role in driving behavioral outcomes. Functional connections are inherently more flexible and dynamically reconfigurable in response to task demands, making them better suited to support time-sensitive processing adaptively. In contrast, white matter provides the structural scaffolding for signal transmission,

but this alone does not account for the moment-to-moment routing required for efficient visuomotor transformations.

The enhanced functional connectivity observed in the left dorsal stream reflects a CRR-driven adaptation, in which prolonged task engagement, such as that experienced during sustained action video game play, leads to cognitive resource reallocation that promotes localized refinement supporting more efficient integration and processing of visuomotor information. This adaptation is especially relevant in the context of action video games, where rapid and successive visuomotor decisions are required throughout gameplay. Such reallocation likely reduces cognitive friction, facilitating low-latency decision-making through more functionally connected visuomotor pathways.

3.2.1 **Concluding Remarks**

This study provides strong evidence that long-term action video game play could plausibly induce a neuroplastic refinement within visuospatial and sensorimotor networks, particularly in the dorsal stream and right parietal cortex. Gamers showed increased white matter integrity and cortical thickness in key visuospatial regions, along with enhanced FC within the dorsal visual stream, specifically between L SOG and L SPL. The functional measures, FC and TGC, were moderately correlated with faster response times, highlighting the importance of functional integration in supporting rapid visuomotor decision-making. Although the study was completed before the formal development of CRR, the findings align directly with its core premise that when task engagement induces cognitive strain, it triggers a redistribution of neural resources toward behaviorally relevant circuits**.**

In this light, enhanced dorsal stream connectivity in gamers reflects not just reinforcement through use but a dynamic adaptation shaped by task demands. The lack of correlation between structural measures and response time supports this view, suggesting that while white matter and cortical thickness provide scaffolding, it is functional integration that is more associated with real-time performance.

CRR accounts for this distinction by predicting that long-term adaptations emerge in networks exposed to high cognitive load, which match the demands of rapid visuomotor decision-making in action video games. In sum, the results of this chapter offer converging structural and functional evidence for experience-driven plasticity in task-relevant systems. They retrospectively validate CRR's logic and show how regionally focused connectivity analyses can uncover the neural basis of behavioral adaptation in high-performance environments.

4 WHOLE-BRAIN ANALYSIS: TRACTOGRAPHY CONSTRAINED FUNCTIONAL AND DIRECTED CONNECTIVITY

Within the context of video game–based neuroimaging studies, relatively few have integrated both structural and functional MRI data within a unified analysis; fewer still have done so in healthy, non-addicted gamers (Bediou *et al.,* 2023; Brilliant *et al.,* 2019; Kühn *et al.,* 2019; Palaus *et al.,* 2017). Moreover, while neuroimaging evidence strongly supports widespread plasticity in gamers, many of these studies lack behavioral validation via direct cognitive assessments, making it difficult to determine which connectivity differences translate into measurable cognitive advantages (Brilliant *et al*., 2019). As a result, the relationship between specific neural adaptations and behavioral performance remains an open question, particularly in how functional network coordination operates within the fundamental constraint that rapid interregional communication is gated by white matter anatomy (Filley & Fields, 2016).

This chapter investigates how long-term action video game play impacts both functional and structural connectivity within anatomically plausible white matter pathways. While mechanisms of neuroplasticity, such as Hebbian plasticity, long-term potentiation, synaptic pruning, neurogenesis, and myelination, have been studied extensively at the mesoscale (Puderbaugh & Emmady, 2024), a unifying framework that links these processes to large-scale adaptations remains elusive.

To address this gap, Cognitive Resource Reallocation (CRR) is introduced as a candidate explanatory principle for how mesoscale neuroplasticity gives rise to large-scale, experience-driven changes in network dynamics. CRR is defined as the dynamic redistribution of metabolic and functional resources toward behaviorally relevant, anatomically plausible circuits in response to strenuous cognitive demands. Within the context of action video games (AVGs),

CRR promotes the progressive optimization of neural systems in response to sustained cognitive strain, as imposed by challenging, sensory-rich environments characteristic of AVGs.

Over time, sustained engagement with AVGs may establish a baseline level of visuomotor efficiency, driving adaptive refinement of cognitive functions that support enhanced visuomotor decision-making such as visual processing (Churchland & Shadlen, 2009; Goodale *et al.,* 1991; Green & Bavelier, 2007), visuomotor integration (Cahill *et al.,* 2024; Kravitz *et al.,* 2011), attentional control (Bavelier & Green, 2019; Bavelier & Green, 2025), and cognitive flexibility (Glass *et al.,* 2013; Okazawa & Kiani, 2023). This would account for the enhanced visuomotor decision performance observed in gamers exhibiting approximately 190ms faster response times compared to non-gamers, without compromising accuracy.

To formally test the CRR hypothesis, we constrain both undirected and directed functional connectivity by anatomically plausible white matter tracts. Structurally constrained functional connectivity FC (SC-FC) and structurally constrained directed connectivity dFC (SC-dFC) matrices are derived using binarized whole-brain tractography masks, as described in Section 2.2.3. This approach ensures that both FC, estimated by pairwise Pearson correlation, and dFC, estimated by time-domain Granger causality, are grounded in biologically valid anatomical substrates (Greaves *et al*., 2025; Dhamala *et al*., 2008).

By integrating functional and structural information, we can identify behaviorally relevant, anatomically constrained connectivity differences between gamers and non-gamers. This approach offers a structurally informed measure of effective connectivity (Bajaj *et al.,* 2016), allowing us to assess whether prolonged gameplay reshapes neural communication patterns in ways that are both biologically feasible and behaviorally advantageous.

In doing so, this chapter provides a crucial test of CRR as a formal mechanism of experience-driven neuroplasticity. If supported, this work may not only explain how gamers optimize visuomotor decision-making but also reinforce the value of video games as a rigorous experimental medium for probing cognitive adaptation and, ultimately, as a tool for designing theoretically guided cognitive interventions.

4.1 Structurally Constrained Functional and Directed Connectivity Results

4.1.1 SC-FC and SC-dFC Group Differences Between Gamers and Non-Gamers

To investigate large-scale task-relevant connectivity adaptations associated with action video game playing, we examined SC-FC and SC-dFC between long-term action video gamers and non-gamers, within distinct major anatomical groups of the AAL3 atlas. A detailed categorization of the AAL3 atlas regions by these anatomical groups is outlined in Section 2.2.3.3. By constraining our analysis with underlying white matter pathways, this approach ensures that observed group differences reflect meaningful adaptations rather than arbitrary or spurious connections.

The SC-FC results of the significant connections are presented as a heat map of mean differences between groups, displayed as a connectivity matrix in Figure 4.1a. Connections where gamers showed stronger structurally constrained functional connectivity are indicated by warm colors (red, orange), whereas connections stronger in non-gamers are indicated by cool colors (cyan, blue). Gamers exhibited a significantly greater number of enhanced ($p < 0.05$) SC-FC connections compared to non-gamers (278 ± 17 vs. 220 ± 15; $Z = 2.60$, $p < 0.01$). Significance was determined using a Gaussian approximation to estimate the standard error of total connection counts. SC-FC analyses revealed greater connectivity in gamers across occipital-

limbic, occipital-parietal, frontal-limbic, and frontal-parietal pathways. In contrast, non-gamers exhibited stronger SC-FC between frontal-occipital regions and within the cerebellum (Figure 4.1a).

The SC-dFC results are shown in Figure 4.1b as a heat map of mean group differences, using the same matrix format as Figure 4.1a. Although non-gamers exhibited a greater total number of significantly stronger SC-dFC (313 ± 18 vs. 249 ± 16; Z = 2.70, $p < 0.01$), gamers showed greater SC-dFC between frontal and occipital regions, suggestive of more targeted top-down visual processing. Non-gamers showed significantly greater SC-dFC within cerebellar regions, consistent with the SC-FC findings and reinforcing a distinct inter-cerebellar profile.

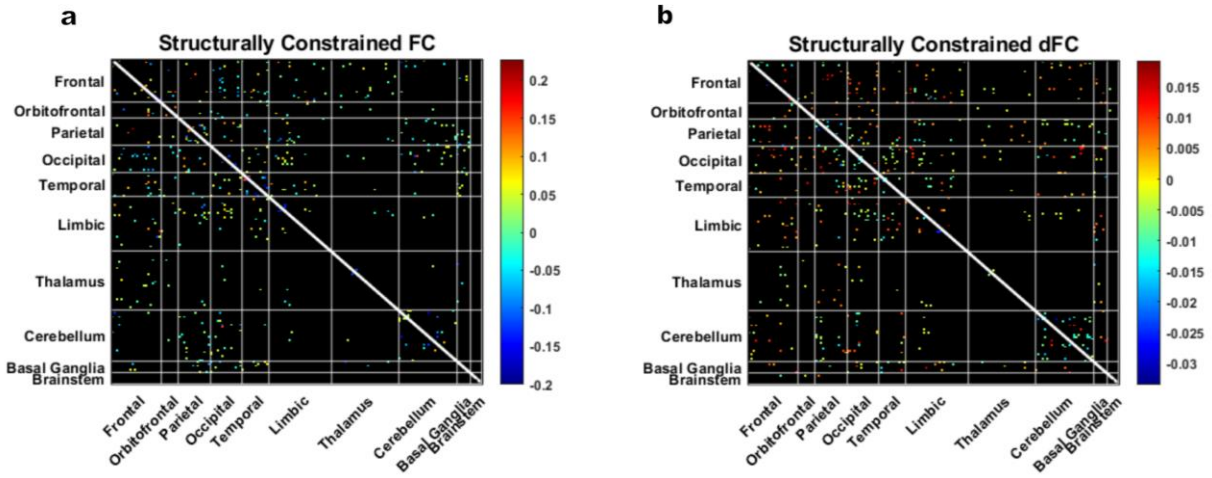

Figure 4.1 Group Differences in SC-FC and SC-dFC Between Gamers and Non-Gamers (a) SC-FC (-) group differences, where positive values indicate greater connectivity in gamers and negative values indicate stronger connectivity in non-gamers ($p < 0.05$). (b) SC-dFC (→) group differences measured using time-domain Granger causality (TGC) to capture effective connectivity ($p < 0.05$).

4.1.2 SC-FC and SC-dFC Correlations with Response Times

To evaluate how response time (RT) relates to structurally constrained functional connectivity, we examined its Spearman correlation with both SC-FC and SC-dFC. This analysis identified behaviorally relevant connections and revealed which group differences may help explain the response time advantage observed in gamers within anatomically constrained pathways. Results are shown in Figure 4.2 and summarized in Tables 4.1 and 4.2.

4.1.2.1 SC-FC Correlations with Response Times

Several SC-FC pairwise relationships showed significant negative correlations with RT, indicating that stronger connectivity was associated with faster performance. These included connections between the left inferior temporal and left cerebellum crus I ($r = –0.40$, $p = 0.012$), right lingual and right cerebellum crus I ($r = –0.38$, $p = 0.016$), and left insula and left superior temporal cortex ($r = –0.37$, $p = 0.019$). Additional correlations were observed in early visual areas, including left cuneus – left middle occipital ($r = –0.35$, $p = 0.029$) and right calcarine – left cuneus ($r = –0.33$, $p = 0.039$). The cuneus, positioned just above the calcarine sulcus, is thought to play a key role in routing visual input into the dorsal stream (Cohen, 2011; Zhang *et al*., 2019). The cuneus' involvement here suggests that faster responders may engage more early-stage dorsal relays for visuomotor integration.

Several SC-FC relationships showed significant positive correlations with RT, indicating that stronger connectivity was associated with slower performance. These included left supramarginal – left middle temporal ($r = 0.40$, $p = 0.012$), left cerebellum crus I – Vermis 4,5 ($r = 0.38$, $p = 0.015$), and left middle temporal – left inferior temporal ($r = 0.37$, $p = 0.018$). Additionally, SC-FC between the left hippocampus and left parahippocampus was positively

correlated with response time ($r = 0.36$, $p = 0.021$). All results are summarized in Table 4.1 and displayed in Figure 4.2a.

Table 4.1 Significant Spearman correlations between pairwise SC–FC connectivity and response time involving AAL3 atlas regions

Region A	**Region B**	***r***	***p***
Temporal Inf L	Cerebellum Crus1 L	-0.403	0.012
SupraMarginal L	Temporal Mid L	0.396	0.012
Cerebellum Crus1 L	Vermis 4,5	0.385	0.015
Lingual R	Cerebellum Crus1 R	-0.379	0.016
Temporal Mid L	Temporal Inf L	0.373	0.018
Fusiform R	Cerebellum Crus1 R	-0.352	0.026
Precuneus L	Precuneus R	-0.32	0.043
Cerebellum 8 L	Cerebellum 10 L	0.32	0.044

4.1.2.2 SC-dFC (→) Correlations with Response Times

A wide array of effective pairwise causal relationships given by SC-dFC was negatively correlated with RT. The strongest correlation was observed between the right subgenual and supracallosal anterior cingulate cortex ($r = –0.51$, $p = 0.0009$). Additional SC-dFC relationships associated with faster response times included left temporal middle → left lingual ($r = –0.46$, $p = 0.003$), left rolandic operculum → left insula ($r = –0.46$, $p = 0.003$), left insula → left superior temporal ($r = –0.46$, $p = 0.003$), and left superior temporal → left rolandic operculum ($r = –0.44$, $p = 0.004$).

Several subcortical and frontal pathways were also significant, including left putamen → left insula (r = –0.45, p = 0.005), left frontal operculum → left insula (r = –0.43, p = 0.006), and left putamen → left superior frontal gyrus (r = –0.41, p = 0.009). Right hemisphere relationships included right frontal inferior triangularis → right insula (r = –0.37, p = 0.019), right frontal inferior orbitalis → right rolandic operculum (r = –0.37, p = 0.021), and right insula → right frontal inferior operculum (r = –0.35, p = 0.026).

Additional significant SC-dFC findings included right rolandic operculum → left supramarginal (r = –0.37, p = 0.019), left superior parietal → itself (r = –0.36, p = 0.022), right frontal medial orbital → right rectus (r = –0.37, p = 0.022), and left parahippocampus → left superior temporal pole (r = –0.36, p = 0.022). One relationship, right insula → right posterior orbitofrontal cortex (r = 0.36, p = 0.025), showed a significant positive correlation with RT. All results are summarized in Table 4.2 and displayed in Figure 4.2b.

Table 4.2 Significant Spearman correlations between pairwise SC–dFC connectivity (source to target) and response time involving AAL3 atlas regions

Source Region	**Target Region**	***r***	***p***
ACC sub R	ACC sup R	-0.517	0.001
Rolandic Oper L	Insula L	-0.461	0.003
Heschl L	Temporal Sup L	-0.457	0.003
Temporal Sup L	Rolandic Oper L	-0.445	0.004
Cerebellum Crus2_R	Cerebellum Crus1 R	0.457	0.005
Putamen L	Insula L	-0.452	0.005
Frontal Inf Oper R	Insula_R	-0.427	0.006
Vermis 8	Cerebellum 8 R	-0.429	0.008
Putamen L	Frontal Sup 2 L	-0.41	0.009
Heschl L	Insula L	-0.409	0.009
Cerebellum_Crus1_R	Vermis 6	-0.421	0.01
Temporal Inf L	Lingual L	-0.41	0.01
Vermis 4,5	Vermis_6	-0.402	0.012
ACC pre L	ACC sup R	-0.377	0.017
Cerebellum Crus2 L	Cerebellum Crus1 L	0.382	0.019
Rolandic Oper L	SupraMarginal L	-0.37	0.019
Frontal Inf Tri R	Insula R	-0.37	0.019
Insula L	Rolandic Oper L	-0.365	0.021
ParaHippocampal L	Temporal Pole Sup L	-0.364	0.022
Frontal Med Orb R	Rectus L	-0.373	0.022
Parietal Inf_R	Parietal Sup R	-0.362	0.022
Insula R	OFCpost R	0.355	0.025
Insula R	Frontal Inf Oper R	-0.353	0.026
Frontal Inf Orb 2 R	Frontal Inf Tri R	-0.353	0.026
Temporal Sup L	Insula_L	-0.349	0.028
Cerebellum 4,5 R	Vermis_6	-0.348	0.029
Lingual R	Cerebellum 6 R	-0.341	0.032
ACC pre R	ACC pre_L	-0.334	0.036
ACC pre R	ACC sup R	-0.331	0.038
Cuneus L	Cuneus R	-0.323	0.043
Occipital Mid L	Lingual L	-0.323	0.043

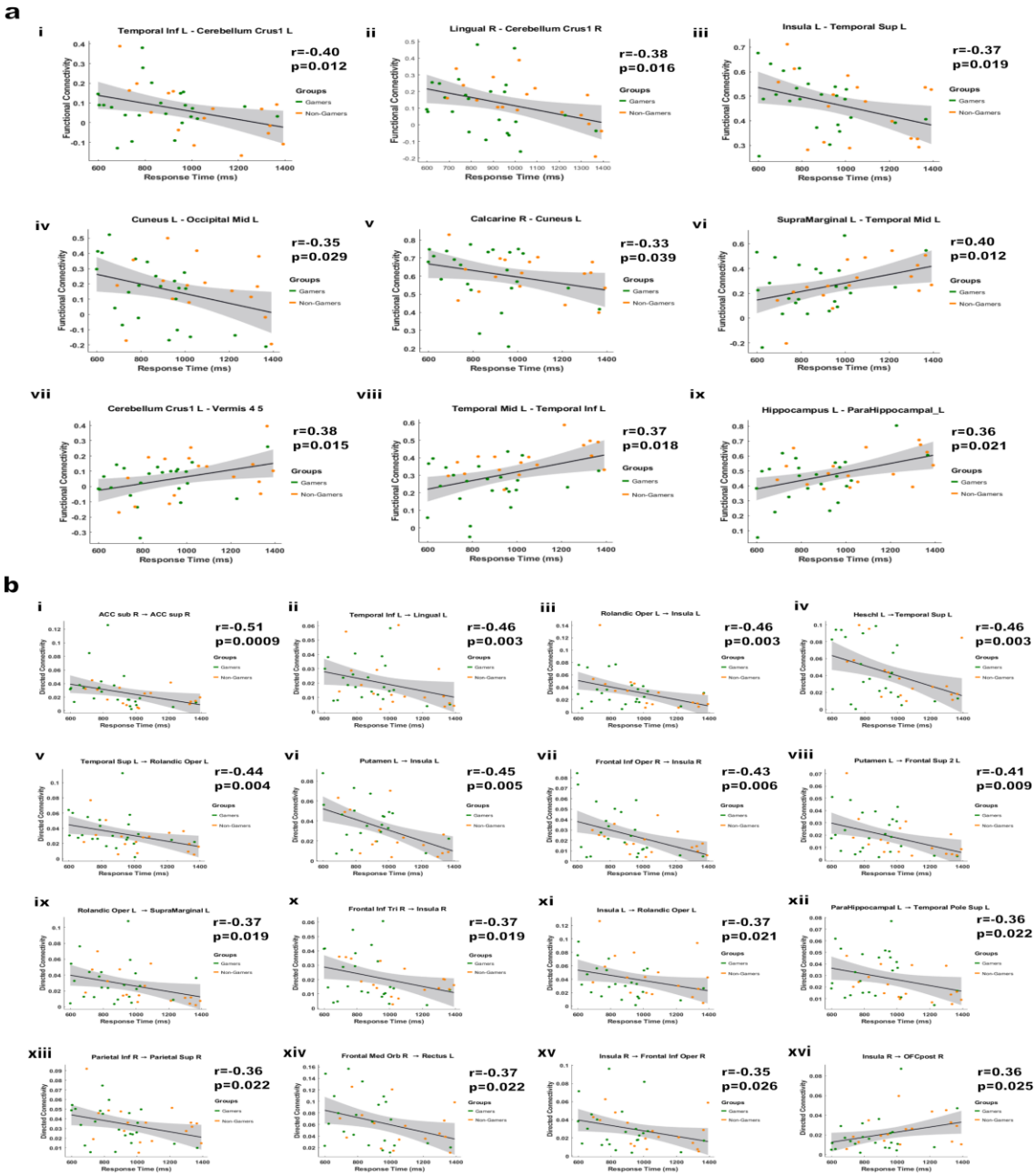

Figure 4.2 Correlations Between Functional Connectivity Measures and Response Times. (a) Significant Spearman correlations ($p < 0.05$) between structurally constrained functional connectivity (SC-FC) and response time (RT), ranked by ascending p-values, separated by (i-v) negative and (vi-ix) positive correlation coefficients. Negative correlations reflect connections where increased SC-FC predicts faster decision-making, while positive correlations indicate connections where stronger SC-FC is associated with delayed RT. (b) Significant Spearman correlations ($p < 0.05$) between structurally constrained directed functional connectivity (SC-dFC) and response times, ranked from lowest to highest p-values, separated by negative (i-xv) and positive (xiv) correlation, capturing effective connectivity linked to visuomotor decision RT. Region names are derived from the AAL3 atlas.

4.1.3 Behaviorally Relevant Group Differences in SC-FC and SC-dFC

Among the behaviorally relevant SC-FC connections, a significant group difference was observed between the left middle temporal and inferior temporal gyri. This connection was significantly stronger in non-gamers ($p = 0.002$) as shown in Figure 4.3a(i) and showed a positive correlation with response times ($r = 0.37$, $p = 0.018$) which is displayed in Figure 4.2a(vii).

In addition, two behaviorally relevant SC-dFC group differences emerged. The effective connection from the left parahippocampus to the left superior temporal pole was stronger in gamers ($p = 0.034$) shown in Figure 4.3a(ii), and was negatively correlated with response times ($r = –0.36$, $p = 0.022$) shown in Figure 4.2b(xii). In contrast, the effective connection from the right insula to the right posterior orbital cortex was stronger in non-gamers ($p = 0.046$) shown in Figure 4.3a(iii), and was positively correlated with response times ($r = 0.36$, $p = 0.025$) demonstrated in Figure 4.2b(xvi). Figure 4.3b provides a visual representation of these connections in gamers and non-gamers, rendered using DSI Studio.

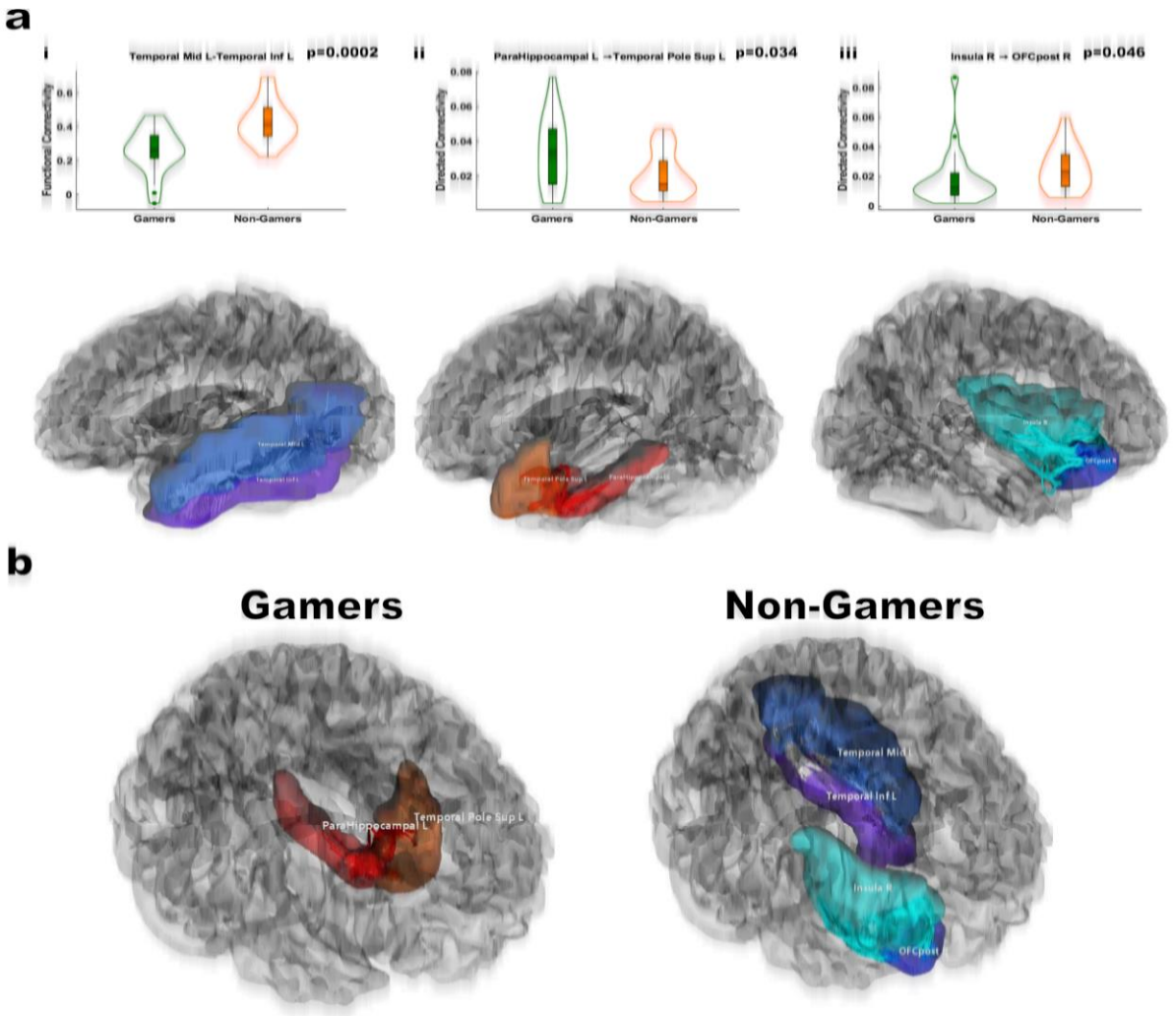

Figure 4.3 Behaviorally Relevant Connectivity Differences Between Gamers and Non-Gamers. (a) Violin plots are depicted comparing functional (i) and directed (ii, iii) connectivity for key brain regions, including Temporal Mid L – Temporal Inf L, Parahippocampal L →Temporal Pole Sup L, and Insula R →OFCpost R, with significant group differences indicated by p-values. (b) 3D renderings of the respective regions for Gamers (left) and Non-Gamers (right), highlighting the anatomical locations where significant connectivity differences were observed, are shown. The brain regions shown are left mid-temporal gyrus, left inferior temporal gyrus, left parahippocampus, left superior temporal pole, right insula, and right orbitofrontal cortex. The renderings were created using the AAL3 atlas and visualized in DSI Studio.

4.1.4 SC-FC Graph-Theoretic Network Analysis

After applying structural connectivity (SC) constraints to the functional connectivity (FC) data, we retained the top 95% of the strongest connections to construct binarized SC-FC graphs for network analysis. This threshold maximized the characterization of the SC-FC network while maintaining sparsity. At the global level, network measures, including characteristic path length, assortativity, and global efficiency, did not significantly differ between gamers and non-gamers.

To further investigate topological differences, we examined local graph-theoretic metrics, specifically local efficiency and node degree. Local efficiency reflects regional integration by measuring how effectively information is exchanged among a node's immediate neighbors if the node itself is removed. Node degree, a local measure of centrality based on how many direct links a node has to other regions in the network, reflects the extent to which a region participates in the SC-FC network.

4.1.4.1 Group Differences in Local Efficiency and Node Degree

Gamers exhibited significantly greater local efficiency in the right middle occipital gyrus ($p = 0.02$) and right supramarginal gyrus ($p = 0.047$), suggesting stronger localized integration within dorsal visual and parietal circuits. In contrast, non-gamers showed greater local efficiency in the left pallidum ($p = 0.047$), a subcortical region involved in motor regulation and reinforcement learning.

For node degree, gamers demonstrated significantly higher values in the right inferior frontal gyrus (triangular part) ($p = 0.015$), right insula ($p = 0.017$), and two subdivisions of the left anterior cingulate cortex subgenual ($p = 0.028$) and pregenual ($p = 0.032$). These are key nodes in the salience and cognitive control networks, supporting integration of internal state

monitoring and goal-directed action. By contrast, non-gamers showed higher node degree in the left cerebellum 3 ($p = 0.009$) and left hippocampus ($p = 0.047$), reflecting greater centrality in circuits involved in motor coordination and memory-based retrieval. These results are summarized using violin plots, which show the group distributions in Figure 4.4a.

4.1.4.2 Correlations Between Local Efficiency and Node Degree and Response Times

Several SC-FC graph metrics were significantly correlated with response times across participants. Negative correlations were found for local efficiency in the left superior occipital gyrus ($r = –0.38$, $p = 0.016$) and node degree in the right insula ($r = –0.32$, $p = 0.047$), indicating that higher values were associated with faster responses. Positive correlations were observed for node degree in the left superior occipital gyrus ($r = 0.38$, $p = 0.019$) and left cerebellum 3 ($r = 0.32$, $p = 0.044$), where higher values were associated with slower responses. The brain–behavior correlations between SC-FC and RT are shown in Figure 4.4b.

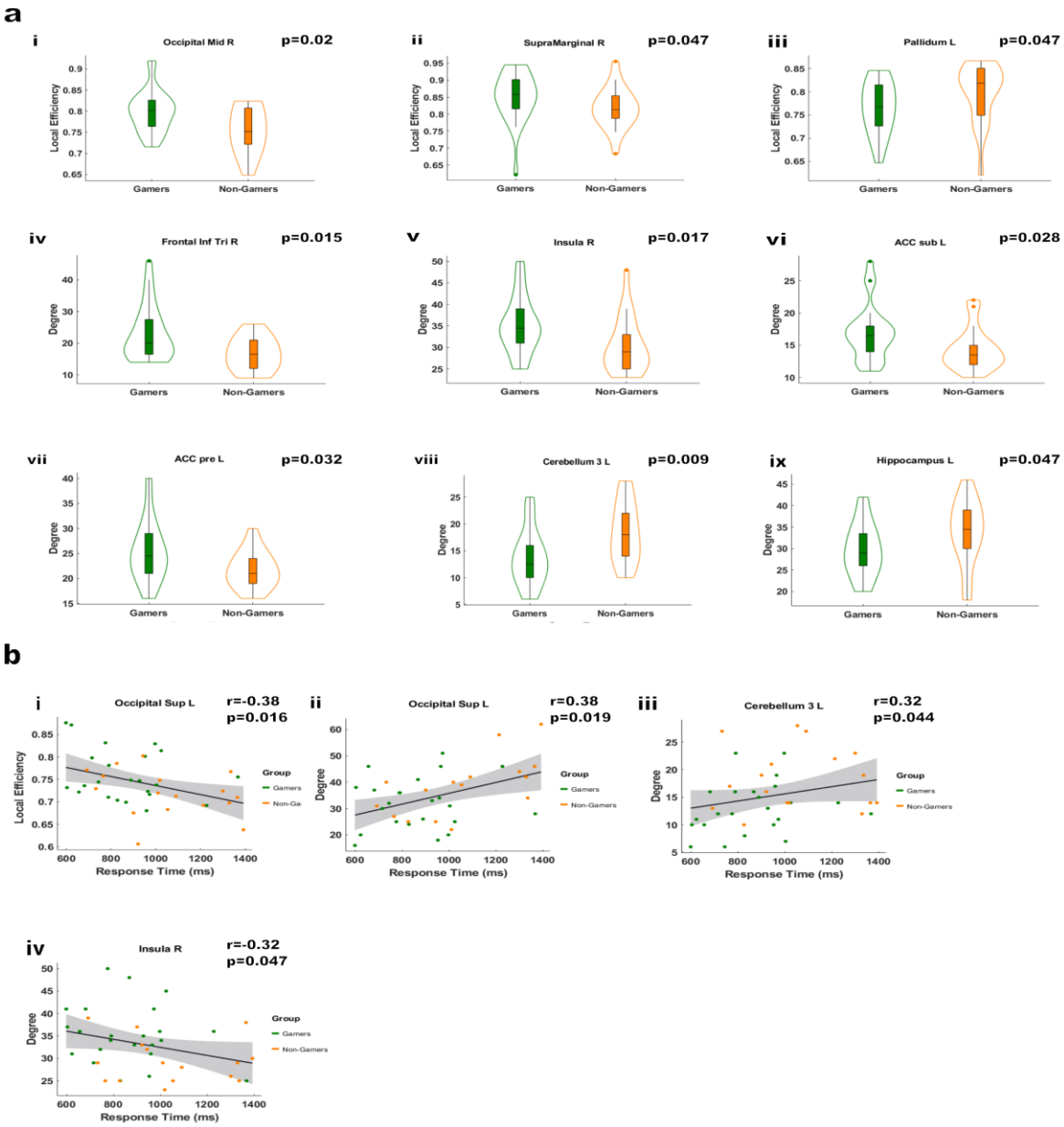

Figure 4.4 Group Differences in Binarized Undirected Connectivity Network Metrics and Brain-Behavior Correlations. (a) Violin plots depicting group differences in binarized directed functional connectivity network metrics, including (i-vii) local efficiency and (ix-xii) node degree, for gamers and non-gamers.(b) Spearman correlations between directed functional connectivity network metrics and response times. Negative correlations indicate an association with faster responses, while positive correlations reflect an association with slower responses. Region names are taken from the AAL3 atlas.

4.1.5 SC-dFC Graph-Theoretic Network Analysis

For the binarized graph-theoretic analysis of structurally constrained directed functional connectivity (SC-dFC), we retained the top 10% of the strongest directed connections, accounting for the sparser and asymmetric nature of effective connectivity. As in the SC-FC analysis, global network measures—including characteristic path length, assortativity, and global efficiency—did not significantly differ between gamers and non-gamers.

We again focused on local efficiency and node degree, metrics that capture regional integration and network centrality, respectively.

4.1.5.1 **Group Differences in SC-dFC Local Efficiency and Node Degree**

Gamers exhibited significantly greater local efficiency in the right middle occipital gyrus ($p = 0.026$) and left precentral gyrus ($p = 0.044$), suggesting more integrated local processing within early visual and motor areas. Non-gamers, by contrast, had greater local efficiency in the left pallidum ($p = 0.034$) and vermis 4,5 ($p = 0.047$), indicating increased localized interaction within subcortical and cerebellar structures.

For node degree, gamers showed significantly higher values in multiple frontal and salience-related regions, including the left anterior cingulate (pregenual) ($p = 0.008$), right insula ($p = 0.018$), right rectus ($p = 0.026$), left superior medial frontal ($p = 0.027$), right inferior frontal (opercular) ($p = 0.027$), left posterior orbital ($p = 0.045$), and right inferior frontal (triangular) ($p = 0.047$). Non-gamers had significantly greater node degree in the left cerebellum 3 ($p = 0.013$) and left hippocampus ($p = 0.031$), consistent with stronger centrality in motor and memory-related regions. These results are summarized using violin plots, which show the group distributions in Figure 4.5a.

4.1.5.2 Correlations Between SC-dFC Graph Metrics and Response Times

Both local efficiency and node degree were significantly correlated with response times (RT) across participants. We observed several negative correlations, indicating that higher graph values were associated with faster responses. For local efficiency, significant negative correlations were found in the left superior occipital ($r = –0.48$, $p = 0.002$), left supplementary motor area ($r = –0.45$, $p = 0.005$), left supramarginal ($r = –0.40$, $p = 0.013$), left superior temporal pole ($r = –0.39$, $p = 0.016$), left amygdala ($r = –0.39$, $p = 0.016$), left rectus ($r = –0.34$, $p = 0.036$), left parahippocampus ($r = –0.43$, $p = 0.006$), and left middle frontal gyrus ($r = –0.41$, $p = 0.009$). For node degree, faster response times were associated with higher values in the left insula ($r = –0.51$, $p = 0.001$), left posterior orbital ($r = –0.37$, $p = 0.018$), left anterior cingulate (pregenual) ($r = –0.33$, $p = 0.045$), and right postcentral gyrus ($r = –0.32$, $p = 0.048$). Only one positive correlation was observed, with higher node degree in the left superior occipital gyrus associated with slower response times ($r = 0.32$, $p = 0.048$). The brain–behavior correlations between SC-dFC and RT are shown in Figure 4.5b.

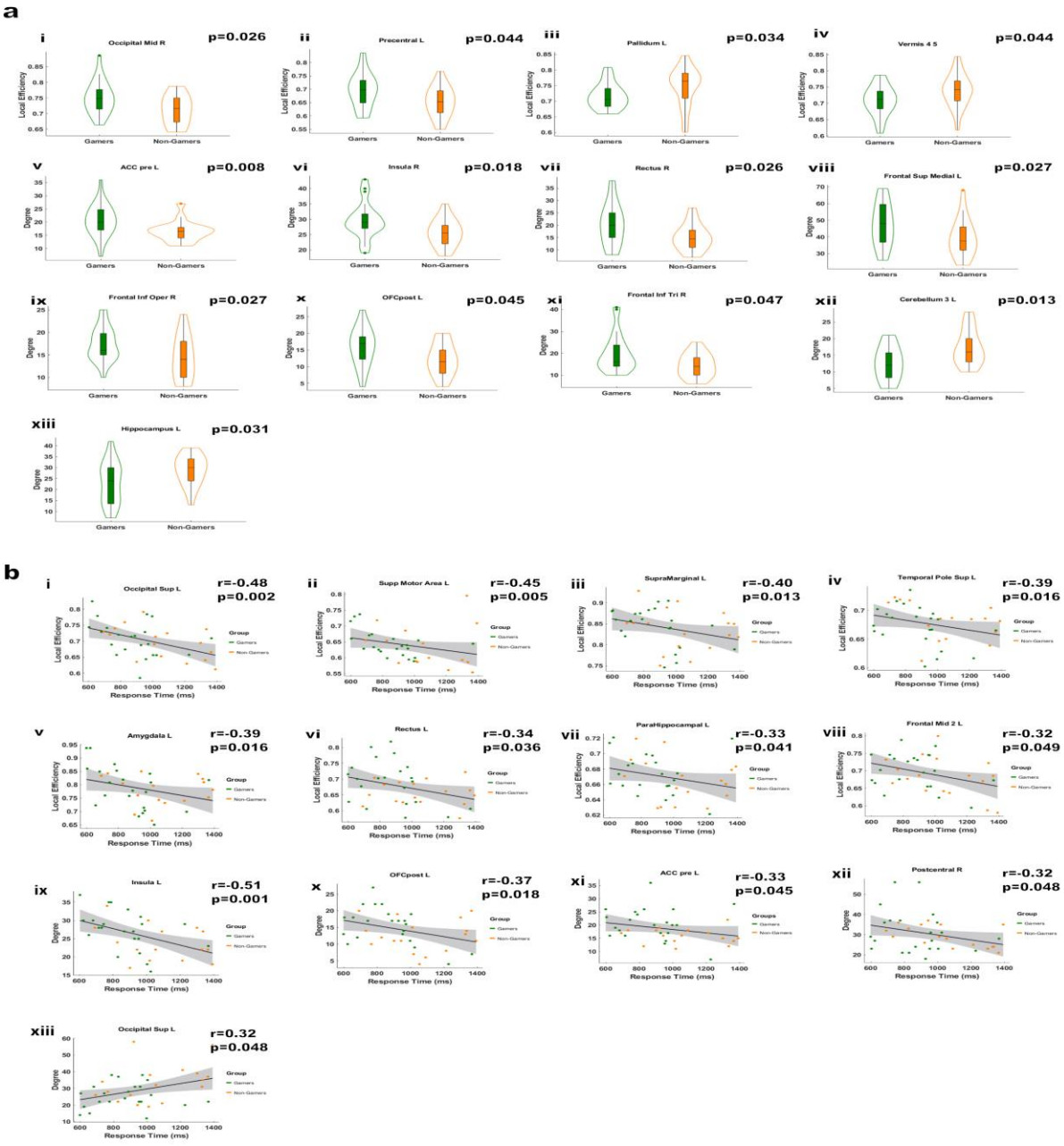

Figure 4.5 Group Differences in Binarized Directed Connectivity Network Metrics and Brain-Behavior Correlations. (a) Violin plots depicting group differences in binarized directed functional connectivity network metrics, including (i-vii) local efficiency and (ix-xii) node degree, for gamers and non-gamers.(b) Spearman correlations between directed functional connectivity network metrics and response times. Negative correlations indicate an association with faster responses, while positive correlations reflect an association with slower responses. Region names are taken from the AAL3 atlas

4.2 Discussion of Findings and Interpretation

The results of this analysis provide compelling evidence that long-term action video game playing induces neuroplastic changes in structurally constrained functional and directed connectivity, leading to more efficient decision-making. These findings reveal distinct differences between gamers and non-gamers in connectivity patterns, brain-behavior relationships, and local network properties, suggesting a fundamental shift in visuomotor processing and decision-making strategies.

4.2.1 Structurally Constrained Functional Connectivity Profiles

4.2.1.1 SC-FC Gamer and Non-Gamer Connectivity Patterns

Gamers exhibited a significantly greater number of enhanced ($p < 0.05$) SC-FC connections than non-gamers (278 ± 17 vs. 220 ± 15, $Z = 2.60$, $p < 0.01$). The SC-informed FC connectivity matrix shown in Figure 4.1a revealed more prominent connectivity shifts in favor of gamers across occipital-limbic, occipital-parietal, frontal-limbic, and frontal-parietal pathways. This pattern is consistent with the predictions of Cognitive Resource Reallocation (CRR), suggesting that video game experience enhances neural synchrony within circuits that support visual processing, attentional control, visuomotor integration, flexible action selection, and efficient decision-making under time pressure.

In the occipital-limbic pathway, increased SC-FC suggests stronger synchronization between regions involved in salience detection and early visual processing, potentially facilitating more effective extraction of task-relevant visual cues (Menon, 2015). Enhanced occipital-parietal connectivity supports the integration of spatial and motion cues necessary for tracking object trajectories, indicating a greater reliance on endogenous attentional mechanisms

to guide action (Beffara *et al.,* 2022; Goodale & Milner, 1992). Strengthened frontal-limbic connections reflect improved integration of executive and affective signals relevant to attentional control and adaptive behavior (Chen *et al*., 2018; Kennerley & Walton, 2011). Finally, increased frontal-parietal coupling aligns with enhanced intentional action planning and selection during decision-making tasks, consistent with prior models of visuomotor coordination (Andersen & Cui, 2009).

In contrast, non-gamers exhibited stronger SC-FC connectivity between frontal and occipital regions, suggesting a greater reliance on executive-visual synchrony rather than the anticipatory visuomotor response selection observed in gamers (Gonzalez Alam *et al*., 2024). Additionally, greater intra-cerebellar connectivity in non-gamers indicates a heavier reliance on feedback-driven motor adjustments, given the cerebellum's known role in motor modulation (Stoodley & Schmahmann, 2018), which likely reflects a compensatory mechanism for less adaptive top-down motor planning and response execution. These findings suggest that non-gamers' visuomotor processing strategies are less optimized, characterized by broader, more reactive, back-and-forth engagement between the visual, executive, and motor correction systems rather than the targeted, feedforward, adaptive response selection characterized by SC-FC connectivity patterns found in gamers.

4.2.1.2 SC-dFC Gamer and Non-Gamer Connectivity Patterns

Non-gamers exhibited a greater total number of significantly stronger ($p < 0.05$) SC-dFC connections (313 ± 18 vs. 249 ± 16, $Z = 2.70$, $p < 0.01$) shown by the SC-dFC connectivity matrix in Figure 4.1b, suggesting a greater need for directed interactions to support their visuomotor decision-making. In contrast, gamers displayed more frontal-occipital and frontal-

parietal SC-dFC connections, indicating a shift toward more targeted signaling between executive, visual, and motor regions, whereas non-gamers seem to rely more on broader, frontal-occipital engagement. Additionally, non-gamers exhibited significantly greater intra-cerebellar SC-dFC interactions, reinforcing their reliance on corrective motor adjustments rather than anticipatory control mechanisms.

4.2.2 SC-FC and SC-dFC Brain–Behavior Correlations

The following interpretations are grounded in well-established canonical neural anatomy and physiology of the involved brain regions, where functional roles are less well established in the literature.

4.2.2.1 SC-FC Correlations with Response Times

Stronger connectivity between occipital, cerebellar, and multimodal sensory regions was associated with faster response times (RTs), suggesting that these pathways facilitate efficient visuomotor processing. This pattern is demonstrated clearly in Figure 4.2a. For example, connectivity between the left inferior temporal gyrus and the left cerebellum Crus I ($r = –0.40$, $p = 0.012$) suggests that motor planning and control processes, synchronized with object recognition (such as identifying moving target dots), facilitate faster decision-making and response execution. Similarly, connectivity between the right cerebellum Crus I and the right lingual gyrus ($r = –0.38$, $p = 0.016$) implies that visual scene processing paired with anticipatory motor planning plays a key role in rapid response execution.

Connectivity between the left insula and the left superior temporal gyrus ($r = –0.37$, $p = 0.019$) modulates interoceptive attention to auditory stimuli, effectively gatekeeping salient auditory information from executive engagement and optimizing cognitive resources for efficient visuomotor decision-making. Additional connectivity between the right calcarine and the left

cuneus *(r* = –0.33, *p* = 0.039), as well as between the left cuneus and left middle occipital gyrus (*r* = –0.35, *p* = 0.029), indicates that enhanced early-stage visual processing supports rapid extraction of motion cues and enables quicker decision-making.

Conversely, stronger SC-FC connectivity in memory-related and feedback-driven motor regions has a positive correlation with RT, which is tracked with slower responses. This pattern suggests a reliance on deliberative processing rather than real-time visuomotor integration. For instance, connectivity between the left hippocampus and the left parahippocampus (*r* = 0.36, *p* = 0.021) points to an antagonism between scene-specific spatial configuration and object-in-place cognitive mapping, which may slow decision-making. Similarly, stronger connectivity between the left cerebellum Crus I and the left vermis 4,5 (*r* = 0.38, *p* = 0.015) indicates increased reliance on corrective motor feedback, which could prolong response execution.

4.2.2.2 SC-dFC Correlations with Response Times

To investigate how structurally constrained directed functional connectivity (SC-dFC) influences response time (RT), we assessed correlations between connectivity strength and RT across all participants, as depicted in Figure 4.2b.

Several SC-dFC connections were significantly associated with faster response times. For instance, directed connectivity from the right anterior cingulate (subgenual) to the right anterior cingulate (supracallosal) (*r* = –0.51, *p* = 0.0009) was linked to urgency-driven response selection. This pathway is a major constituent of the dorsal attention network and likely serves as a high-priority signal that prompts executive systems to initiate rapid decision-making.

SC-dFC from the left middle temporal gyrus to the left lingual gyrus (*r* = –0.46, *p* = 0.003) supports the integration of high-level visual processing, such as object recognition, given

the middle temporal gyrus's proximity to the ventral stream, with color discrimination in the lingual gyrus. This integration may support rapid discrimination of color-based target dots from distractors during the sensory accumulation stage of a visuomotor decision.

Interactions from the left rolandic operculum to the left insula ($r = –0.46$, $p = 0.003$) and from the left insula to the left superior temporal gyrus ($r = –0.46$, $p = 0.003$) taken together suggest enhanced modulation of interoceptive attention to salient stimuli (Menon, 2015). These pathways likely act to gate salient auditory information away from executive resources, facilitating scanner noise to be more of a persistent background feature than a salient distraction. Additionally, SC-dFC from the left superior temporal gyrus to the left rolandic operculum ($r = –0.44$, $p = 0.004$) further supports streamlined sensory integration, likely under insular modulation, facilitating faster RT. Furthermore, based on known physiology, this loop may reflect interoceptive signaling prompting the retrieval or prioritization of high-level sensory information to guide an imminent motor response (Blefari *et al.,* 2017).

Connectivity from the left putamen to the left insula ($r = –0.45$, $p = 0.005$) and from the left putamen to the left superior frontal gyrus ($r = –0.41$, $p = 0.009$) highlights the putamen's role in motor preparation and control (Purves D, 2001), suggesting that basal ganglia–insular circuits support the rapid coordination of motor action under time pressure.

Fronto-insular interactions were also predictive of faster response times. Directed signaling from the right inferior frontal gyrus (triangularis) to the right insula ($r = –0.37$, $p = 0.019$) suggests unconscious perceptual priming and enhanced attentional control (Shi *et al*., 2022). Likewise, connectivity from the right inferior frontal gyrus (orbital) to the right rolandic operculum ($r = –0.37$, $p = 0.021$) likely reflects a goal-directed control mechanism that bridges

the brain's interoceptive goal-directed map, such as the intention to make the correct decision, with voluntary motor execution of finger movement (Blefari *et al*., 2017; Shi *et al.,* 2023).

Inter-parietal connections also tracked with faster responses. Directed signaling from the left supramarginal gyrus to the left superior parietal lobule ($r = –0.37$, $p = 0.019$), and from the left inferior parietal lobule to the left superior parietal lobule ($r = –0.36$, $p = 0.022$), supports visuospatial attention, motor planning, and sensorimotor integration. These dorsal stream pathways likely enhance rapid action selection by engaging the dorsal attention network.

SC-dFC from the right medial orbital frontal gyrus to the right rectus gyrus ($r = –0.37$, $p = 0.022$) may reflect goal-directed control over response selection. Although the precise cognitive role of the gyrus rectus remains under investigation, prior work suggests its involvement in value-based decision-making and executive control (Rudebeck & Rich, 2018; Rolls, 2021).

A SC-dFC connection from the left parahippocampal gyrus to the left superior temporal pole ($r = –0.36$, $p = 0.022$) supports the integration of scene-specific contextual information, which may facilitate quicker decisions by rapidly resolving target–distractor dynamics in complex visual environments by more readily integrating relative motion of the target compared to the distractor. Finally, signaling from the right insula to the right inferior frontal operculum ($r = –0.35$, $p = 0.026$) suggests close coordination between interoceptive and motor regions (Dziedzic *et al*., 2022), further reinforcing the importance of insular modulation in facilitating fast, goal-oriented actions.

One SC-dFC connection had a positive correlation and was significantly associated with slower response times, namely, the SC-dFC interaction from the right insula to the right posterior orbitofrontal cortex ($r = 0.36$, $p = 0.025$). Given the insula's role in interoception and the orbitofrontal cortex's function in decision inhibition and uncertainty evaluation, this connection may reflect a shift toward internal state monitoring and deliberative control, which slows down response execution (Gogolla, 2017; Rolls, 2004; Rudebeck & Rich, 2018).

4.2.3 Behavioral Correlates of SC-FC and SC-dFC Group Differences

We observed group-level differences in SC-FC and SC-dFC patterns between gamers and non-gamers that tracked with RT. Non-gamers exhibited stronger connectivity between the left middle temporal gyrus and left inferior temporal gyrus ($p = 0.002$) and showed a positive correlation with response times ($r = 0.37$, $p = 0.018$) suggesting a greater reliance on detailed object recognition (Conway, 2018; Holdstock, 2005; Kakaei *et al.,* 2021) before committing to a decision. In contrast, gamers exhibited stronger connectivity from the left parahippocampal gyrus to the left superior temporal pole ($p = 0.034$) and was negatively correlated with response times ($r = –0.36$, $p = 0.022$). The parahippocampus is crucial for spatial scene processing (Burgess & O'Keefe, 2003), while the superior temporal pole is known as a convergent hub of high-level sensory information and perhaps of high-level information convergence in general (Herlin *et al.,* 2021).

Stronger SC-dFC from the parahippocampus to the superior temporal pole in gamers suggests greater integration of scene-specific contextual information, likely allowing for more efficient decision-making by more readily facilitating the rapid integration of the relative motion of target dots compared to distractors. Rather than solely relying on detailed object recognition, gamers place greater emphasis on the broader spatial and contextual relevance of the scene to

guide their actions compared to non-gamers. This shift from object-based analysis to greater context-driven reasoning would contribute to greater decision efficiency in dynamic environments, reinforcing that long-term action video game playing experience leads to enhancements in adaptive visuomotor processing.

Additionally, non-gamers demonstrated stronger SC-dFC from the right insula to the right posterior orbitofrontal cortex (OFC) ($p = 0.046$) and had a positive correlation with RT ($r = 0.36$, $p = 0.025$). The right insula plays a key role in internal state monitoring and uncertainty assessment (Gogolla, 2017). The posterior OFC contributes to evaluating outcomes and creating cognitive maps to navigate goal-directed behavior, such as the goal of picking the correct direction that target dots are moving in a visuomotor decision (Shi *et al.,* 2023). Stronger connectivity involving these regions in non-gamers likely reflects a heightened emphasis on progressively reducing uncertainty before committing to a goal-directed decision of selecting the correct direction the target dots were moving, resulting in longer stimulus evaluation times at the expense of RT. This aligns with the well-established speed-accuracy tradeoffs in visuomotor decision-making, where prioritizing certainty and deliberation comes at the cost of slower response times (Drugowitsch *et al*., 2014; 2015).In contrast, gamers likely engage in more real-time error correction to maintain accuracy and more effectively address uncertainty earlier in the decision-making process, enabling less reliance on feedback-driven inter-cerebellar corrections. This is supported by a shift in visuomotor decision strategy that more readily incorporates integration of scene-relevant information provided by their enhanced parahippocampal → superior temporal pole connectivity.

Together, these findings support the CRR hypothesis, demonstrating that long-term AVG experience plausibly promotes the reallocation of neural resources toward context-sensitive

circuits that enable rapid, adaptive visuomotor decision-making. In contrast, non-gamers appear to rely more heavily on evaluative and uncertainty-monitoring systems that prioritize accuracy at the cost of speed. This divergence reflects distinct visuomotor decision-making strategies between gamers and non-gamers.

4.2.4 SC-FC Local Efficiency & Node Degree

For the undirected graph-theoretic network analysis, we applied a 95% threshold to binarize the SC-FC data, retaining the top 95% of the strongest connections after applying tractography constraints. This approach was chosen to capture as much of the structural network as possible while ensuring that only valid, non-spurious connections were included.

As in previous sections, the following interpretations are grounded in canonical neural anatomy and physiology of the involved brain regions, with references provided where functional roles are less well established in the literature.

4.2.4.1 Local Efficiency Group Differences

Graph-theoretic analysis revealed significant group-level differences in local efficiency, highlighting distinct patterns of network integration between gamers and non-gamers displayed in Figure 4.4a. Gamers exhibited significantly greater local efficiency in the right middle occipital gyrus (MOG) ($p = 0.02$). The right MOG plays a central role in integrating visual input with egocentric spatial orientation and processing spatial information, supporting visuomotor coordination (Renier et al., 2010). Increased local efficiency in this region likely facilitates low-latency visual processing and rapid motion tracking, advantages that are particularly beneficial in fast-paced visuomotor decision-making tasks requiring dynamic scene integration.

Gamers also demonstrated greater local efficiency in the right supramarginal gyrus (p = 0.047), a key node within the ventral attention network. This may reflect enhanced reorienting capacity, enabling more efficient shifts of attention to salient visual cues in dynamic environments such as action video games.

In contrast, non-gamers exhibited significantly greater local efficiency in the left pallidum (p = 0.047), a basal ganglia structure implicated in regulating voluntary movement and motor inhibition. This finding suggests a greater reliance on response inhibition mechanisms among non-gamers, which may contribute to slower, more deliberative decision-making strategies characterized by increased uncertainty monitoring.

4.2.4.2 Node Degree Differences

Significant group differences were also observed in node degree, further elucidating the network-level reorganization associated with long-term gaming experience. Gamers exhibited higher node degree in several functionally relevant regions. These included the right inferior frontal gyrus triangularis (p = 0.015), a region central to executive control, unconscious perceptual priming, and information processing (Shi *et al.,* 2022). Increased node degree here may reflect heightened readiness for rapid stimulus-response mapping and rule-based action selection.

Gamers also showed a greater degree in the right insula (p = 0.017), a salience network hub responsible for integrating sensory inputs and modulating attentional and decision-making processes. Elevated node degree was also observed in two subregions of the anterior cingulate cortex (ACC). In the subgenual ACC (p = 0.028), this increase is linked to urgency and

affectively driven decisions, while in the pregenual ACC ($p = 0.032$), it reflects involvement in conflict monitoring and the adjustment of cognitive strategies in response to prediction errors. Together, these findings suggest that gamers leverage a more dynamically responsive network configuration that emphasizes anticipatory control and efficient adaptation to environmental demands.

In contrast, non-gamers exhibited higher node degree in regions associated with object-in-place cognitive mapping and feedback-driven motor regulation. Specifically, the left hippocampus ($p = 0.047$), a key structure for spatial memory and contextual mapping, showed greater centrality, indicating a strategy that relies more heavily on object-based spatial reasoning. Additionally, increased node degree was observed in the left cerebellar lobule 3 ($p = 0.009$), which is involved in motor feedback correction. This suggests that non-gamers depend more on feedback-driven motor adjustments, potentially resulting in slower response execution due to ongoing corrective processes rather than optimized feedforward planning.

4.2.4.3 SC-FC Local Efficiency and Node Degree Correlations with Response Time

Stronger SC-FC local efficiency and node degree in visual and attentional regions were significantly associated with faster response times (RT), supporting their role in efficient visuomotor processing as shown in Figure 4.4b.

Higher SC-FC local efficiency in the left superior occipital cortex ($r = –0.38$, $p = 0.016$) was associated with enhanced early visual processing, likely facilitating more efficient motion cue extraction and rapid response execution. Higher SC-FC node degree in the right insula ($r = –0.32$, $p = 0.047$), which was also significantly elevated in gamers ($p = 0.017$), was associated

with faster response times. This aligns with the insula's role in salience detection and adaptive attentional control, supporting the enhanced decision speed observed in gamers.

Conversely, stronger SC-FC node degree in early visual and feedback-driven motor regions was associated with slower response times, suggesting that an over-reliance on early-stage perceptual processing or corrective motor feedback may introduce inefficiencies. Specifically, higher node degree in the left superior occipital cortex ($r = 0.38$, $p = 0.019$) may reflect diffused or redundant spatial information processing that burdens downstream decision mechanisms. Similarly, increased node degree in the left cerebellar lobule 3 ($r = 0.32$, $p = 0.044$), which was significantly higher in non-gamers ($p = 0.009$), likely indicates greater reliance on feedback-based motor corrections, potentially delaying response execution due to slower, corrective adjustments during deliberation.

Taken together, these findings align with the CRR hypothesis by demonstrating that more efficient SC-FC integration in gamers supports a shift toward feedforward-dominant processing. This would enable more rapid visuomotor decisions based on salient visual cues. In contrast, non-gamers appear to rely more heavily on slower, feedback-dependent strategies, which impose greater cognitive load and contribute to delayed motor responses.

4.2.5 SC-dFC Local Efficiency and Node Degree Differences

SC-dFC is inherently asymmetric, meaning that a connection from source A to target B does not imply the same or a similar connection from B to A. This asymmetry results in dFC networks exhibiting greater variability and a sparser structure compared to FC networks.

To address this sparsity, we applied a 10% threshold to binarize the SC-dFC network, retaining only the top 10% of the strongest and most reliable directed interactions. This threshold

minimized the influence of invalid or spurious connections, while preserving as many effective connections as possible. By doing so, we ensured that the global density of the SC-dFC network remained comparable to that of the SC-FC network within the same participant. This thresholding strategy aligned with our goal of maintaining as many meaningful connections as possible for an accurate characterization of the SC-dFC network while excluding invalid and spurious ones.

As with earlier sections, the following interpretations are grounded in canonical neural anatomy and physiology of the involved brain regions, with references provided where functional roles are less well established in the literature.

4.2.5.1 SC-dFC Local Efficiency Differences

Gamers demonstrated significantly greater SC-dFC local efficiency in two regions. First, the right middle occipital gyrus ($p = 0.026$), a region involved in motion perception and spatial processing, exhibited enhanced efficiency. This region likely serves as a transitional node linking early-stage visual areas, such as the superior occipital and calcarine cortices, to higher-order visuomotor networks. Greater local efficiency in this region suggests more effective directional information transfer, potentially enabling faster, low-latency visual processing of spatial information that is advantageous for rapid response execution (Renier *et al.,* 2010). Second, gamers also showed increased local efficiency in the left precentral gyrus ($p = 0.044$), a primary motor area. This enhancement indicates improved sensorimotor coupling, allowing for more direct and efficient communication between visual input and motor output pathways.

In contrast, non-gamers exhibited significantly greater SC-dFC local efficiency in two different regions. The left pallidum ($p = 0.034$), a basal ganglia structure critical for

proprioception and habitual motor actions, showed higher efficiency, suggesting a greater reliance on pre-learned or routine motor responses rather than executive planning. Additionally, the vermis 4,5 ($p = 0.047$), part of the cerebellum involved in error correction and feedback-driven motor coordination, also exhibited greater efficiency in non-gamers. This pattern implies a heavier dependence on corrective strategies, which may introduce temporal delays in response execution during time-sensitive tasks.

4.2.5.2 SC-dFC Node Degree Differences

Examining SC-dFC node degree revealed that gamers exhibited significantly higher connectivity in several regions associated with executive control and adaptive decision-making. The left anterior cingulate cortex pregenual ($p = 0.008$), known for its role in performance monitoring and adaptive control, showed enhanced node degree, suggesting greater integration of cognitive control mechanisms to support rapid response selection. The right insula ($p = 0.018$), a core node of the salience network, also displayed increased connectivity, reinforcing the idea that gamers are more adept at optimizing sensory-cognitive interactions for stimulus-driven decision-making.

Additional regions showing increased node degree in gamers included the right rectus gyrus ($p = 0.026$), thought to contribute to motivational behavior and reward-based decision-making (Rolls, 2021; Rudebeck & Rich, 2018), and the left superior medial frontal gyrus ($p = 0.027$), which is associated with higher-order motor planning and strategic control. Furthermore, the right inferior frontal gyrus, both opercular ($p = 0.027$) and triangular ($p = 0.047$) parts, showed elevated node degree, pointing to more effective executive suppression of irrelevant signals and potentially enhanced unconscious priming. Finally, the left posterior orbital cortex

($p = 0.045$), involved in response evaluation and strategic adjustment, also demonstrated increased connectivity in gamers.

In contrast, non-gamers showed significantly higher node degree in regions associated with memory-guided and feedback-driven motor processing. These included the left hippocampus ($p = 0.031$), implicated in spatial memory and object-in-place mapping, and the left cerebellum lobule 3 ($p = 0.013$), which plays a role in corrective motor control. These patterns suggest that non-gamers rely more on feedback-dependent and memory-guided decision-making strategies rather than streamlined, stimulus-response circuits.

Collectively, these results support the notion that gamers exhibit more feedforward-driven visuomotor integration and executive control, enabling rapid response selection without the need for extensive uncertainty reduction. This is evidenced by greater SC-dFC local efficiency in key visual and motor integration areas, as well as increased node degree in salience and control-related regions. In contrast, non-gamers appear to rely more on habitual, feedback-corrective strategies involving memory and cerebellar coordination, which may introduce delays in rapid decision-making contexts.

4.2.5.3 SC-dFC Efficiency and Node Degree Correlations with Response Times

Spearman correlations revealed that enhanced SC-dFC local efficiency in several regions was significantly associated with faster response times. Notably, efficiency in the left superior occipital cortex ($r = -0.48$, $p = 0.002$) supported enhanced early-stage visual processing and motion cue extraction, while the left supplementary motor area ($r = -0.45$, $p = 0.005$) contributed to motor planning and rapid visuomotor responses. The left parahippocampal gyrus ($r = -0.43$, p

= 0.006), known for scene-based spatial memory, and the left supramarginal gyrus (r = -0.40, p = 0.013), involved in sensorimotor integration and attentional shifts, were also significantly correlated with response speed. Additionally, the left superior temporal pole (r = -0.39, p = 0.016), thought to serve as a hub for perceptual integration (Herlin *et al*., 2021), and the left amygdala (r = -0.39, p = 0.016), involved in emotional salience processing, both showed significant negative correlations with response time. Finally, local efficiency in the left rectus (r = -0.34, p = 0.036) was associated with faster response times, consistent with its role in motivational orientation and goal-directed behavior (Rolls, 2021; Rudebeck & Rich, 2018).

In terms of node degree, several regions demonstrated significant associations with faster response times. These included the left insula (r = –0.51, p = 0.001), a salience network hub that integrates sensory and interoceptive inputs and also showed significantly greater node degree in gamers (p = 0.017); the left posterior orbital cortex (r = –0.37, p = 0.018), involved in adaptive decision-making and similarly elevated in gamers (p = 0.045); and the left anterior cingulate cortex pregenual (r = –0.33, p = 0.045), which supports performance monitoring and adaptive control and was also higher in gamers (p = 0.008). The right postcentral gyrus (r = –0.32, p = 0.048), associated with sensorimotor integration and proprioception, also showed a significant behavioral correlation, although this region did not show a group difference in node degree.

Interestingly, a higher node degree in the left superior occipital gyrus was associated with slower response times (r = 0.32, p = 0.048), suggesting a potential tradeoff in information distribution. From the perspective of CRR, this may reflect a diffusion of vital visual information of object trajectory across multiple processing routes, analogous to current splitting in a parallel electrical circuit, which may slow decision-making.

Altogether, these findings underscore the role of enhanced SC-dFC efficiency and node degree in visuomotor and executive regions as contributors to faster response execution in gamers. Enhanced efficiency in early visual and sensorimotor regions, along with greater connectivity in salience and control hubs, appears to facilitate rapid stimulus-response transformations. These results align with the CRR hypothesis, suggesting that gamers optimize directional communication along more effective pathways, which would minimizing reliance on cerebellar feedback loops and reducing response latency. In contrast, non-gamers' greater reliance on memory and feedback-driven control systems may underlie slower, more deliberative response strategies.

4.2.6 Integration with Prior Research

This section builds on prior research into video game-induced neuroplasticity by further contextualizing previously reported findings from this dataset and demonstrating how structurally constrained functional and directed connectivity changes contribute to enhanced visuomotor decision-making response time (RT) (Jordan & Dhamala, 2022a; Jordan & Dhamala, 2022b; Jordan, 2021). Several key regions previously identified as critical for video game-related neural enhancements reappear in the current analysis, particularly in the domains of visuomotor processing and attentional coordination.

One notable example is the right lingual gyrus, which in earlier work showed significant group differences in BOLD activation between gamers and non-gamers. In the present analysis, this region exhibited stronger SC-FC connectivity with the cerebellum ($r = –0.38$, $p = 0.016$), a relationship that also correlated with faster RT. This finding reinforces the lingual gyrus's role in supporting rapid visual-motor transformations (Jordan & Dhamala, 2022b).

Additionally, improvements in connectivity between the dorsal attention network (DAN) and the salience network (SN) were observed in gamers, surviving Bonferroni correction ($p < 0.05$). These enhancements suggest more efficient attentional coordination and flexible network switching, likely enabling gamers to focus more effectively on task-relevant stimuli (Jordan & Dhamala, 2022a). Expanding on these results, the current findings indicate that gamers differ from non-gamers not only in top-down DAN→SN attention allocation but also in how they process motion information. Specifically, the data support the idea that, through long-term engagement with action video games, cognitive resources are gradually reallocated toward more optimized neural pathways that incorporate scene-specific visual information, particularly relative motion cues, which in turn improve RT during visuomotor decision-making tasks.

A central region in this dynamic is the supracallosal (dorsal) anterior cingulate cortex (ACC), a key node within the salience network involved in top-down attention and internal conflict monitoring between competing motor plans. In the current study, gamers exhibited significantly higher SC-dFC node degree in both the subgenual ($p = 0.028$) and pregenual ($p = 0.008$) ACC, suggesting greater centrality in circuits involved in urgency signaling, adaptive control, and performance monitoring. Notably, node degree in the left pregenual ACC was also correlated with faster RT ($r = –0.33$, $p = 0.045$), consistent with its role in resolving action conflicts under pressure and optimizing behavioral responses.

Although the subgenual ACC did not correlate with RT, its elevated connectivity likely reflects affective modulation, heightening motivational salience and time-sensitive urgency signaling to the suprarcallosal ACC. These two regions appear to work in tandem, with the subgenual ACC driving arousal and the supracallosal ACC coordinating rapid executive

responses. Supporting this view, stronger directed connectivity from the right subgenual to right supracallosal ACC was significantly associated with faster RT ($r = –0.51$, $p = 0.0009$), suggesting that a streamlined affective-to-executive signaling pathway is a strong indicator of decision-making RT.

Additional SC-dFC connections involving pregenual and supracallosal ACC regions also tracked with faster RT. These included connections from the right pregenual ACC to the left pregenual ACC ($r = –0.33$, $p = 0.036$), from the left pregenual ACC to the right supracallosal ACC ($r = –0.38$, $p = 0.0169$), and from the right pregenual ACC to the right supracallosal ACC ($r = –0.33$, $p = 0.038$).

Our results from this chapter also reinforce earlier findings from Chapter 3, which showed that functional connectivity in the left dorsal stream is enhanced in gamers (Holm-Bonferroni corrected, $p < 0.05$), with a significant correlation to faster response times ($r = –0.41$; Holm-Bonferroni corrected, $p < 0.05$). Specifically, gamers exhibited increased FC in the left superior occipital gyrus (L SOG) and superior parietal lobule (L SPL), core dorsal stream regions essential for visuomotor integration. In this chapter, faster response times were significantly associated with higher local efficiency in both SC-FC ($r = –0.38$, $p = 0.016$) and SC-dFC ($r = –0.48$, $p = 0.002$) within the left superior occipital gyrus (L SOG), supporting the interpretation that enhanced dorsal stream function in gamers facilitates more efficient trajectory estimation and visuomotor integration.

Interestingly, however, greater SC-FC node degree in the L SOG had a positive correlation with RT ($r = 0.38$, $p = 0.019$), suggesting that excessive reliance on early-stage visual

processing may lead to a less efficient visuomotor strategy—analogous to splitting current across too many paths in a parallel circuit.

Collectively, these findings lend further support to the CRR hypothesis, which posits that long-term action video game experience drives a reallocation of cognitive resources toward more efficient visuomotor decision-making circuits. By reinforcing salience detection and motion tracking systems, AVG experience would enable rapid, accurate responses in high-pressure environments. These results underscore the potential role of adaptive neural processing and network refinements as key mechanisms that underlie AVG-induced neuroplasticity.

4.2.7 Evaluation of the CRR Hypothesis

The goal of this chapter was to formally evaluate the Cognitive Resource Reallocation (CRR) hypothesis as a mechanistic explanation for the enhanced visuomotor decision-making observed in long-term action video game (AVG) players. CRR posits that sustained AVG engagement gradually reallocates cognitive resources toward more efficient, feedforward visuomotor pathways, favoring circuits that support rapid, goal-directed responses over slower, deliberative feedback loops. This reallocation is expected to manifest as anatomically plausible changes in both the structure and dynamics of neural networks, supporting more efficient visuomotor decision making through enhancements in visual processing, visuomotor integration, attentional control, and cognitive flexibility. To test this hypothesis, this section focuses on group-level differences that also showed significant correlations with response time (RT). These findings represent the most direct evidence with which to evaluate CRR as a candidate explanation of the behavioral advantage observed in gamers.

We observed group-level differences in SC-FC and SC-dFC that tracked with RT. For example, non-gamers exhibited stronger SC-FC between the left middle temporal gyrus and left inferior temporal gyrus ($p = 0.002$), a connection positively correlated with slower RTs ($r = 0.36$, $p = 0.025$). This suggests a decision-making strategy weighted toward detailed object recognition, potentially increasing stimulus evaluation time. By contrast, gamers showed stronger SC-dFC from the left parahippocampal gyrus to the left superior temporal pole ($p = 0.034$), a connection negatively correlated with RT ($r = –0.36$, $p = 0.022$). This pathway likely facilitates more efficient integration of scene-specific contextual information and relative motion, aligning with a context-driven decision-making strategy.

This interpretation is supported by greater SC-dFC local efficiency in both the left superior temporal pole ($p = 0.029$, $r = –0.33$) and the left parahippocampus ($p = 0.033$, $r = –0.34$), indicating more efficient local integration of scene-relevant information in gamers. While efficiency in these regions did not differ between groups, the fact that gamers demonstrated stronger SC-dFC between them, coupled with the negative RT correlation, supports a shift toward optimized visuospatial processing of salient scene-specific cues.

In contrast, non-gamers demonstrated stronger SC-dFC from the right insula to the right posterior orbitofrontal cortex (OFC) ($p = 0.043$), a connection positively correlated with RT ($r = 0.36$, $p = 0.025$), tracking with slower response times. The right insula is involved in interoception and uncertainty monitoring, while the posterior OFC supports outcome evaluation and decision inhibition. Stronger SC-dFC signaling from the right insula to the right posterior OFC likely reflects a heightened emphasis on internal deliberation and iterative uncertainty

reduction in non-gamers, amplifying the speed-accuracy tradeoff by promoting accuracy at the cost of RT.

In line with this interpretation, gamers exhibited significantly higher SC-FC node degree in the right insula ($p = 0.017$), which was associated with faster RT, as indicated by its negative correlation ($r = –0.32$, $p = 0.047$). While both groups appear to engage the right insula during visuomotor decision-making, gamers were shown to benefit more from its involvement due to greater network centrality, amplifying its role in rapid salience detection and adaptive interoceptive control. From this evidence, it is clear that gamers tend to leverage right insular engagement more effectively by tending to establish it as more central to the decision-making process to interoceptively monitor more regions, tending to devote less resources to support a directed connection to the posterior OFC, while non-gamers tend to recruit the right insula in such a way that aligns more closely with canonical speed-accuracy tradeoffs.

SC-FC and SC-dFC node degrees also revealed consistent enhancements in gamers. SC-FC node-degree of the left cerebellum lobule 3 tended to be greater in non-gamers ($p = 0.009$), and correlated with slower RTs ($r = 0.32$, $p = 0.044$), indicative of a more feedback-dependent motor correction strategy, once again aligning with a canonical speed-accuracy tradeoff. In contrast, the pregenual ACC had a higher SC-dFC node degree in gamers ($p = 0.008$) and was significantly correlated with faster RTs ($r = –0.33$, $p = 0.045$), suggesting a role in top-down attentional control and more effective resolution of internal conflict regarding competing motor plans.

Higher local efficiency in the left superior occipital gyrus (SOG) was associated with faster response times in both SC-FC ($r = –0.38$, $p = 0.016$) and SC-dFC ($r = –0.48$, $p = 0.002$).

Although no group differences were observed in SOG efficiency, these results reinforce the dorsal stream's critical role in visuomotor integration, particularly during the sensory accumulation phase of decision-making, where object motion and trajectory must be rapidly estimated and an imminent motor response is required. As shown in Section 3.1.2, this system is functionally enhanced in gamers, underscoring the dorsal stream's contribution to more efficient visuomotor decision-making.

Taken together, the evidence from this study rejects the null hypothesis that CRR is not a plausible explanatory principle for the visuomotor decision-making advantage observed in gamers. Across SC-FC and SC-dFC modalities, local network properties, and response time correlations, we observed converging evidence that long-term AVG engagement reflects a reallocation of cognitive resources, which would induce neuroplastic refinements that support a more effective visuomotor decision-making strategy. Notably, no contradictions were observed within this dataset, providing unilateral support for CRR as a viable mechanistic account of experience-driven neuroplastic refinement associated with enhanced visuomotor decision-making in the context of AVG experience.

While CRR was found to be strongly supported as a plausible mechanistic explanation for enhanced visuomotor performance in gamers, it is important to consider what kinds of findings would have contradicted the hypothesis. CRR would be challenged if non-gamers showed stronger connectivity or network properties in task-relevant circuits that also predicted faster response times, especially if such markers were absent or weaker in gamers. It would also raise concerns if neural enhancements in gamers were limited to only part of the visuomotor decision process, while non-gamers showed stronger tuning in other equally relevant

components. Another challenge to CRR would come from evidence that pre-existing individual differences, such as globally more efficient networks unrelated to task relevance, predisposed individuals both to faster performance and a higher likelihood of gaming. This would suggest a selection effect rather than a plasticity-driven process. Similarly, if non-gamers showed stronger brain–behavior correlations in task-relevant areas than gamers, that too would challenge CRR. However, none of these patterns were observed. Instead, we found consistent adaptations in gamers across task-relevant networks that closely track behavioral performance. These findings support cognitive resource reallocation as the mechanism underlying the observed neuroplastic changes.

4.2.8 Concluding Remarks

This study investigates how long-term action video game play could induce neuroplastic refinements that enhance visuomotor decision-making and its supporting cognitive functions. While prior research has established that gamers exhibit faster response times and cognitive benefits, the specific neural mechanisms underlying these improvements have remained unclear.

Our findings unilaterally support Cognitive Resource Reallocation (CRR) as the underlying principle governing gaming-related neuroplasticity, with no contradictions observed across any facet of our results. This shift reflects a transition from feedback-driven motor correction to anticipatory, feedforward processing, optimizing response efficiency and enhancing relative motion tracking between targets and distractors. These improvements are supported by strengthened connectivity in circuits involved in visual processing, visuomotor integration, attentional control, and cognitive flexibility, resulting in a more streamlined neural architecture for action selection in dynamic environments.

This conclusion, evidenced by SC-FC and SC-dFC connectivity analyses, graph-theoretic metrics, and behavioral correlations with response time, is consistent with CRR's mechanistic account of how cognitive resources are selectively reallocated to task-relevant pathways. This reallocation leads to measurable behavioral advantages, including an average improvement of approximately 190 milliseconds in response time among gamers. By supporting CRR as a plausible explanatory framework for experience-dependent neuroplasticity, this work advances our understanding of how intense visuomotor engagement refines brain networks to support rapid, adaptive decision-making in fast-paced, graphically rich environments such as AVGs.

5 WHOLE BRAIN ANALYSIS: PCA-BASED ROI SELECTION

This chapter addresses the challenge of understanding large-scale neuroplasticity in the context of long-term action video game (AVG) play using multimodal neuroimaging data. The overarching goal of this analysis is to investigate how AVG experience shapes structural (SC), functional (FC), and directed (dFC) connectivity, as well as region-specific structure–function coupling, both undirected (SFC) and directed (SdFC sender), as described in Section 2.2.4.5. However, whole-brain connectivity matrices derived from these modalities are extremely high-dimensional relative to the sample size, making exploratory analyses difficult without a principled strategy for dimensionality reduction.

By the time this analysis was conducted, Cognitive Resource Reallocation (CRR) had already received strong empirical support from the tractography-constrained findings presented in Chapter 4. While tractography offers a powerful means of reconstructing white matter pathways, it remains an indirect, model-based estimate of anatomical connectivity, subject to algorithmic limitations such as minimum streamline length, angular threshold, and spatial resolution. As such, even though the tractography-constrained framework leverages biologically plausible reconstructions of white matter tracts using the AAL3 atlas, it may still miss fine-grained or multi-synaptic interactions that support emergent coordination across distributed brain networks. Consequently, behaviorally relevant functional and directed connectivity may go undetected or be overlooked when filtered through these structural constraints. Furthermore, the tractography data itself had not been analyzed directly in Chapter 4, but was instead used as a structural mask to constrain the functional analysis. A more complete account of how CRR would refine neural pathways in gamers in response to prolonged AVG experience requires

examining structural and functional adaptations in parallel, as each modality may capture distinct yet complementary aspects of experience-dependent plasticity.

Initial attempts to isolate meaningful whole-brain functional effects using conventional statistical thresholding (e.g., $p < 0.05$) without tractography constraints yielded an overwhelming number of results across AAL3's 166 × 166 pairwise connections, with no principled way to distinguish signal from noise. The need to correct for multiple comparisons—27,390 pairwise tests in the case of dFC, and half as many for FC due to its undirected, symmetric structure across 166 regions (excluding self-connections), severely diminished statistical power.

To address this, a complementary data-driven PCA-based approach was developed to sweep across the entire dataset and identify the strongest sources of inter-subject signal variance. If any meaningful adaptation was missed by the tractography-constrained analysis, this method would be well-positioned to detect it. In this way, data-driven and anatomically constrained frameworks work synergistically, with the former broadening discovery and improving statistical power and the latter anchoring findings in neurobiological plausibility. Unlike traditional PCA approaches that reduce time series or select top ROIs from early components, the region-cumulative PCA (rcPCA) method utilizes cumulative variance-weighted contribution scores across all components, up to a defined cumulative explained variance threshold. This balances the goal of capturing meaningful inter-subject variation while excluding spurious components that reflect noise or isolated variance.

An ICA-based approach to dimensionality reduction was initially considered, but rcPCA was ultimately developed as a more suitable alternative for this study's goal of investigating how AVG experience shapes SC, FC, dFC, SFC, and SdFC sender profiles within a predefined

anatomical atlas such as AAL3. Independent Component Analysis (ICA) is a powerful tool for uncovering distributed functional networks via blind source separation, using higher-order statistics such as kurtosis or negentropy (Calhoun *et al*., 2001; 2009), and has yielded valuable insights into large-scale brain organization. While ICA excels at detecting latent sources and identifying network-level structure, it does not natively support anatomically localized, region-level ranking. Techniques such as spatial template matching, dual regression, ICN labeling, and joint ICA each extend ICA's utility with template matching aiding anatomical alignment, dual regression estimating subject-level component expression, ICN labeling providing network-level categorization, and joint ICA enabling multimodal data fusion. However, none of these approaches cleanly resolve the core challenge of identifying which anatomical regions within a predefined atlas like AAL3 contribute most meaningfully to inter-subject variability across connectivity modalities.

By contrast, the variance-based rcPCA method retains direct anatomical interpretability by operating within a predefined atlas (AAL3) from the outset. It leverages variance, a foundational statistical measure, rather than more abstract higher-order moments, offering a conceptually transparent and analytically targeted approach tailored to the needs of this study. This makes rcPCA particularly well-suited to the goal of identifying high-variance regions that meaningfully contribute to individual differences, enabling focused, region-level statistical comparisons across structural, functional, and directed connectivity measures.

To test CRR using a multimodal approach at the whole-brain level, we examined connectivity differences in high-variance ROIs identified using rcPCA in SC, FC, dFC, SFC, and SdFC sender modalities. This allowed us to ask which mechanistic shifts in information-rich

brain areas are most involved in the neural adaptations distinguishing action gamers from non-gamers, and how these adaptations support enhanced visuomotor performance.

Our primary hypothesis is that gamers, due to their long-term AVG experience, will reflect neuroplastic refinements that reduce visuomotor surprise in task-relevant pathways by increasing anticipatory feedforward processing and decreasing reliance on uncertainty-reducing feedback loops, patterns typically observed in canonical speed–accuracy tradeoffs (Drugowitsch *et al*., 2014; 2015) and consistent with CRR predictions. Visuomotor surprise, in this context, refers to unresolved prediction error (Friston, 2010), arising throughout all stages of a visuomotor decision from sensory accumulation to action execution, and is expected to be more effectively minimized through the refinement of efficient, task-relevant circuits. In the context of our modified moving-dots task, gamers are expected to adapt more effectively to either possible outcome of a 50/50 decision, reflecting enhanced cognitive flexibility and attentional control.

Our secondary hypothesis is that rcPCA will reveal behaviorally relevant structure–function couplings and connectivity patterns that further elucidate the ~190 ms response time advantage observed in gamers, complementing the tractography-constrained findings presented in Chapter 4. We expect these effects to align with CRR's prediction that long-term AVG experience drives resource reallocation toward efficient visuomotor decision pathways and away from redundant or compensatory circuits, thereby refining the task-specific networks that support proficient AVG performance.

Although we do not directly quantify visuomotor surprise, it is treated as a latent cognitive property inferred from features like feedforward transformation, motor readiness, and anticipatory connectivity. Gamers are expected to show stronger alignment in task-relevant brain

regions between structural and functional signals (e.g., SFC, SdFC sender) and more selective engagement of task-relevant circuits. Non-gamers, by contrast, are expected to rely more heavily on early visual processing, broader compensatory feedback mechanisms, and less efficient transformations from perception to action.

In summary, this chapter utilizes rcPCA as a data-driven tool for identifying consistent covarying patterns in multimodal neuroimaging data and for further evaluating CRR as a formal mechanism of experience-driven neuroplasticity associated with long-term AVG experience. The results are expected to extend and complement the findings presented in earlier sections.

5.1 Results

The rcPCA ROI selection strategy followed standard PCA-based practices (Jolliffe & Cadima, 2016; Lee *et al*., 2021) commonly used in neuroimaging studies (Lee *et al.,* 2021; Mwangi *et al*., 2014), prioritizing high-loading features from each principal component (Kucukboyaci *et al*., 2014). Specifically, we selected the top 20 contributing ROIs per component to highlight regions that most strongly account for structured variance, while minimizing the inclusion of low-weight contributors across each modality, as described in Section 2.2.4.6. Figure 5.1 illustrates this selection for FC and dFC modalities, including sender, receiver, and total modes. This approach is consistent with established PCA interpretation practices, which emphasize the most dominant features from early components to enhance interpretability.

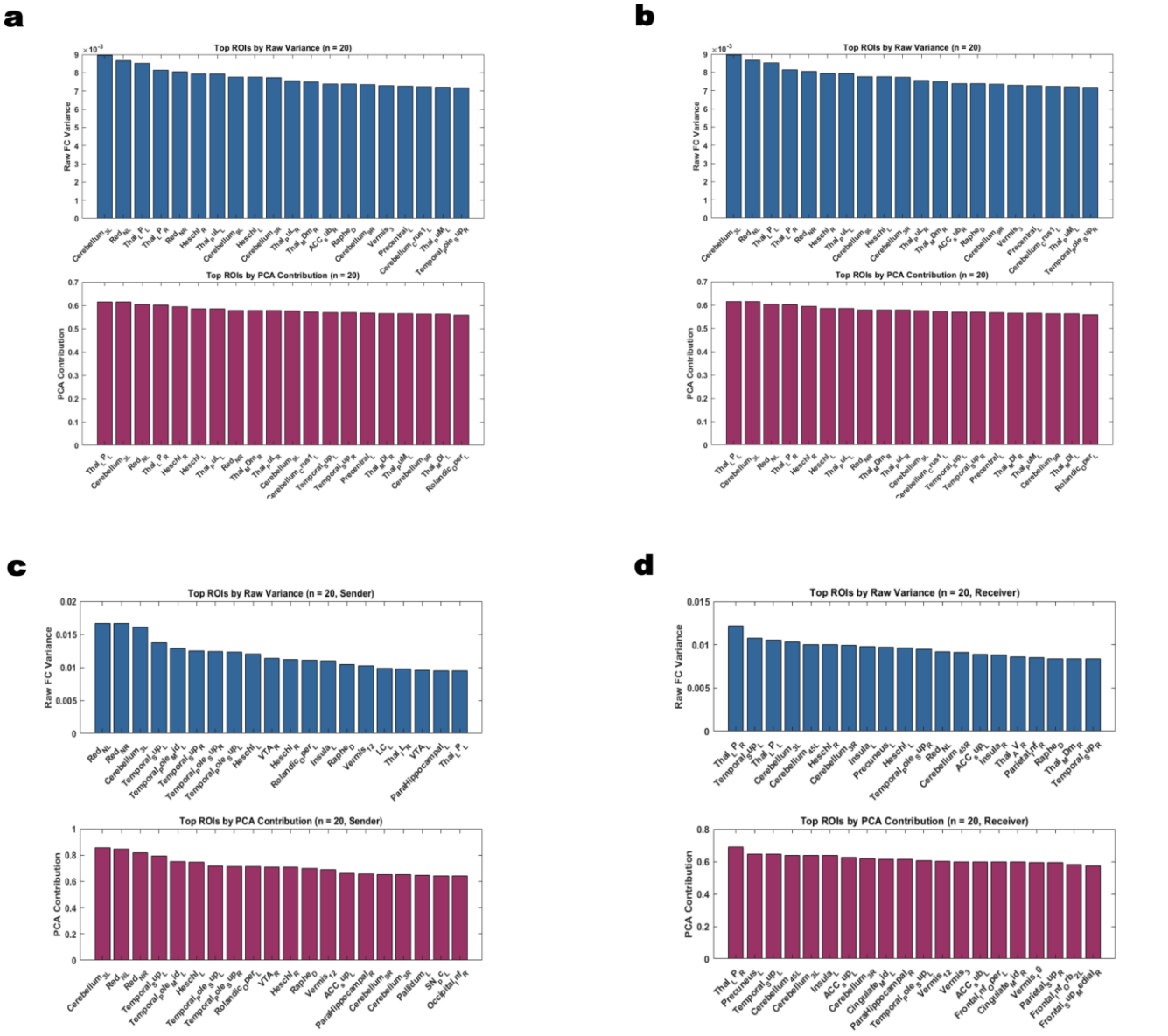

Figure 5.1 Top 20 PCA Selected ROIs from FC and dFC Explained Variance. Principal component analysis (PCA) was applied to undirected functional connectivity (FC) and directed functional connectivity (dFC), with dFC further decomposed into total, sender, and receiver modes. ROIs names taken from the AAL3 atlas were ranked by their contribution to across-subject variance, and the top 20 were selected based on a cumulative 80% explained variance threshold. (a) FC: undirected Pearson correlations. (b) dFC total: summed Granger causality across source and target roles. (c) dFC sender: variance from outgoing influences. (d) dFC receiver: variance from incoming influences. This decomposition highlights asymmetric functional dynamics and distinguishes ROIs involved in information transmission versus reception.

Validation of rcPCA-derived ROIs utilized a combination of rank correlation, permutation testing, and hypergeometric overlap statistics. Using a significance threshold of $p < 0.001$, this approach confirmed that the observed alignments between PCA-derived ROI rankings and raw variance were statistically robust and unlikely to occur by chance. The full validation procedure is described in Section 2.2.4.7. For subsequent group-level comparisons, the Storey–Tibshirani (ST) method was applied only to FC, where its assumptions held; all other modalities used the Benjamini–Hochberg (BH) procedure for FDR correction. Further details on modality-specific correction rationale are provided in Section 2.2.4.8.

5.1.1 Group Differences in Functional and Directed Connectivity

5.1.1.1 Group Differences in Functional Connectivity

Whole-brain FC analysis revealed significant group differences ($p < 0.05$) between gamers and non-gamers, concentrated in thalamic, cerebellar, midbrain, and temporal regions (Figure 5.2a). PCA-selected ROIs, validated in Figure 5.2b, showed robust effects following FDR correction. Gamers exhibited significantly stronger functional connectivity between the right red nucleus and the right pulvinar thalamic nucleus ($p = 0.0061$, $q = 0.02$, $d = 0.85$), and between left cerebellar lobule 3 and both the right superior temporal pole ($p = 0.0014$, $q = 0.035$, $d = 1.12$) and the left caudate nucleus ($p = 0.00093$, $q = 0.03$, $d = 1.00$). In contrast, non-gamers showed stronger connectivity between left cerebellar lobule 3 and the left intralaminar thalamic nuclei ($p = 0.00085$, $q = 0.042$, $d = –1.26$), the left substantia nigra pars reticulata ($p = 0.002$, $q = 0.042$, $d = –1.10$), and both the right and left ventrolateral thalamic nuclei ($p = 0.01$, $d = –0.76$; $p = 0.03$, $d = –0.87$, respectively). These effects reflect consistent, large-magnitude differences in functional connectivity across subcortical–cerebellar circuits. Absolute effect sizes were consistently large, ranging from $d = 0.76$ to 1.26 across significant connections. Full statistical

results are organized in Table 5.1 and violin plot distributions illustrating these effects are shown in Figure 5.2c.

Table 5.1 Group differences in functional connectivity between action video game players and non-gamers, derived from rcPCA-selected ROIs taken from the AAL3 atlas

Functional Connectivity		***p*-value**	***q*-value (ST)**	**Cohen's *d***
Red N R	Thal Pul R	0.0061	0.02	0.85
Cerebellum 3L	Temporal Pole Sup R	0.0014	0.035	1.12
Cerebellum 3L	Caudate L	0.00093	0.03	1.00
Cerebellum 3L	Thal IL L	0.00085	0.042	-1.26
Cerebellum 3L	SN pr L	0.002	0.042	-1.10
Cerebellum 3L	Thal VL R	0.01	_	-0.76
Cerebellum 3L	Thal VL L	0.03	_	-0.87

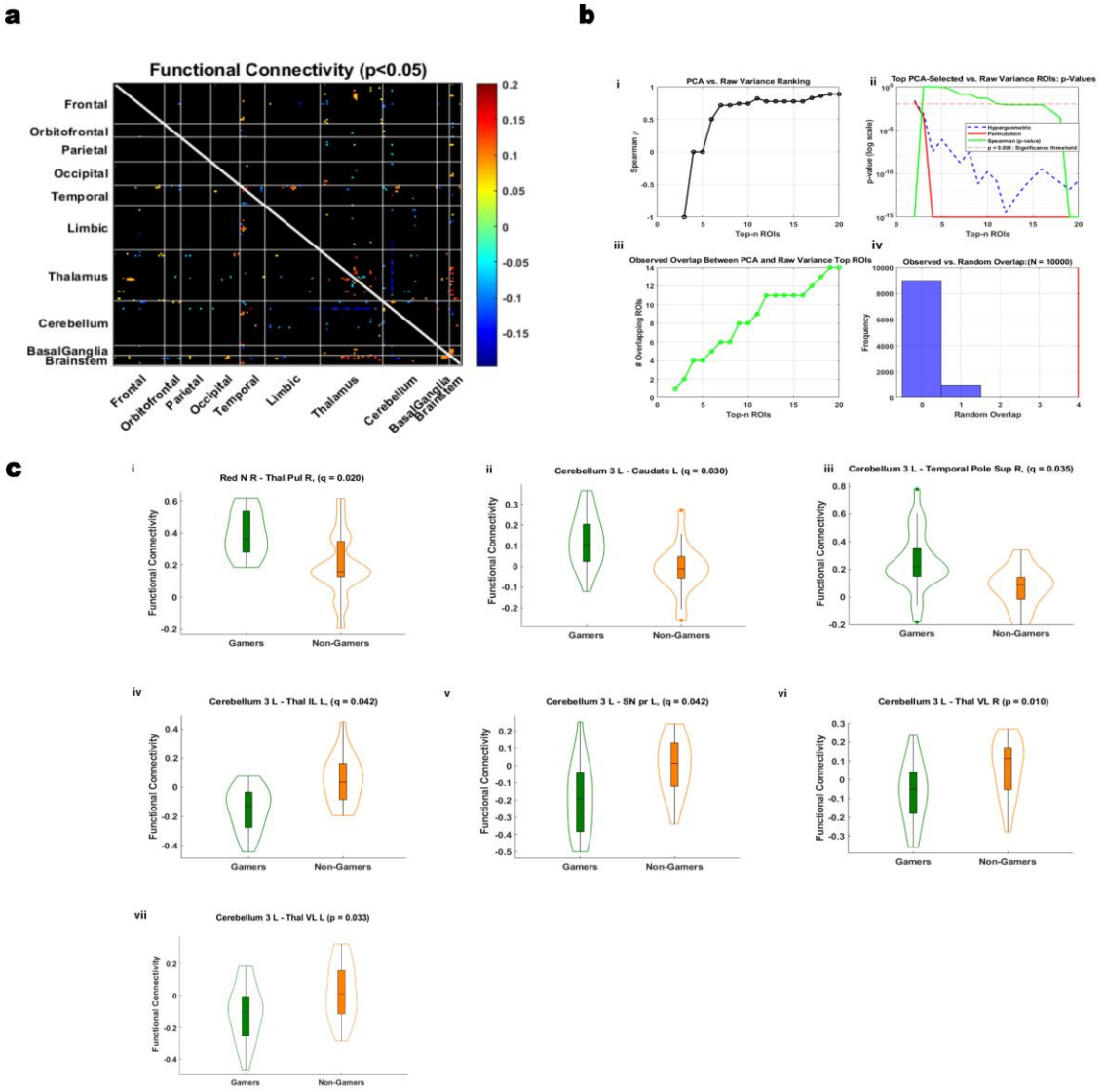

Figure 5.2 Functional Connectivity Differences Involving Top PCA ROIs (a) Whole-brain FC matrix showing significant group differences ($p < 0.05$, uncorrected), organized by anatomical region.(b) Validation of the PCA-based method involved (i) Spearman's rank correlation (ρ) across top-n selections comparing PCA-weighted and raw variance-based rankings; (ii) Comparison of statistical sensitivity using Spearman correlation, hypergeometric overlap p-values, and permutation-derived p-values between PCA- and raw-ranked ROIs; (iii) Overlap between PCA- and raw-ranked ROIs increases systematically with top-n selections; (iv) PCA-selected ROI overlap exceeds chance across 10,000 permutations. Region names are taken from the AAL3 atlas

5.1.1.2 Group Differences in Directed Functional Connectivity

Directed connectivity analyses using Granger causality revealed significant differences in directed functional connectivity (dFC) between gamers and non-gamers across sender, receiver, and total modes ($p < 0.05$, uncorrected). These effects were concentrated in midbrain, thalamic, cerebellar, and anterior cingulate cortex (ACC) regions (Figure 5.3a–c). In sender mode, non-gamers exhibited stronger directed influence from the left supracallosal ACC to the right ventrolateral thalamus ($p = 0.0003$, $q = 0.042$, $d = –0.91$), the only connection that survived false discovery rate (FDR) correction. Additional uncorrected differences included stronger non-gamer outflow from the left ACC to the left cerebellar lobule 7b ($p = 0.004$, $d = –0.65$) and from the right ventral tegmental area (VTA) to both the right ventrolateral thalamus ($p = 0.006$, $d = –0.96$) and the left cerebellar lobule 3 ($p = 0.012$, $d = –0.75$).

In receiver mode, non-gamers showed greater inflow to the left supracallosal ACC from the left cerebellar lobule 3 ($p = 0.004$, $d = –1.00$) and the right locus coeruleus ($p = 0.031$, $d = –0.83$), while bilateral VTA and right thalamus also showed elevated input to the left cerebellum. Total mode effects reflected overlapping but distinct connectivity patterns, including stronger non-gamer influence from the left ACC to the right thalamus ($p = 0.002$, $d = –0.98$) and from the left cerebellar lobule 3 to the left ACC ($p = 0.011$, $d = –0.87$).

Effect size magnitudes across modes ranged from $d = 0.59$ to 1.00, indicating robust directional asymmetries in dFC across groups. Full statistical results are reported in Table 5.2, and violin plots showing group distributions for these effects are provided in Figure 5.3.

Table 5.2 Group differences in directed connectivity (sender, receiver, and total modes) between action video game players and non-gamers, based on rcPCA-selected AAL3 ROIs

Directed Connectivity (Sender)		***p*-value**	***q*-value (BH)**	**Cohen's *d***
ACC sup L	Thal VL R	0.0003	0.042	-0.91
ACC sup L	Cerebellum 7b L	0.004	_	-0.65
VTA R	Thal VL R	0.006	_	-0.96
VTA R	Cerebellum 3L	0.012	_	-0.75
Directed Connectivity (Receiver)		***p*-value**	***q*-value (BH)**	**Cohen's *d***
Cerebellum 3L	ACC sup L	0.004	_	-1.00
LC R	ACC sup L	0.031	_	-0.83
VTA L	Cerebellum 3L	0.0008	_	-0.91
VTA R	Cerebellum 3L	0.008	_	-0.75
Thal VL R	Cerebellum 3L	0.029	_	-0.61
Directed Connectivity (Total)		***p*-value**	***q*-value (BH)**	**Cohen's *d***
ACC sup L	Thal VL R	0.002	_	-0.98
Cerebellum 3L	ACC sup L	0.011	_	-0.87
Red N R	SN pc R	0.024	_	-0.79
Thal LP R	Cerebellum 3L	0.038	_	-0.59

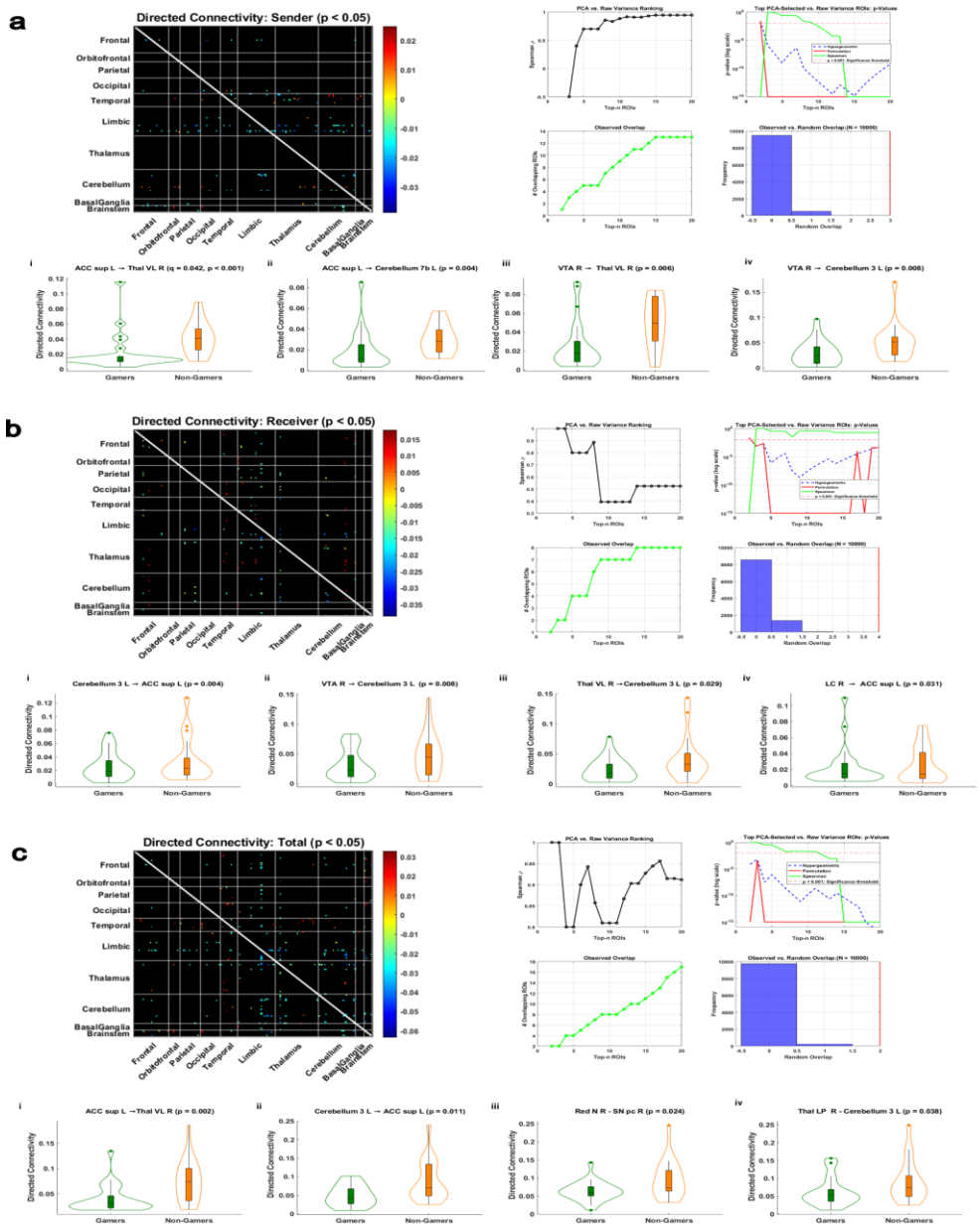

Figure 5.3 Directed connectivity differences involving top PCA ROIs. Group-level differences in directed functional connectivity (dFC) between gamers and non-gamers based on PCA-derived regions of interest. Each panel displays the dFC matrix of significant group differences ($p < 0.05$), selection stability validation, and violin plots highlighting the strongest effects. Panel (a) shows sender-mode results reflecting group differences in outgoing influence, including a connection from the left superior anterior cingulate cortex to the right ventrolateral thalamus that survived FDR correction ($q < 0.05$), alongside uncorrected effects from the right ventral tegmental area to cerebellar and thalamic targets. Panel (b) presents receiver-mode results indicating group differences in incoming influence, with effects observed in the left cerebellar lobule 3 (from the right VTA and right ventrolateral thalamus) and the left superior anterior cingulate cortex (from the right locus coeruleus). Panel (c) shows total influence results, combining sender and receiver roles, with significant effects involving the left superior anterior cingulate cortex, the right substantia nigra pars compacta, and the left cerebellar lobule 3.

5.1.2 Extensions of PCA-Based ROI Selection Beyond Functional Connectivity

5.1.2.1 Group Differences in Structural Connectivity

Structural connectivity (SC) analysis using diffusion measures, fractional anisotropy (FA), axial diffusivity (AD), isotropy (ISO), and non-restricted diffusion imaging (NDRI) described in Table 2.3 revealed significant group-level differences between gamers and non-gamers involving rcPCA-derived ROIs ($p < 0.05$), as shown in Figure 5.4. For FA, reduced connectivity in non-gamers was observed between the left calcarine cortex and the left superior occipital gyrus ($p = 0.036$, $d = –0.78$), a connection also associated with slower response times in behavioral analysis (see Figure 5.6).

In the AD measure, a robust group difference emerged between the left superior medial frontal gyrus and the left middle cingulate cortex ($p = 0.0003$, $q = 0.047$, $d = 1.16$), the only FA or AD comparison to survive FDR correction. ISO-based analyses revealed stronger connectivity in gamers between the left lingual gyrus and the left caudate ($p = 0.0002$, $q = 0.026$, $d = 1.22$) and between the right lingual gyrus and the left cerebellar lobule 6 ($p = 0.0007$, $q = 0.047$, $d = 0.96$). These region pairs also showed significant differences in the NDRI measure, with both comparisons maintaining significance following FDR correction.

Absolute effect sizes across all measures were consistently large, with *d* values ranging from 0.78 to 1.22. These findings underscore robust SC differences within posterior cortical and subcortical circuits relevant to visuomotor integration. Full statistical results, including all p-values, FDR-adjusted q-values, and Cohen's *d* effect sizes, are presented in Table 5.3. Violin plots visualizing these effects are shown in Figure 5.4.

Table 5.3 Group differences in structural connectivity measures (FA, AD, ISO, NDRI) between action video game players and non-gamers based on rcPCA-selected AAL3 ROIs

Fractional Anisotropy (FA)		***p*-value**	***q*-value (BH)**	**Cohen's *d***
Calcarine L	Occipital Sup L	0.036	_	-0.78
Axial Diffusivity (AD)		***p*-value**	***q*-value (BH)**	**Cohen's *d***
Frontal Sup Medial L	Cingulate Mid L	0.0003	0.047	1.16
Isotropy (ISO)		***p*-value**	***q*-value (BH)**	**Cohen's *d***
Lingual L	Caudate L	0.0002	0.026	1.22
Lingual R	Cerebellum 6 L	0.0007	0.047	0.96
None-Restricted Diffusion (NDRI)		***p*-value**	***q*-value (BH)**	**Cohen's *d***
Lingual L	Caudate L	0.00008	0.037	0.97
Lingual R	Cerebellum 6 L	0.0007	0.047	0.87

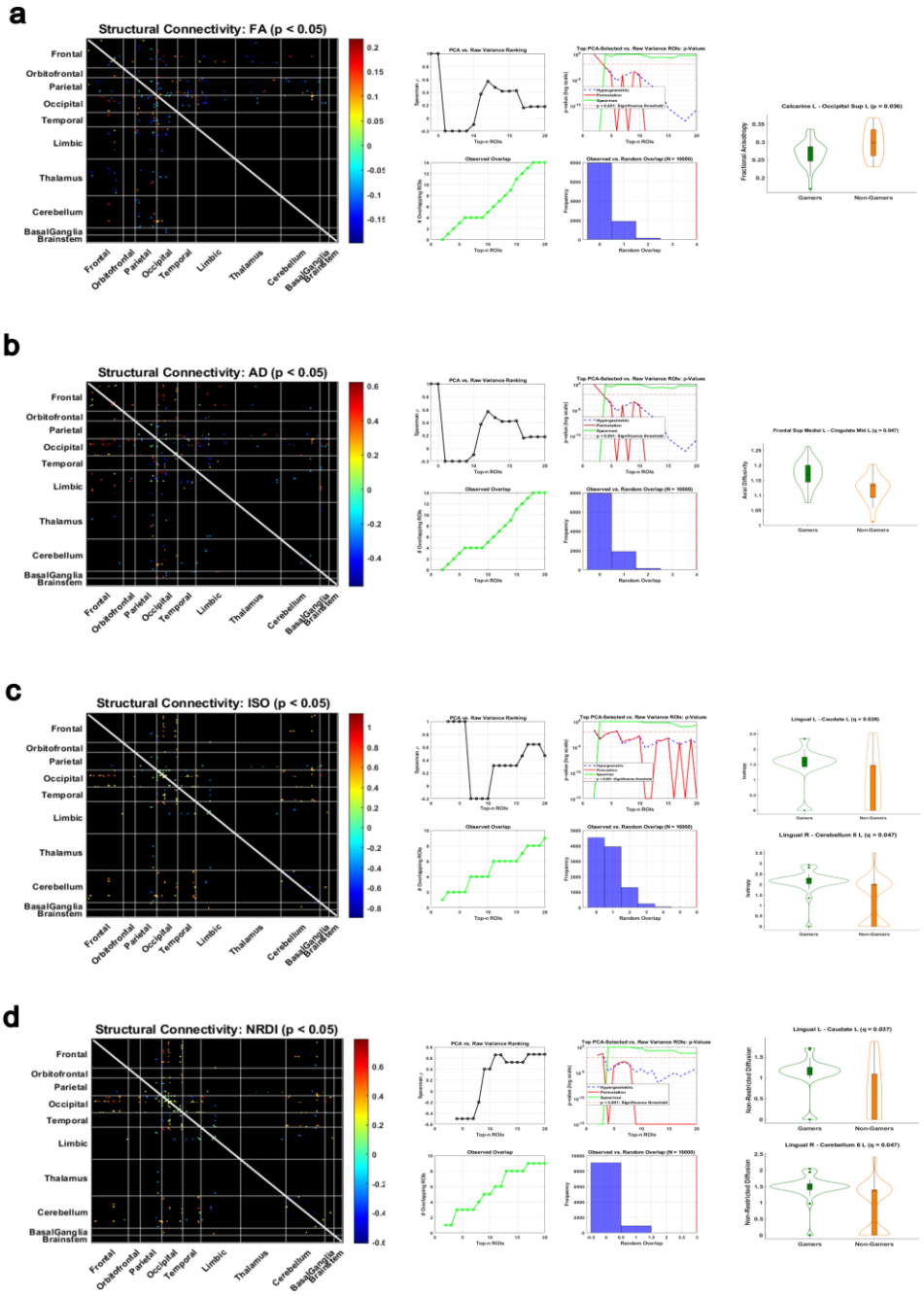

Figure 5.4 Structural connectivity differences filtered by top PCA ROIs Group-level structural connectivity (SC) differences between gamers and non-gamers across four diffusion MRI measures, limited to regions of interest (ROIs) identified through PCA-based selection from the AAL3 atlas. Each panel presents the SC matrix of significant group differences ($p < 0.05$), validation of selection stability, and violin plots highlighting the strongest effects. Panel (a) shows uncorrected differences in fractional anisotropy (FA) between the left calcarine cortex and the left superior occipital gyrus. Panel (b) displays axial diffusivity (AD) differences involving the left superior medial frontal gyrus and the left mid-cingulate cortex. Panel (c) illustrates isotropy (ISO) differences in connections between the lingual gyrus and cerebellar lobule 6. Panel (d) shows corresponding differences in non-restricted diffusion imaging (NRDI) across the same regions.

5.1.2.2 Group Differences in Structure–Function Coupling

Structure-function coupling measures the alignment between a region's structural connectivity measure and its corresponding capacity for functional load (Fotiadis *et al*., 2024). To quantify this relationship, Pearson correlations were computed between structural connectivity (SC) and both functional connectivity (FC) and directed functional connectivity (dFC sender mode). The undirected correlation with FC is referred to as SFC, while the correlation with sender-mode dFC is termed SdFC (sender). In the SFC condition, gamers exhibited significantly stronger coupling in the cerebellum. These included Vermis 3 with mean diffusivity ($p = 0.046$, $d = 0.64$), Vermis 9 with both mean length ($p = 0.024$, $d = 0.64$) and fractional anisotropy ($p = 0.049$, $d = 0.55$), and Cerebellum 10L with fractional anisotropy ($p = 0.046$, $d = 0.65$) and quantitative anisotropy ($p = 0.049$, $d = 0.65$).

In the SdFC sender condition, non-gamers showed significantly stronger coupling in Vermis 7 across multiple measures, including axial diffusivity ($p = 0.002$, $q = 0.048$, $d = –1.00$), isotropy ($p = 0.004$, $d = –0.97$), and restricted diffusion ($p = 0.004$, $d = –0.97$). Additional effects favoring non-gamers were found in the right calcarine cortex for count ($p = 0.038$, $d = –0.74$), ncount ($p = 0.015$, $d = –0.82$), and ncount2 ($p = 0.023$, $d = –0.82$), as well as in the left calcarine cortex ($p = 0.043$, $d = –0.59$).

Gamers, in contrast, exhibited stronger SdFC sender coupling in the left supracallosal anterior cingulate cortex for both ncount ($p = 0.020$, $d = 0.82$) and ncount2 ($p = 0.021$, $d = 0.83$), in the left medial orbitofrontal cortex for count ($p = 0.032$, $d = 0.74$), and in the right paracentral lobule for ncount ($p = 0.028$, $d = –0.67$).

Effect size magnitudes were moderate to large across both coupling modes, with *d* values ranging from 0.55 to 1.00. The Vermis 7–axial diffusivity pair was the only comparison to survive FDR correction. These findings highlight distinct structure–function coupling profiles between groups, particularly in cerebellar and occipital regions. Full statistical results are provided in Table 5.4, and violin plots illustrating these effects are shown in Figure 5.5.

Table 5.4 Group differences in structure–function coupling (SFC and sender dFC modes) between action video game players and non-gamers based on rcPCA-selected AAL3 ROIs

Coupling	Region	SC Measure	*p*	*q*	*d*
SFC	Vermis 3	Mean Diffusivity (MD)	0.046	—	0.64
	Vermis 9	Mean Length	0.024	—	0.64
	Vermis 9	Fractional Anisotropy (FA)	0.049	—	0.55
	Cerebellum 10L	Fractional Anisotropy (FA)	0.046	—	0.65
	Cerebellum 10L	Quantitative Anisotropy (QA)	0.049	—	0.65
SdFC (Sender)	Vermis 7	Axial Diffusivity (AD)	0.002	0.048	-1.00
	Vermis 7	Isotropy (ISO)	0.004	—	-0.97
	Vermis 7	Restricted Diffusion (RDI)	0.004	—	-0.97
	Calcarine R	count	0.038	—	-0.74
	Calcarine R	ncount	0.015	—	-0.82
	Calcarine R	ncount2	0.023	—	-0.82
	Calcarine L	count	0.043	—	-0.59
	ACC sup L	ncount	0.02	—	0.82
	ACC sup L	ncount2	0.021	—	0.83
	Frontal Medial Orb L	count	0.032	—	0.74
	Paracentral Lobule R	ncount	0.028	—	-0.67

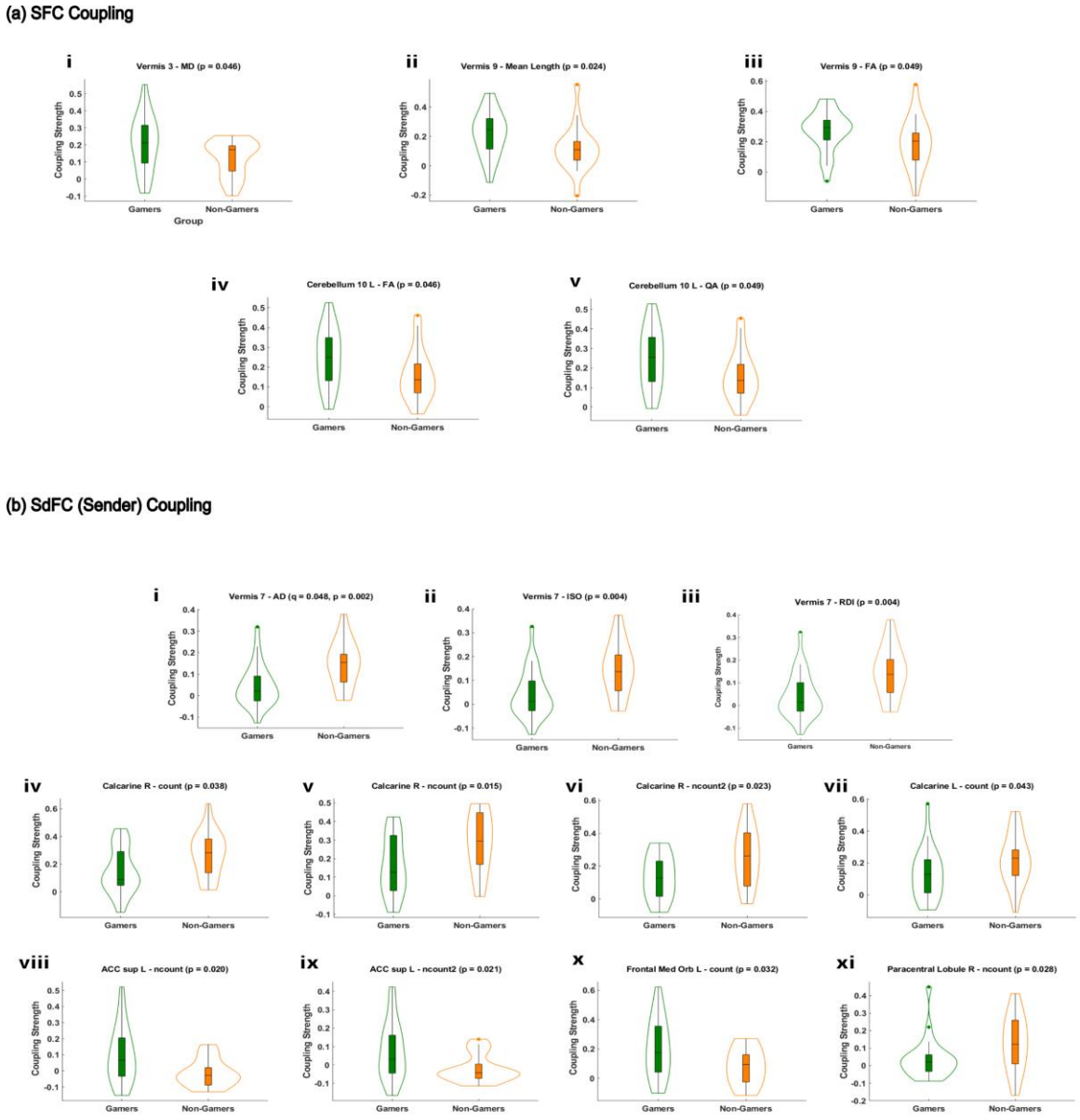

Figure 5.5 SFC and SdFC (Sender) Coupling Differences Involving Top PCA ROIs. Group-level differences in structure–function coupling strength between gamers and non-gamers, using rcPCA-derived ROI selections from the AAL3 atlas.(a) SFC coupling: Significant effects ($p < 0.05$) were observed across multiple structural measures—including mean diffusivity (MD), mean length, fractional anisotropy (FA), and quantitative anisotropy (QA)—involving Vermis 3, Vermis 9, and Cerebellum 10L. (b) SdFC (sender) coupling: Significant group differences emerged in Vermis 7 across intensive diffusion measures (AD, ISO, RDI), and in Calcarine cortex (bilaterally), ACC sup L, Frontal Med Orb L, and Paracentral Lobule R across extensive measures (count, ncount, ncount2). ROI selection and validation followed the same rcPCA-based procedure used in other connectivity modalities. A significant FDR-corrected effect ($q = 0.048$) was observed in Vermis 7–AD SdFC sender coupling.

5.1.3 Brain–Behavior Relationships

Response time was significantly associated with connectivity strength and structure–function coupling across modalities. Faster responses were linked to negatively sloped Spearman correlations, while slower responses were associated with positively sloped trends.

In functional connectivity, faster responses were linked to stronger connectivity between the right red nucleus and the right pulvinar thalamus ($r = –0.41$, $p = 0.009$), whereas slower responses were associated with increased connectivity in cerebellar and thalamic circuits, including the left cerebellar lobule 3 and the right substantia nigra pars compacta ($r = 0.33$, $p = 0.036$), as well as the left ventrolateral thalamus and the left cerebellar lobule 3 ($r = 0.33$, $p = 0.037$).

In directed connectivity, slower responses were correlated with increased influence from the right ventral tegmental area to the left cerebellar lobule 3 ($r = 0.41$, $p = 0.008$), from the right substantia nigra pars compacta to the right red nucleus ($r = 0.40$, $p = 0.003$), and from the left supracallosal anterior cingulate cortex to the left cerebellar lobule 7b ($r = 0.34$, $p = 0.032$). Additional significant effects included connections from the right lateral posterior thalamus to the left cerebellar lobule 3 ($r = 0.40$, $p = 0.009$) and from the right locus coeruleus to the left supracallosal anterior cingulate cortex ($r = 0.40$, $p = 0.010$).

In structural connectivity, slower responses were associated with higher fractional anisotropy between the left calcarine cortex and the left superior occipital gyrus ($r = 0.35$, $p = 0.020$), while faster responses were linked to lower fractional anisotropy between the left parahippocampal gyrus and the left precuneus ($r = –0.36$, $p = 0.011$), and to lower quantitative

anisotropy between the left superior temporal pole and the left orbital part of the inferior frontal gyrus ($r = –0.42$, $p = 0.005$).

In structure–function coupling, faster response times were associated with stronger coupling in the right mid-occipital cortex, including axial diffusivity ($r = –0.31$, $p = 0.050$) and non-restricted diffusion imaging ($r = –0.32$, $p = 0.042$). Stronger coupling in the right supracallosal anterior cingulate cortex was also associated with faster responses across multiple measures: axial diffusivity ($r = –0.44$, $p = 0.006$), fractional anisotropy ($r = –0.44$, $p = 0.006$), normalized quantitative anisotropy *(*$r = –0.39$, $p = 0.015$), and non-restricted diffusion imaging (r = –0.37, $p = 0.020$). In sender-mode coupling, faster responses were further linked to greater structure–function alignment from the right anterior cingulate cortex (*e.g.,* FA: $r = –0.44$, $p = 0.006$; NRDI: $r = –0.37$, $p = 0.020$; NQA: $r = –0.39$, $p = 0.015$), as well as from the left medial orbital frontal cortex ($r = –0.34$, $p = 0.035$) and the left calcarine cortex ($r = –0.34$, $p = 0.032$).

All brain–behavior correlations supporting these effects are organized in Table 5.5 and displayed in Figure 5.6.

Table 5.5 Significant Spearman correlations between multimodal brain connectivity measures, including functional, directed, structural, and structure–function coupling, and response time

Modality	Connection	Measure	*r*	*p*
Functional Connectivity	Red N R – Thal PuL R	FC	–0.41	0.009
	Cerebellum 3 L – SN pc R	FC	0.33	0.036
	Thal VL L – Cerebellum 3 L	FC	0.33	0.037
Directed Connectivity	VTA R → Cerebellum 3 L	dFC	0.41	0.008
	VTA R → Thal VL R	dFC	0.38	0.013
	ACC sup L → Cerebellum 7b L	dFC	0.34	0.032
	LC R → ACC sup L	dFC	0.40	0.01
	SN pc R – Red N R	dFC	0.40	0.003
	Thal LP R – Cerebellum 3 L	dFC	0.40	0.009
Structural Connectivity	Calcarine L – Occipital Sup L	FA	0.35	0.02
	Parahippocampal L – Precuneus L	FA	–0.36	0.011
	Temporal pole sup L – Frontal Inf Orb 2 L	AD	–0.42	0.005
Structure–Function Coupling (Undirected)	Occipital Mid R	AD	–0.31	0.05
	Occipital Mid R	NRDI	–0.32	0.042
Structure–Function Coupling (Sender)	ACC sup R	AD	–0.44	0.006
	ACC sup R	FA	–0.44	0.006
	ACC sup R	NQA	–0.39	0.015
	ACC sup R	NRDI	–0.37	0.02
	Frontal medial orbital L	Count	–0.34	0.035
	Calcarine R	NRDI	0.34	0.032

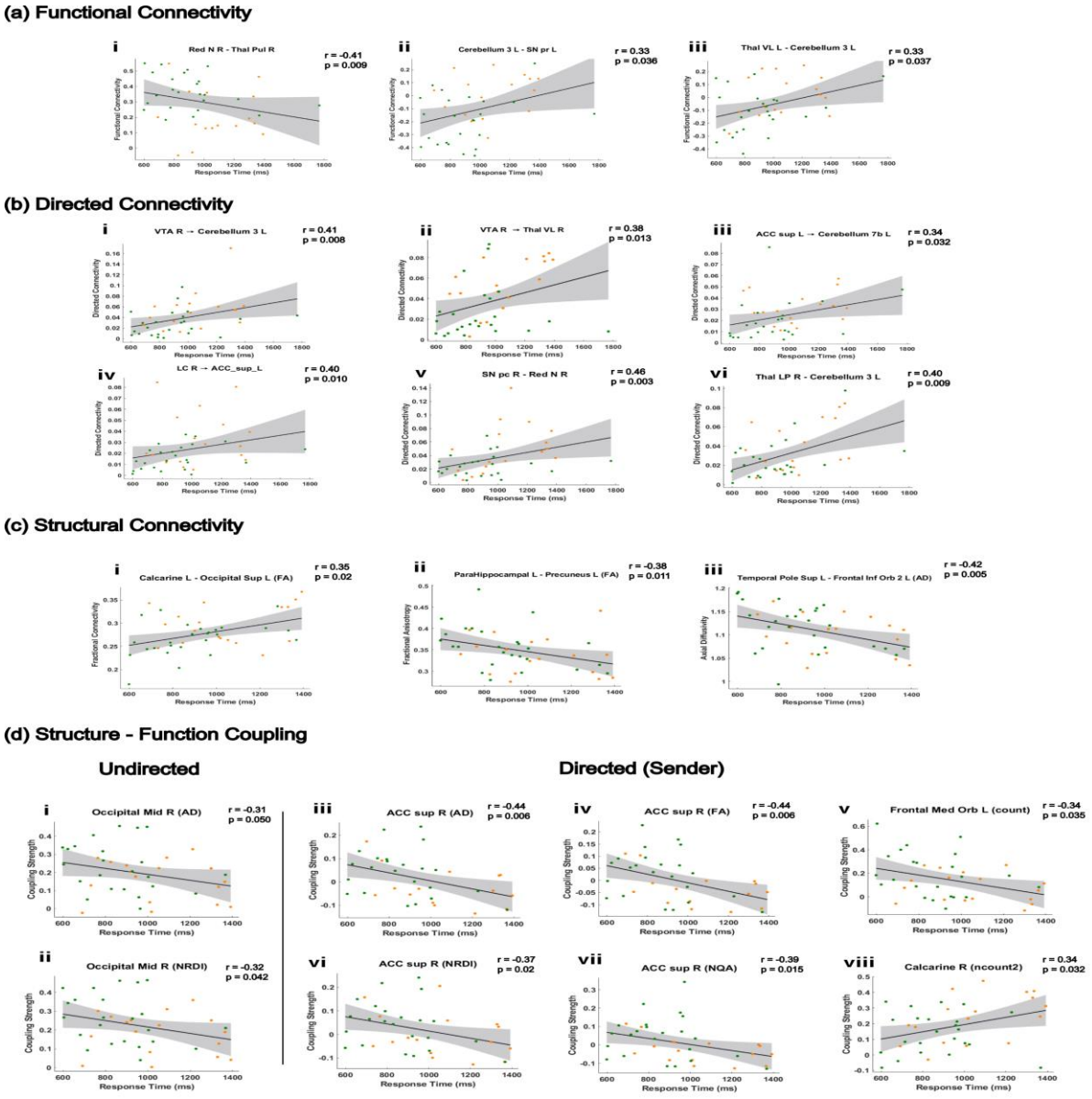

Figure 5.6 Brain–Behavior Correlations Across Connectivity Modalities. Connectivity strength and structure–function coupling among PCA-derived ROIs from the AAL3 atlas were significantly associated with response time. Negative correlations reflect faster performance. (a) In functional connectivity, faster responses were linked to stronger connectivity between the red nucleus and right pulvinar thalamus, while slower responses were associated with enhanced connectivity across midbrain–thalamic–cerebellar pathways.(b) In directed connectivity, slower responses corresponded to greater influence among midbrain (VTA R, SN pc R), thalamic (Thal VL R), cerebellar, and left supracallosal anterior cingulate regions.(c) In structural connectivity, slower responses were linked to higher FA between the left calcarine cortex and superior occipital gyrus, while faster responses were associated with reduced FA between the left parahippocampal and precuneus and decreased AD between the superior temporal pole and inferior frontal gyrus.(d) In structure–function coupling, stronger SC–FC and SC–dFC coupling in mid-occipital, frontal, and anterior cingulate regions tracked with faster responses

5.2 Discussion of Findings and Interpretation

5.2.1 A Novel PCA-Based Framework for Region Selection

To address the challenges of navigating the complexity of full-brain connectivity matrices, we developed a novel PCA-based framework that reimagines the role of principal component analysis (PCA) in neuroimaging. Rather than relying on anatomical constraints or arbitrary statistical cutoffs, this method decomposes subject-by-connection matrices into orthogonal principal components and computes the eigenvalue-weighted sum of absolute contributions for the top user-defined regions across all components. The result is a global variance contribution score for each brain region, allowing us to prioritize the most informative regions for downstream group comparisons based on their contribution to explained variance. For our analysis, we selected the top 20 regions contributing up to 80% of the total explained variance, emphasizing the most relevant contributors for downstream analysis while ensuring stability, as detailed in Section 2.2.4.6.

Crucially, this method leverages the mathematical structure of PCA(Mwangi *et al*., 2014; Wall, 2002) to form an orthonormal basis over the space of brain regions, enabling a principled and interpretable ranking of ROI importance. By weighting regional contributions according to the variance explained by each principal component, the method prioritizes dominant, structured inter-subject variance. This orthogonal decomposition avoids redundancy, permitting straightforward accumulation of variance-weighted contributions.

Moreover, this region-centric approach flexibly handles both undirected and directed connectivity matrices. For directed measures, such as Granger causality, the method separately calculates contribution scores for the sender, receiver, and total contributions, allowing for a nuanced interpretation of directional asymmetries in brain networks. This increases the

interpretability and relevance of the selected ROIs. Altogether, this novel application of PCA provides a mathematically robust alternative to traditional thresholding and anatomical filtering, focusing on variance-based selection that generalizes across structural, functional, directed connectivity, and coupling modalities.

To evaluate the internal consistency and robustness of our PCA-based ROI selection method, we developed a multi-pronged validation strategy using rank correlation, permutation testing, and hypergeometric overlap statistics with a conservative significance threshold of $p < 0.001$ as our primary validation criteria. This strategy enabled a drastic reduction in the number of statistical comparisons required for downstream testing, significantly improving our ability to detect FDR-corrected ($q < 0.05$) results that would have been obscured by multiple comparison corrections.

In the previous chapter, we applied a structurally constrained functional neuroimaging analysis, limiting connectivity assessments to anatomically plausible tracts informed by white matter tractography. While this approach enhanced biological plausibility, it was inherently limited by tractographic reconstruction and macro-level user-defined parameters such as allowable streamline length and angular thresholds. The PCA-based method introduced here offers a complementary perspective by identifying dominant, behaviorally relevant patterns of variance without relying on anatomical priors. By combining tractography-informed constraints to ensure biological plausibility with PCA-driven selection to surface robust inter-subject variability, we constructed a methodological framework capable of supporting a comprehensive and principled investigation of the neuroplastic adaptations associated with video game experience.

5.2.2 Group Differences Between Gamers and Non-Gamers Across Modalities

Group-level comparisons between gamers and non-gamers revealed widespread differences across multiple connectivity domains, all of which involved at least one PCA-identified region of interest (ROI).

In functional connectivity (FC), shown in Figure 5.2, gamers exhibited significantly stronger FC between the right red nucleus and the right pulvinar thalamus, the left cerebellum lobule 3 and the left caudate nucleus, and the left cerebellum lobule 3 and the right superior temporal pole. In contrast, non-gamers showed stronger FC between the left cerebellum lobule 3 and the left intralaminar thalamus, the left cerebellum lobule 3 and the left substantia nigra pars reticulata, and the left cerebellum lobule 3 and the ventrolateral thalamus bilaterally. All FC differences, except for the connections involving the ventrolateral thalamus, survived FDR correction. Several of these FC connections were also significantly correlated with response time (RT), indicating behavioral relevance. These patterns suggest that non-gamers may rely more heavily on feedback-based loops involving cerebellar–thalamic–midbrain circuits, potentially as a mechanism to reduce uncertainty during motor action selection. Effect sizes were consistently large, with Cohen's *d* magnitudes ranging from 0.76 to 1.26.

In directed functional connectivity (dFC), presented in Figure 5.3, sender-mode results revealed a robust group difference in directed influence from the left superior anterior cingulate cortex to the right ventrolateral thalamus, which survived FDR correction. Additional uncorrected differences favoring non-gamers included projections from the left superior anterior cingulate cortex to the left cerebellum lobule 7b, from the right ventral tegmental area to the right ventrolateral thalamus, and from the right ventral tegmental area to the left cerebellum

lobule 3. Notably, each of these connections also showed significant positive correlations with RT.

Receiver-mode differences also favored non-gamers, with several directed connections showing stronger influence toward key target regions. These included projections from the left cerebellum lobule 3 to the left superior anterior cingulate cortex, from the right ventral tegmental area to the left cerebellum lobule 3, and from the right locus coeruleus to the left superior anterior cingulate cortex. Several of these connections also showed significant positive correlations with RT. Total-mode results closely mirrored the sender- and receiver-mode patterns, with notable unique group differences such as increased connectivity from the right red nucleus to the right substantia nigra pars compacta and from the left thalamus to the left cerebellum lobule 3 in non-gamers.

The consistency of these effects across all directed functional connectivity (dFC) modes, coupled with moderate to large effect sizes (d = 0.59 to 1.00), reinforces the earlier findings from tractography-constrained analyses presented in Chapter 4, which revealed that non-gamers exhibit a greater number of directed connections. The current results build on that observation, suggesting that non-gamers engage in a broader, more distributed pattern of targeted information flowlikely reflecting compensatory network recruitment to signal the need for an imminent motor response during rapid visuomotor decision-making.

In structural connectivity (SC) analysis using diffusion measures (FA, AD, ISO, and RDI), we observed group-level differences involving PCA-derived regions of interest ($p < 0.05$) as shown in Figure 5.4. For FA, a notable and seemingly counterintuitive difference emerged that FA was significantly higher in non-gamers between the left calcarine cortex and the left

superior occipital gyrus—early visual areas (Huff *et al.,* 2025), which also had a positive correlation with RT thus associated with slower response times in behavioral analysis (see Figure 5.6). This finding suggests that non-gamers may over-rely on early-stage visual processing to compensate for inefficiencies further downstream. For AD, group differences emerged between the left superior medial frontal gyrus and the left mid-cingulate cortex ($q < 0.05$). ISO revealed significant effects in connections between the right lingual gyrus and the left cerebellum lobule 6, as well as between the left lingual gyrus and the left caudate nucleus. Both connections remained significant in NRDI and under FDR correction. Absolute effect sizes across all SC measures were substantial, with Cohen's *d* magnitudes ranging from 0.78 to 1.22, indicating consistently large group-level differences.

Structure–function coupling findings displayed in Figure 5.5 provided further insight into group differences by measuring the alignment between a region's structural connectivity profile and its capacity for functional load (Fotiadis *et al*., 2024). Gamers exhibited stronger structure–function coupling (SFC) within cerebellar regions, including vermis lobule 3 (MD), vermis lobule 9 (mean length, FA), and the left cerebellum lobule 10 (FA, QA). In contrast, non-gamers showed stronger structure–directed functional coupling (SdFC sender) in bilateral calcarine cortices and vermis lobule 7. One of these connections, involving vermis lobule 7 and AD-based SdFC sender coupling, survived FDR correction.

Gamers also demonstrated stronger SdFC sender coupling in key frontal and cingulate regions, including the left superior anterior cingulate cortex (ncount, ncount2), the left medial orbital frontal cortex (count), and the left paracentral lobule (ncount). These findings underscore a functional distinction between undirected synchrony, as measured by SFC, and directional

signaling capacity, as captured by SdFC sender. Stronger coupling in gamers may reflect more efficient transmission channels for dynamic signaling, consistent with prior evidence of increased dorsal attention to salience network (DAN-to-SN) switching and which the superior anterior cingulate cortex as a core node in the salience network (SN) (Jordan & Dhamala, 2022).

5.2.3 Brain–Behavior Relationships

Connectivity and coupling strengths across all modalities were significantly associated with response time (RT), as shown in Figure 5.6. These associations reinforce the behavioral relevance of group differences and suggest that the specific network configurations observed in gamers versus non-gamers reflect divergent visuomotor strategies. Non-gamers exhibited greater engagement in cerebellar–midbrain–thalamic circuits, which were consistently associated with slower responses and may indicate less efficient allocation of cognitive resources.

5.2.3.1 Functional Connectivity

Faster RTs, indicated by negative correlations, were linked to stronger functional connectivity (FC) between the right red nucleus and right pulvinar thalamus. In contrast, slower RTs were associated with stronger FC in cerebellar–thalamic and cerebellar–midbrain connections, particularly between the left cerebellum lobule 3 and the left intralaminar thalamus, left substantia nigra pars reticulata, and bilateral ventrolateral thalamus, connections that were more prominent in non-gamers. These patterns suggest that reliance on cerebellar–thalamic error correction signals (Ide & Li, 2011) slows visuomotor transformations by promoting tighter inhibitory control. This is evidenced by increased synchrony between the substantia nigra and ventrolateral thalamus in non-gamers (Walter & Shaikh, 2014), implying reduced motor readiness due to greater inhibitory gating of thalamic output. Such dynamics may delay

resolution of competing motor plans (Sonne, 2025), ultimately prolonging response times under conditions of uncertainty.

5.2.3.2 Directed Functional Connectivity

In addition to undirected connectivity patterns, directed functional connectivity (dFC) analyses revealed several behaviorally relevant group differences linked to response time.

All three sender-mode dFC favoring non-gamers, left superior anterior cingulate cortex → left cerebellum lobule 7b, right ventral tegmental area → right ventrolateral thalamus, and right ventral tegmental area → left cerebellum lobule 3, also exhibited significant positive correlations with RT, indicating slower responses. Similarly, several receiver-mode dFC favoring non-gamers (e.g., left cerebellum lobule 3 → left superior anterior cingulate cortex, right ventral tegmental area → left cerebellum lobule 3, and right locus coeruleus → left superior anterior cingulate cortex) were positively correlated with RT.

These results point to a more distributed routing of information in non-gamers, involving regions implicated in error correction (cerebellum; Caligiore *et al*., 2017), stress responses (locus coeruleus; Borodovitsyna *et al*., 2020), and dopaminergic impulsivity (ventral tegmental area; Aurelian *et al*., 2016). In this context, increased VTA signaling may serve as a compensatory mechanism for a lack of goal-directed strategy instead opting for greater reward-seeking pathway signaling trying to "search" for the correct direction of the target dots, which incurs a performance cost.

5.2.3.3 Structural Connectivity

In terms of structural connectivity (SC), higher FA between the left calcarine cortex and the left superior occipital gyrus predicted slower RTs in non-gamers. While gamers showed elevated FA in the left superior occipital–inferior parietal dorsal stream (see Section 3.1.1.2;

Cahill *et al.,* 2024), neither this tract nor the FA tract between the calcarine and occipital cortex showed a behavioral correlation with RT. However, functional connectivity between the left superior occipital gyrus and the left superior parietal lobule was significantly associated with faster RTs. Additionally, higher local efficiency in the left superior occipital gyrus predicted faster responses, whereas greater node degree was associated with slower performance. SdFC sender coupling analyses revealed that increased tract counts with the right calcarine cortex tracked with slower response times and was elevated in non-gamers.

These findings suggest that non-gamers tend to invest more cognitive resources into early visual processing, likely to enhance object discrimination and resolution of individual dot trajectories, compensating for reduced visuomotor integration. Prior work showed that dorsal stream structural integrity does not predict performance in this dataset (Cahill *et al*., 2024), implying that tracts linked to slower RTs likely fall outside core visuomotor pathways (Goodale and Milner 1992; Kravitz *et al.,* 2011; Mishkin *et al*., 1983). These results support the view that while early sensory encoding is necessary, behavioral efficiency depends more on effective visuomotor transformation and action selection. Cognitive resources yield greater returns when used to convert perceptual input into action, rather than for continuous refinement of early-stage representations.

Additional behaviorally relevant SC connections reinforce this view. Faster RTs were associated with higher AD between the left superior temporal pole and left inferior frontal orbital cortex, regions implicated in integrating high-value sensory input (Herlin *et al.,* 2021) with value-based action selection (Rolls, 2023; Rudebeck and Rich, 2018; Shi *et al*., 2023). The left temporal pole more readily receives contextual scene information from the left parahippocampus

a key finding in Chapter 4, see Section 4.1.3, enabling the orbital frontal cortex to transform learned value representations into goal-directed actions.

Similarly, greater FA between the left parahippocampal gyrus and the left precuneus was associated with faster RTs. The parahippocampus supports recognition of spatial layouts (Burgess and O'Keefe, 2003), while the precuneus enables visuospatial simulation (Blihar *et al*., 2020; Cavanna and Trimble, 2006; Hahn *et al*., 2006), both essential for anticipating movement trajectories during visuomotor tasks.

5.2.3.4 Structure–Function Coupling

Structure–function coupling metrics further clarified behaviorally meaningful dynamics by measuring how well a region's anatomical infrastructure aligns with its functional load (Fotiadis *et al*., 2024). Both intensive (e.g., FA, AD, NQA, NRDI) and extensive (e.g., count, ncount2) SC measures showed behavioral relevance.

Stronger NDRI–FC and AD–FC coupling in the right mid-occipital gyrus predicted faster responses. This region is known to support spatial information processing (Renier *et al*., 2010), and these findings suggest that stronger coupling reflects greater alignment between incoming visual load and the region's capacity to relay information downstream. Prior analyses showed that gamers exhibited greater local efficiency in both SC constrained FC and SC constrained dFC networks involving this same region (see Sections 4.1.4 and 4.1.5), so at equal coupling strength, gamers' networks are better structured to disseminate spatial input and facilitate visuomotor transformations.

Additionally, coupling between streamline count and dFC sender mode in the left medial orbital frontal cortex was greater in gamers and negatively correlated with RT, indicating faster behavioral responses. This aligns with findings that higher AD between the left superior

temporal pole and the left inferior frontal orbital cortex — anatomically proximal and functionally similar to the left medial orbital frontal cortex — also tracked with faster RT. Both regions are critical for integrating value-based information with motor planning (Rolls, 2023; Rudebeck and Rich, 2018). In contrast, elevated ncount2 dFC sender coupling in the right calcarine cortex in non-gamers reflects continued reliance on early visual processing, which likely contributes to bottlenecks that hinder decision-making performance.

Finally, enhanced SdFC sender coupling from the right supracallosal anterior cingulate cortex was associated with faster response times across multiple SC measures (AD, FA, NQA, NRDI). While these findings highlight its role as a sender, they converge with prior reports of increased dorsal attention network (DAN) input to the salience network (SN) in gamers (Jordan and Dhamala, 2022). Together, these results suggest that the ACC, as a core node within the salience network, may integrate high-priority signals, such as those originating from DAN regions, more readily in gamers and transmit top-down control signals to resolve competition between motor plans. The fact that SdFC sender coupling aligns with multiple SC metrics reinforces the idea that, whenever the ACC is engaged, its core functional role is to reduce uncertainty and resolve conflict between competing actions. The strengthened DAN-to-SN interaction in gamers further supports the findings of this analysis, suggesting that gamers display better attentional control, leading to integration of high-value visual information more readily than non-gamers, allowing them to discern the direction of target dots and make a confident selection more quickly.

5.2.4 Synthesis of Findings Across Modalities

Across modalities, a consistent pattern emerged that faster response times were associated with stronger connectivity in circuits involved in transforming high-value sensory information into goal-directed action and supporting goal-directed motor execution, *i.e.,* regions implicated in resolving perceptual ambiguity more effectively tracked with faster RT. Central to this process was the superior anterior cingulate cortex (ACC sup), a region traditionally associated with conflict monitoring and the resolution of competing motor plans (Brockett & Roesch, 2021). More recent work suggests the ACC functions as a key hub for uncertainty-driven cognitive control, particularly in dynamic and feedback-sensitive decision environments (Chen *et al*., 2024; Monosov, 2017; Monosov *et al*., 2020; Mushtaq *et al*., 2011). These areas likely serve to clarify salience signals and commit to goal-relevant actions once monitoring demands have been satisfied. The superior ACC was previously found to be a significant node involved with the increased DAN-to-SN interaction observed in gamers which that tracked with improved RT (Jordan & Dhamala, 2022) and within the right ACC a node by which enhanced SdFC sender coupling tracked with improved response times across multiple SC measures.

Conversely, increased activity among regions involved in motor correction, stress reactivity, and dopaminergic signaling was positively correlated with response time, indicating slower performance and stronger involvement in non-gamers. This pattern may reflect reduced access to high-value salient cues, as suggested by greater engagement of early visual areas and cerebellar–midbrain–thalamic circuits (Caligiore *et al.,* 2017; Popa & Ebner, 2019; Seidler *et al.,* 2013). These compensatory pathways likely reflect increased reliance on bottom-up processing and corrective feedback, with the anterior cingulate cortex (ACC) potentially recruited to manage elevated uncertainty during response selection.

Examples of regions implicated in resolving ambiguity in these findings include the left medial frontal orbital cortex, an executive region critical for integrating value-based information with motor planning. SdFC sender coupling with streamline count in this region was significantly stronger in gamers ($p = 0.32$, $d = 0.74$) and negatively correlated with response time ($r = –0.34$, $p = 0.035$), consistent with improved performance. Another example includes increased synchrony, measured by functional connectivity, between the red nucleus—a lower midbrain structure canonically linked to limb control—and the pulvinar thalamus, reflecting enhanced bottom-up and top-down coordination. This connection likely contributes to perceptual disambiguation by signaling motor readiness (Basile *et al.,* 2021; Brockett *et al*., 2020; Krimmel *et al*., 2024), effectively facilitating the "I'm ready to press the button" moment.

This finding parallels prior work in Go/No-Go paradigms, where red nucleus activity modulates motor output based on recent trial history, speeding responses after Go trials and promoting caution after Stop trials. Critically, red nucleus neurons amplify directional signals during successful Stop trials, suggesting a role in reshaping ongoing motor plans when initial responses must be inhibited. This capacity for rapid, context-sensitive motor adjustment reflects a form of feedforward control, in which the system anticipates task demands and dynamically tunes motor output in real time. The functional connection between the red nucleus and pulvinar thalamus is supported by a group-level difference favoring gamers ($p = 0.0061$, $q = 0.02$, $d = 0.85$), and negatively correlated with response time ($r = –0.41$, $p = 0.009$), which suggests that long-term exposure to high-stakes, fast-paced environments fosters a neurocognitive strategy that prioritizes feedforward conflict resolution—facilitating swift action and flexible, real-time motor adjustments under uncertainty.

These findings collectively confirm our second hypothesis that a novel, data-driven approach based on explained cumulative structured variance (rcPCA) can successfully identify behaviorally relevant connections and structure–function couplings. This method provided a more granular and meaningful view of the neuroplastic refinements observed in gamers and laid the groundwork for testing our primary hypothesis.

Overall, gamers demonstrate enhanced top-down cognitive clarity, unobstructed translation of learned value into action, and bottom-up motor readiness when making visuomotor decisions under uncertainty. This configuration reduces the need for prolonged internal conflict resolution between competing motor plans and offers what may be a functionally necessary and sufficient explanation for their accelerated decision-making compared to non-gamers.

This neurocognitive visuomotor decision making profile supports a feedforward, proactive strategy for visuomotor transformation, through which gamers exhibit an optimized neural architecture for fast, adaptive, goal-directed behavior—one that more readily anticipates possible task outcomes and enables flexible, real-time motor corrections. By reducing internal uncertainty more efficiently, this yields a more effective cognitive architecture for action selection under dynamic, time-sensitive conditions.

In the context of our modified moving-dots task, this strategy was expressed as greater reliance on top-down selection of goal-directed responses based on scene-specific contextual cues, such as the motion of target dots relative to distractors. Gamers adapted more effectively to either possible outcome of a 50/50 visuomotor decision, reflecting enhanced cognitive flexibility and attentional control.

Our results support the primary hypothesis that long-term action video game (AVG) play reflects neuroplastic refinements that reduce visuomotor surprise by shifting toward superior decision-making strategies—ones that more effectively resolve prediction error and minimize internal conflict regarding competing motor plans. This facilitates a more optimal cognitive state for visuomotor decisions, one that is primed to rapidly incorporate salient, task-relevant information and execute swift, accurate, and decisive actions.

Ultimately, these neuroplastic refinements reflect a reallocation of cognitive resources toward circuits that minimize visuomotor surprise more efficiently. Cognitive Resource Reallocation (CRR) thus emerges once again as a viable mechanistic explanation hypothesized to drive the enhancement of a baseline cognitive state over time, enabling refinements in neural configuration adapted to repeated task demands. This shift toward optimizing internal conflict resolution may not merely reflect a gaming-related adaptation but a broader principle regarding how cognitive systems respond to prolonged cycles of strenuous task engagement and recovery—gradually reallocating resources to stabilize changes in cognitive action over time, promoting local refinements that enhance overall efficiency during task performance by targeting regions and connections most involved in reducing task-induced strain.

In the case of AVG experience, this would lead to neuroplastic refinements that translate into more efficient visuomotor decision-making—a common and frequent demand during gameplay, where errors often come with significant costs. Over time, the brain learns to prioritize high-value visual cues, promote goal-directed action, and increase motor readiness to respond to uncertainty in dynamically changing environments. This ultimately results in quantifiable improvements, establishing a new set point by which the brain makes visuomotor

decisions—leading to the ~190 ms response time improvement observed in this dataset, without any loss in accuracy.

As gamers repeatedly engage in high-stakes, rapid-response tasks, the CRR framework posits that the brain reallocates resources toward pathways that facilitate more proficient AVG performance. These reallocations map cleanly onto cognitive improvements consistently reported in the literature, including enhanced visual acuity (Green & Bavelier, 2007), visuomotor integration (Cahill *et al*., 2024; Granek *et al*., 2010), attentional control (Bavelier & Green, 2019), and cognitive flexibility (Glass *et al*., 2013). The point to be emphasized here is that, rather than endlessly refining early sensory representations beyond a sufficiently reliable threshold, long-term AVG experience encourages the brain to avoid diminishing returns—its priority is to execute the task as efficiently as possible while incurring minimal strain. Over repeated cycles of task engagement and recovery, resources are reallocated toward downstream processes more directly involved in effective gameplay, particularly those supporting visuomotor decision-making and perception–action coupling. This shift offers a comprehensive and mechanistically grounded account of the functional gains observed in gamers and provides a clear neural signature of long-term adaptive plasticity associated with AVG play.

5.2.5 Concluding Remarks

This study introduces a novel, data-driven PCA-based method for ROI selection (rcPCA) that reveals significant neuroplastic adaptations consistent with what would be expected from long-term action video game (AVG) experience. Our findings, based on a multimodal whole-brain neuroimaging analysis, provide empirical support for the Cognitive Resource Reallocation (CRR) framework, which posits that the brain optimizes performance by reallocating functional

and metabolic resources toward anatomically plausible, behaviorally relevant circuits to better meet demanding task conditions—ultimately mitigating costly prediction errors.

We show that AVG experience reflects more efficient visuomotor decision-making through enhanced top-down cognitive clarity, unobstructed transformation of learned value into goal-directed action, and heightened bottom-up motor readiness. The convergence of these factors reduces internal conflict, mitigates visuomotor surprise, and enables rapid yet skillful action selection through greater anticipation of multiple possible outcomes under uncertainty.

Our PCA-based structured variance method offers ample room for future development, including the integration of demographic or clinical covariates and the application of nonlinear dimensionality reduction approaches, such as kernel PCA, to capture more complex representational variance. This work not only demonstrates the utility of principled, data-driven neuroimaging tools but also provides a foundation for future research aimed at enhancing human performance through targeted cognitive adaptation. While future studies are needed to assess the broader generalizability and nonlinear dynamics of rcPCA, the present findings offer both a novel analytical method and a mechanistically grounded view of how experience reshapes cognition. They highlight the brain's remarkable ability to "level up" through repeated encounters with cognitively demanding challenges. Through adaptive resource reallocation, these challenges become less effortful over time, minimizing internal conflict, reducing uncertainty, and ultimately enabling more efficient, high-performance behavior. The findings from this chapter strongly support that action video game play could drive targeted neuroplastic refinement and offers a generalizable blueprint for cognitive optimization through adaptive resource reallocation.

6 SYNTHESIS OF FINDINGS AND THEORETICAL UNIFICATION

6.1 Synthesis of Findings

Across all three analytical domains that were considered (structural connectivity, functional connectivity, and directed functional connectivity), gamers consistently demonstrated neural patterns indicative of enhanced visuomotor decision-making that align with their behavioral advantage of ~190ms in our moving-dots visuomotor decision task without loss of accuracy. These patterns, presented independently across Chapters 3 through 5, were marked by reduced redundancy and streamlined functional clarity. They align with neuroplastic refinements that would reasonably be expected to support improved performance during action video game play.

Although each modality was evaluated separately, a convergent mechanistic signature emerged. The findings provided clear and consistent support for Cognitive Resource Reallocation (CRR). The empirical results presented throughout this dissertation showed no contradictions to CRR as the mechanism driving the neuroplastic refinements observed in gamers. Instead, they point to a reallocation process in which repeated episodes of task engagement and recovery in cognitively demanding environments compel the brain to refine itself through internal redistribution of resources.

CRR has emerged as a strong explanatory candidate for enhanced visuomotor performance. When paired with the structural and functional evidence documented in this dissertation, it becomes clear that a formal, physically grounded framework is warranted. This led to the development of Cognitive Resource Theory (CRT), which provides a quantifiable

structure for CRR. CRT is not intended as a heuristic but as a principled model that can be evaluated, tested, and refined using real data.

If future predictions derived from CRT do not hold up broadly, from the author's perspective this would not represent failure. Such an outcome would offer an opportunity to reassess how cognitive energy is managed under physical constraint, as well as to evaluate whether the proposed mechanisms are overly rigid, too broad, or incomplete. Even if CRT does not ultimately provide a complete first-principles account of cognition, it would still represent meaningful progress toward uncovering the physical mechanisms governing neuroplastic phenomena underlying cognitive adaptations.

However, it is worth noting that CRT also generated a prediction not explicitly contained in the original dataset. Specifically, it anticipated a relationship between connectivity dynamics and sleep–wake modulation. When subjected to internal consistency checks, CRT produced a true *a priori* prediction, as detailed in Section 6.2.7.

Within the scope of this dissertation, CRR consistently aligned with observed patterns. Although the formalization of CRR came after the visual stream analysis presented in Chapter 3, the theory remains compatible with those results. It also served as the leading hypothesis throughout Chapters 4 and 5. CRR was not applied retroactively. It was evaluated in real time as a proposed explanation for the behavioral advantages observed in gamers. CRT, in turn, formalizes how CRR could arise in a dynamic and energy-constrained system such as the human brain.

Altogether, this synthesis supports the conclusion that CRR is not just a descriptive label. It is a core mechanism of neural adaptation under pressure. To develop this mechanism further and place it within a physically grounded theory of cognition, the next section introduces Cognitive Resource Theory (CRT), a unified framework that treats cognition as a constrained energetic process governed by fundamental physical principles.

6.2 Theoretical Unification: Cognitive Resource Theory (CRT)

A Gauge-Theoretic, Thermodynamic Framework of Cognition

6.2.1 Cognitive Resource Theory: Introduction

CRR has demonstrated empirical validity as the latent organizing principle across every major analysis presented in this dissertation. Multiple data modalities—spanning structural, functional, and directed functional connectivity—and diverse statistical approaches consistently supported the same explanatory mechanism. This convergence suggests that the observed effects are not incidental, but instead reflect a deeper, underlying principle of neural adaptation. Such consistency calls for a precise, physically grounded theoretical framework.

Cognitive Resource Theory (CRT) was developed to meet this need. CRT formalizes the mechanisms of cognitive resource allocation and reallocation as dynamic energetic processes embedded in physically lawful neural dynamics. By unifying structural, functional, and behavioral considerations into a single coherent formalism, CRT elevates CRR from a descriptive concept to a quantifiably testable principle of cognition under constraint. If further validated, CRT may inform new theoretical, computational, and applied paradigms across neuroscience, cognitive modeling, and adaptive systems research.At its core, CRT is a physics-based framework for modeling cognition as a process of energy-constrained optimization. It is

built on two complementary components that operate in tandem: Cognitive Resource Allocation (CRA) and Cognitive Resource Reallocation (CRR).

CRA refers to the brain's baseline distribution of energy across cognitive systems. This allocation reflects a dynamic equilibrium shaped by internal constraints such as metabolic availability, neural efficiency, anatomical connectivity, and ongoing regulatory demands from the nervous system (Alister *et al*., 2024; Longman *et al*., 2023; Saberi *et al*., 2024; Schmidt, 2014). CRA determines the energetic landscape that supports routine cognitive operations such as perception, decision-making, and action when the system is not under duress. In effect, CRA defines a dynamic ground state of cognition characterized by energetic stability and homeostasis.

Up to this point, CRR has been used throughout this dissertation as a conceptual framework to interpret the observed patterns of neuroplasticity, particularly in explaining how repeated engagement in AVG play reflects neuroplastic refinement within task-relevant circuits. While this interpretation has been shown to be empirically valid, CRT now expands CRR into a formal theoretical construct. Within this framework, CRR is no longer treated merely as a descriptive inference but as a physically grounded mechanism defined in energetic terms. It is best understood as a dynamic perturbation of the baseline configuration defined by CRA. It governs how the system redirects energetic resources in response to cognitive strain—such as uncertainty, frustration, or task demands that exceed CRA capacity. Rather than representing a breakdown, CRR acts as an adaptive response to unaccommodated internal friction. By reallocating energy toward circuits most relevant for successful task performance and downregulating those less critical, the brain recalibrates itself in real time. Through repeated

episodes of engagement and recovery, these perturbations drive neuroplastic refinements that stabilize more efficient neural configurations.

Although concepts resembling CRR have appeared in prior work on learning, attention, working memory, and motor adaptation (Becker *et al*., 1996; Buhusi & Meck, 2009; Barbot *et al*., 2021), they have not been formally defined as physically grounded mechanisms. CRT offers such a formalism by embedding CRA and CRR within a broader energetic model of cognition, using thermodynamic and variational principles to describe how real energetic constraints shape the brain's capacity for adaptive modification. This framework also helps clarify the mechanism by which long-term gameplay would produce a targeted neuroplastic refinement.

For example, as described in Chapter 3, improved functional connectivity between the left superior occipital gyrus (SOG) and left superior parietal lobule (SPL) in gamers can be understood as a direct outcome of repeated CRR episodes. The persistent demand for rapid visual processing of where objects are and how they are moving during gameplay imposes cognitive strain on this pathway, straining CRA baseline support. In response, CRR would episodically reallocate energetic resources to facilitate more efficient signal transmission between these regions. Over time, these repeated perturbations stabilize into more streamlined configurations, reducing overall strain for the same cognitive task, yielding behavioral improvements in visuomotor decision-making. In this way, CRT explains how both baseline support (CRA) and dynamic refinement (CRR) operate in tandem to drive the effects observed in empirical data.

6.2.1.1 CRT Postulates

To formally construct Cognitive Resource Theory (CRT), it is necessary to begin with three foundational assumptions. These assumptions are not arbitrary; rather, they reflect a deliberate extension of core physical principles to the domain of cognition. Each postulate is motivated by both empirical observation and theoretical coherence, providing the scaffolding upon which the remainder of the framework is built.

The first postulate of CRT asserts that cognition is a physical system**.** As with any physical system, cognitive processes unfold within a structure governed by physical laws and well-defined energy dynamics. Accordingly, the state of the cognitive system can be described by a Hamiltonian, which defines the total energy of the system at a given moment

$$H_{\mathrm{CRT}}(t) = H_{CRA}(t) + \varepsilon R_{\mathrm{CRR}}(t).$$

$H_{\mathrm{CRA}}(t)$ describes an unperturbed internally regulated configuration—governed by resting state dynamics, metabolic drift, homeostasis, and slow-timescale fluctuations. $\varepsilon R_{\mathrm{CRR}}(t)$ denotes a first-order perturbation that thermodynamically reallocates cognitive energy in response to cognitive strain.

The second postulate of CRT assumes that cognition follows the principle of stationary action—a unifying principle in physics stating that systems tend to evolve along paths that extremize (typically minimize) total energetic expenditure over time. From this structure, well-known conservation laws such as conservation of energy and momentum are derived based on a system's invariance under continuous transformations in time and space, as formalized by Noether's Theorem. Applying this principle to the brain suggests that cognitive processes, like all physical processes, naturally shift toward more efficient configurations when viable,

minimizing unnecessary energy expenditure. In CRT, this principle is formally expressed using the variational condition

$$\delta \int_{t_0}^{t_1} L_{\mathrm{CRT}}(q, \dot{q}, t)\, d\, t = 0\ ,$$

where q is a generalized coordinate in configuration space and δ is the symbol used to denote the variational derivative of the path taken by the CRT Lagrangian, $L_{\mathrm{CRT}}(q, \dot{q}, t)$.
Applied to the brain, this principle suggests that cognitive processes tend to shift toward energetically favorable configurations when such shifts are viable, minimizing unnecessary work. In this light, cognitive adaptation is not merely reactive but reflects an intrinsic drive toward optimal functioning under physical constraint.

The third and final postulate of CRT is that cognition, like all physical systems, obeys the second law of thermodynamics, which means that it tends toward equilibrium with its surroundings, generating entropy in the process and is classically described by the expression

$$\Delta S > \frac{\delta Q}{T_{surr}},$$

where ΔS is the total change in entropy, δQ is the heat exchanged with the cognitive system's surroundings and T_{surr} is the temperature of the surrounding environment. That is, when the brain is pushed out of CRA equilibrium by cognitive strain, entropy tends to increase—unless counteracted. To achieve reordering or adaptive complexity, two conditions must be met: an energetic drive (work source or exergy) and an instructive signal (Wright, 2017). CRR fulfills both roles, functioning as the energetic and organizational mechanism by which a cognitive system adapts and reconfigures to reduce energetic expenditure and achieve a better alignment with its environment.

In CRT, entropy production serves both as a signal of adaptation and a marker of cognitive load. When task demands strain what CRA can support, CRR enables the brain to explore and realize new configurations, consistent with the second postulate of CRT. This thermodynamic cost of adaptation can be modeled using formal entropy measures, such as the von Neumann entropy of the system's state, as described in Section 6.2.4.1.

6.2.2 Cognitive Resource Allocation

At "rest"—or as restful as the brain ever becomes—the system organizes its resources into a relatively stable configuration aligned with intrinsic network activity, forming a dynamic equilibrium shaped by biological factors such as metabolic efficiency, energetic stability, and internal homeostasis. It reflects the brain's moment-to-moment availability of cognitive energy, influenced by internal fluctuations and regulated by the nervous system. Empirically, this corresponds to resting-state network dynamics, where coordinated activity within systems such as the default mode network (DMN), dorsal attention network (DAN), and salience network (SN) coordinated intrinsic organization within systems such as the DMN, DAN, and SN reflects the brain's default resource distribution in the absence of task-induced strain (Yeo *et al*., 2011) . In CRT, both internal energy and cognitive temperature are treated as dynamic variables. This is not only due to physiological rhythms but also in response to sustained cognitive demands. As these demands accumulate, the system engages CRR to reallocate energy toward efforts that reduce internal friction and help minimize cognitive action. Over time, repeated CRR episodes gradually refine CRA, allowing the brain to stabilize more efficient energy configurations. The baseline allocation updates to better align the system with its environment. CRA thus encodes a dynamic baseline shaped by experience, while CRR functions as the mechanism that perturbs and reshapes that baseline in response to demand.

6.2.2.1 Gauge Theoretic Construction of CRA Energy

To formalize CRA energy, we introduce a gauge-theoretic structure that mirrors classical field theory. Cognitive Resource Allocation (CRA) is modeled as a conserved field over cognitive state space, governed by scalar and vector potentials that distribute energy efficiently across the brain's network architecture.

The dynamics of this field are described by a cognitive field $\vec{\mathrm{C}}_{\mathrm{CRA}}(x,t)$ defined as the negative gradient of a scalar potential $\Phi_{CRA}(x,t)$. This relationship can be expressed as

$$\vec{\mathrm{C}}_{\mathrm{CRA}}(x,t) = -\nabla\Phi_{CRA}(x,t).$$

A cognitive vector potential A_μ governs the dynamic flow of cognitive energy over time and across regions. From this, we can construct the cognitive field tensor for CRA as

$$F^{\mu\nu}_{CRA}(x,t) = \partial^\mu A^\nu_{CRA}(x,t) - \partial^\nu A^\mu_{CRA}(x,t),$$

where the gauge fixing condition is given by $\partial_\mu A^\mu_{(CRA)} = 0$.

In CRT, the vector potential , A^μ, is not introduced as an abstract or metaphorical construct. Rather, since CRT energy is treated as a partitioned subset of total neural energy, any vector field governing neural resource flow would, by necessity, project a real and meaningful component onto the cognitive subspace, while a derivation of this full neural resource field is beyond the scope of this dissertation neural resources may include the delivery and utilization of well-known biological resources such as oxygen, glucose, neurotransmitters, and other substrates required for sustained neural activity.

6.2.3 Cognitive Resource Reallocation

Cognitive Resource Reallocation (CRR) models neuroplasticity as the adaptive reallocation of neural resources toward circuits that support cognitive function that facilitate task

engagement under energetic constraint, focusing on neuroplastic changes within that support task proficiency while moving away from less efficient processing.

CRR dynamically modulates CRA to better support repeated task demands under energetic constraint, to task demands. Therefore, the Hamiltonian for CRT is expressed as the sum of the total CRA energy at a given moment $H_{\mathrm{CRA}}(t)$ and the cognitive resource reallocation term $\varepsilon R_{CRR}(t)$ where R_{CRR} is a thermodynamic reallocation function. This relationship is formalized by the CRT Hamiltonian

$$H_{CRT}(t) = H_{\mathrm{CRA}}(t) + \varepsilon R_{CRR}(t).$$

The parameter ε acts as a perturbation coefficient, quantifying the degree to which CRR modifies baseline cognitive dynamics. It serves as a coupling parameter that scales the influence of reallocation relative to the stability maintained by CRA. In physical terms, ε reflects how sensitively the system responds to task-induced demands or internal fluctuations.

When $\varepsilon = 0$, the system evolves according to its unperturbed baseline (CRA-only); as ε increases, CRR exerts proportionally more influence over the cognitive system. Typically, epsilon is assumed to be small $0 < \varepsilon \ll 1,$ as in other perturbative systems, reflecting that CRR corrections are small relative to CRA, which defines the system's energetic baseline state. This preserves baseline coherence, maintaining a dynamic equilibrium between stability and adaptability. Abnormally large ε would indicate runaway reallocation dynamics, which may reflect some pathological cognitive state. Cognitive states that would require higher-order corrections are beyond the scope of this dissertation and reserved for future investigation.

6.2.4 Thermodynamic Foundations of CRT

6.2.4.1 Helmholtz Free Energy in CRT

To define the total free energy of CRT, we begin by examining the free energy expressions for its two core components: Cognitive Resource Allocation (CRA) and Cognitive Resource Reallocation (CRR). Cognitive Resource Allocatoion (CRA) defines a baseline energetic configuration. It's Helmholtz's free energy $F_{\mathrm{CRA}}(t)$ is defined as the trade-off between the internal energy $U_{\mathrm{CRA}}\,(t)$, and the thermal energy lost to entropy, given by the product $T(t)S_{\mathrm{CRA}}(t)$. This yields the standard expression for Helmholtz free energy

$$F_{\mathrm{CRA}}(t) = U_{\mathrm{CRA}}(t) - T(t)S_{\mathrm{CRA}}(t).$$

Unlike CRA, which defines a relatively stable baseline energy configuration, CRR governs the system's adaptive response to cognitive strain. Because this reallocation process departs from the baseline established by CRA, its thermodynamic contribution cannot be subsumed under CRA's free energy. Instead, CRR warrants its own free energy profile to capture the distinct trade-off between investing internally available energy and overcoming configurational entropy. The energy available for reallocation is denoted $E_{\mathrm{A}}\,(t),$ which represents the portion of the system's energy budget not already committed to baseline cognitive operations or essential maintenance. Accordingly, this quantity defines the internal energy of the CRR subsystem:

$$U_{CRR}(t) \equiv\ E_{\mathrm{A}}\,(t),$$

which allows the system to produce refinements that minimize its action in anticipation of expected future strain—analogous to how repeated training strengthens muscle tissue and reinforces structural integrity. These structural adjustments increase the system's robustness to

energetic perturbations, enabling it to more effectively minimize its action with respect to expected load. The free energy of this reallocation process is given by

$$F_{CRR}(t) = U_{CRR}(t) - T(t)S_{CRR}(t).$$

We now define the total free energy of CRT as the combination of energetic and entropic contributions from both CRA and CRR. This total free energy reflects the system's full cognitive state, incorporating both baseline stability and adaptive flexibility. The general form follows the Helmholtz definition

$$F_{CRT}(t) = U_{CRT}(t) - T(t)S_{CRT}(t).$$

However, we must be careful in describing how internal energy and entropy of CRT are composed. Internal energy is additive by the first law of thermodynamics, which states that the total energy of a closed system is conserved and equals the sum of the energies of its constituent parts. In CRT, this allows us to write

$$U_{CRT}(t) \ = U_{CRA}(t) \ + \ U_{CRR}(t),$$

since CRA and CRR represent distinct energy-contributing. Even if these processes interact or overlap functionally, the total energy remains a conserved scalar quantity and can be meaningfully partitioned and summed.

Entropy like energy is considered an extensive property, meaning it scales with the size of the system under the assumption that subsystems are independent. For example, doubling the number of independent particles in an ideal gas doubles the entropy.

However, in complex interacting systems CRA and CRR are not isolated; they share overlapping circuitry, resource channels, and constraints. As a result, entropy in CRT must be computed holistically from the total system state. This means in general for CRT

$$S_{CRT} \ \neq \ S_{\mathrm{CRA}}(t) \ + S_{CRR}(t),$$

and must instead by calculated holistically using the von Neumann entropy expressed by the system's density matrix ρ_{CRT} which is defined as

$$S_{\mathrm{CRT}} = -\mathrm{Tr}(\rho_{CRT} \ln \rho_{CRT}),$$

where Tr denotes the trace operator. This formulation captures the system's total cognitive uncertainty under both allocation and reallocation dynamics. Therefore, $F_{CRT}(t)$**,** the total free energy of CRT, incorporating both CRA and CRR contributions, is given by

$$F_{CRT}(t) = [\, U_{CRA}(t) + U_{CRR}(t)] - T(t)S_{CRT}(t).$$

6.2.4.2 Free Energy Minimization in CRR

Up to now we have described the CRT Hamiltonian as

$$H_{CRT}(t) = H_{\mathrm{CRA}}(t) + \varepsilon R_{CRR}(t)),$$

where $U_{CRA}(t) = \langle H_{\mathrm{CRA}}(t) \rangle$, and $R_{CRR}(t)$ is a thermodynamic reallocation function but up to now we have declined to specify what form R_{CRR} should take and what are its variable dependencies besides some arbitrary function that evolves in time. Since we are treating cognition as a physical system and R_{CRR} as a physical dynamic reallocation mechanism should depend at least on the available energy for reallocation $E_{\mathrm{A}}(t)$ and reallocation must occur within some physical environment which implies a dependence on T(t) defined as the cognitive temperature of the system. Therefore $R_{CRR}(T\,, E_{\mathrm{A}}(t))$ provides the minimum dependencies which a relocation mechanism can physically exist.

As mentioned, the available energy, $E_{\mathrm{A}}(t)$ denotes the pool of cognitive energy currently accessible for reallocation by CRR. It excludes energy already committed to baseline CRA operations, represented by $E_{\mathrm{CRA}}(t)$ as well as energy locked into essential maintenance functions, such as homeostatic regulation, the support of vital systems or other neural processes that are categorically distinct from cognition as defined by the American Psychological

Association(Association, 2018), denoted E_{L}. Thus, the available energy E_{A} is given by the expression

$$E_{\mathrm{A}}(t) = E_{\mathrm{total}}(t) - E_{\mathrm{CRA}}(t) - E_{\mathrm{locked}}(t),$$

where E_{total} (t) represents total energy at a given moment determined by the system's global metabolic budget.

In order describe how adaptive reallocation unfolds under cognitive strain, it is necessary to formulate a physically plausible expression for the reallocation function $R_{CRR}(T, E_{\mathrm{A}})$. Since CRR is understood as a process that adaptively redistributes energy to reduce internal strain, its behavior should be consistent with thermodynamic principles—namely, the tendency of physical systems to minimize their free energy. In this context, the Helmholtz free energy of CRR, $F_{CRR}(t)$, previously defined in Section 6.2.4.1 is the quantity to be minimized. To determine how the system minimizes $F_{CRR}(t)$, we proceed by substituting $U_{CRR}(t) \equiv E_{\mathrm{A}}(t)$ and taking partial derivative with respect to the available energy, $E_{\mathrm{A}}(t)$, and setting it equal to zero. This yields

$$\frac{\partial F_{CRR}(t)}{\partial E_{\mathrm{A}}(t)} = \frac{\partial E_{\mathrm{A}}(t)}{\partial E_{\mathrm{A}}(t)} - T(t)\frac{\partial S_{CRR}(t)}{\partial E_{\mathrm{A}}(t)} = 1 - T(t)\frac{\partial S_{CRR}(t)}{\partial E_{\mathrm{A}}(t)},$$

where T is cognitive temperature, an S_{CRR} is the CRR entropy.

To ensure that reallocation proceeds toward a physically meaningful equilibrium, we require that the system evolve such that $R_{CRR}(T, E_{\mathrm{A}}) \to 0$ corresponding to the minimization of F_{CRR}, a process widely recognized as gradient descent. The only way this function tends toward zero is if the magnitude of $\frac{\partial F_{CRR}(t)}{\partial E_{\mathrm{A}}(t)} \to 0$ which implies $1 - T(t)\frac{\partial S_{CRR}(t)}{\partial E_{\mathrm{A}}(t)} \to 0$.

However, from dimensional analysis, T, S_{CRR}, and E_{A} are all positive-definite quantities with consistent units. Since the elements of CRR form a dynamic subsystem within CRT—

exchanging energy with other constituents of the full system—their thermodynamic behavior is bounded. If the entire CRT system in equilibrium at a temperature, T, then S_{CRR} per unit of E_{A} must satisfy a constraint such that $0 < \frac{\partial S_{CRR}(t)}{\partial E_{\mathrm{A}}(t)} \leq \frac{1}{T}$. Thus, minimization occurs only when the system saturates its capacity for configurational reordering, and any further energy investment yields no additional changes to S_{CRR}. Therefore, the expression that satisfies the minimization criterion is

$$R_{CRR}(T, E_{\mathrm{A}}) = T\frac{dS_{CRR}}{dE_{\mathrm{A}}} - 1 \ = -\frac{\partial F_{CRR}(t)}{\partial E_{\mathrm{A}}(t)},$$

arriving at a final expression for the reallocation function given by

$$R_{CRR}(T, E_{\mathrm{A}}(t)) = -\frac{\partial F_{CRR}(t)}{\partial E_{\mathrm{A}}(t)}.$$

CRT also supports a generalized, field-based formulation of cognitive resource reallocation. In this view, CRR is treated as a spatially and temporally distributed function shaped by local entropy gradients and directional task constraints. The generalized reallocation function takes the form

$$R_{CRR}(x, t) = f\big(\nabla S_{CRT}(x, t), C(x \to y, t)\big).$$

Here, $\nabla S_{CRT}(x, t)$ denotes the spatial gradient of cognitive entropy at a given moment in time, capturing how rapidly uncertainty or representational conflict changes across the system. The term $C(x \to y, t)$, represents a directional constraint term constraint imposed by task demands or interregional influence. In a field-theoretic formulation of CRT , the causal constraint term can be empirically defined using variance-based Granger causality described by

$$C(x \to y, t) = \Delta R^2 = R^2_{\text{full}} - R^2_{\text{reduced}},$$

where R^2_{full} is the variance in region y explained when the past activity past activity of region x is included, and R^2_{reduced} when it is excluded. ΔR^2, was quantified in our analyses using time-

domain Granger causality (TGC), providing a estimate of directional influence brain regions. These results gain further theoretical insight as stronger values of ΔR^2 indicate more influential paths guiding CRR toward structurally and functionally effective routes of energy reallocation.

6.2.4.2.1 Cognitive Efficiency Index

To quantify how efficiently the brain meets task demands using baseline cognitive resources, CRT defines a cognitive efficiency index, η_{eff}, characterized by the expression

$$\eta_{eff} = \frac{E_{task}(t)}{E_{CRA}(t)}.$$

This index, η_{eff}, expresses the ratio of required task energy, $E_{task}(t)$,to the energy already allocated through CRA, $E_{CRA}(t)$. When $\eta_{eff} < 1$, the task is over-supported. When $\eta_{eff} = 1$, task demands are matched exactly by baseline resources—indicating maximal efficiency. When $\eta_{eff} > 1$ task is under supported. This interpretation reframes cognitive efficiency as a thermodynamic budget CRA defines the system's energetic input, while the task imposes an output requirement. In doing so, it offers a useful lens for interpreting resource mismatch and reallocation dynamics.

This framework also parallels broader theories in dynamical optimization, including control theory, attractor dynamics, and constrained trajectory planning—where systems reconfigure themselves in response to both excess and scarcity to optimize performance under changing conditions (Sussillo & Abbott, 2009; Wang, 2002; Churchland *et al.,* 2012).

6.2.4.3 Neuroplastic Potential

The total amount of energy the system invests in reconfiguring its cognitive architecture can be described by integrating the reallocation function across the range of energy available for adaptation, given by

$$|E_{CRR}(t)| = \left| \int_0^{E_{\mathrm{A}}(t)} R_{CRR}(T, E_{\mathrm{A}})\, dE \right|.$$

This expression captures the extent of energetic reallocation in a cognitive system, but not whether that reallocation was functionally constructive or destructive. To assess the qualitative impact of plasticity, CRT introduces the neuroplastic potential defined as

$$NP(t) \equiv F_{\mathrm{CRA}}(t) - F_{\mathrm{CRR}}(t).$$

This quantity reflects the net change in free energy resulting from cognitive reallocation. If $NP(t) > 0$, then CRR reduces the system's free energy, indicating constructive plasticity—such as integration, upregulation, or the formation of more efficient neural pathways. However, if $NP(t) < 0$ then then CRR increases the system's free energy, suggesting destructive plasticity, such as pruning, downregulation, or loss of redundant pathways.

Both forms of plasticity are adaptive. Constructive plasticity enables improved task performance and long-term robustness, while destructive plasticity conserves resources and streamlines cognitive architecture. CRT treats neuroplastic potential as a continuous, energetically grounded indicator of how the brain reorganizes itself under constraint.

6.2.4.4 Thermodynamic Definition of Cognitive Temperature

In CRT, cognitive temperature is defined with respect to a structurally constrained subspace V which represents the anatomical substrate actively supporting a given cognitive process. This subspace is defined as the combined volume of the engaged regions and the white matter pathways linking them. For example, consider a visuomotor decision task that recruits the superior occipital gyrus (SOG) and superior parietal lobule (SPL) to support the integration of motion trajectories, as we investigated in Chapter 3.

In such a case, V can be approximated as the sum of the volumes of SOG and SPL, along with the intervening white matter tracts that carry information between them. Given the physical separation between these regions, white matter pathways are likely the dominant structure of interaction—minimizing the role of direct gray matter continuity or gap junction coupling. This task-defined subspace serves as the bounded domain over which energy, entropy, and reallocation dynamics are evaluated. It reflects the subset of brain structure that is both anatomically viable and functionally engaged at a specific moment in time.

Within this subspace, the number of active cognitive units is represented by N which denotes the total count of participating units such as neurons, synapses, or glial elements. In practice, the number of active cognitive units can be approximated using structural neuroimaging data. For example, if tractography reveals that a task engages the left superior occipital gyrus (SOG) and left inferior parietal lobule (IPL), we can estimate N by combining the anatomical volumes of these two regions with information about the white matter tracts that connect them. The voxel counts or measured volumes of gray matter regions serve as an approximate index of local tissue volume and, by extension, of the potential number of neurons, glial cells, and synaptic connections within each area. While this approach does not yield precise cellular counts, it offers a coarse-grained proxy for estimating the structural capacity of a region to support cognitive function, especially when interpreted in conjunction with known cortical thickness and cytoarchitectonic profiles from anatomical atlases.

Tractography data would serve as a proxy for the number and density of streamlines linking the two regions—provides an estimate of how many long-range connections are likely active during task performance. As with any tractography-based analysis, it's important to be mindful of methodological details. Streamline counts are influenced by factors such as seeding

strategy and tracking parameters, so their interpretation should always be grounded in the context of the specific analysis. In our analysis in Chapter 3, described in Section 3.1.1.2, we used a seed-based approach to localize tractography to task-relevant regions—specifically to avoid imposing assumptions about what N "should be." Instead, we allowed the data to guide the analysis, using seeding to explore pairwise links within a well-defined cognitive subspace. While streamline counts in this context are not absolute, they still serve as a useful proxy for estimating connectivity strength and, by extension, the number of active cognitive units.

This level of interpretive care is consistent with best practices in neuroimaging and reflects the kind of methodological transparency expected in well-conducted studies. Although this approach does not directly count individual neurons or axons, it provides a principled and empirically grounded way to approximate the size of the system engaged during a given cognitive process. Just as importantly, it keeps the CRT framework practical, transparent, and accessible to researchers working with standard imaging data.

For any given momentary configuration, the system can be treated as a dynamic equilibrium, which is effectively stable. This permits a well-defined partial derivative and allows cognitive temperature, T_{CRT} to reflect the system's capacity to effectively allocate resources to support a cognitive process across a given cognitive subspace. Over longer timescales, neuroplastic changes across the nervous system in general may update both V and N, but such shifts occur outside the local thermodynamic frame used to define an instantaneous cognitive temperature. The physiological plausibility is well founded with respect to modern understanding of brain temperature, which is known to be susceptible to local fluctuations (Kiyatkin, 2019; Wang *et al*., 2014). Cognitive temperature T_{CRT} is thus defined as $T_{CRT} \equiv T(t)$, reflecting a global parameter that modulates cognitive processes. The thermodynamic expression for T_{CRT} is

given by the canonical thermodynamic expression as a partial derivative of a cognitive system's internal energy with respect to its entropy while V and N are held constant

$$T_{\mathrm{CRT}} = \left(\frac{\partial U_{\mathrm{CRT}}}{\partial S_{\mathrm{CRT}}}\right)_{V,N},$$

where U_{CRT} is the internal energy of the cognitive system and S_{CRT} is its entropy.

6.2.4.5 Partition Function in CRT

In CRT, cognitive temperature T_{CRT} is defined as a physical quantity which is aligned with the first postulate of CRT which treats cognitive systems as a physical system from its construction. Formal treatment of how cognitive temperature CRT-governed thermodynamics is discussed in Section 6.2.4.2. Accordingly, all thermodynamic expressions retain Boltzmann's constant: $\beta = \frac{1}{k_B T_{\mathrm{CRT}}}$. In theoretical contexts k_B is often set to 1 for simplicity, but it is retained here to preserve accuracy. At rest, a cognitive system occupies cognitive states probabilistically, like any other physical system, with each state's likelihood determined by its energetic cost E_i and a cognitive temperature parameter T. This yields a Boltzmann distribution that defines a cognitive state in Cognitive Resource Theory (CRT) as

$$P_i = \frac{e^{-\beta E_i}}{Z_{CRT}}, \quad Z_{CRT} = Tr\left(e^{-\beta \widehat{H}_{CRT}}\right)$$

where Tr is denotes the trace which a mathematical operation that means taking a sum over all possible cognitive states. Specifically, this involves adding up the contributions of each state along the diagonal of the matrix representation of the system given by $\widehat{H}$—each corresponding to a distinct energy for every possible cognitive state. The Hamiltonian is expressed as an operator (denoted by the hat), its role in this context is simply to assign an energy to each possible cognitive configuration. This ensures that the resulting probabilities are properly normalized.

Here, $P_i\ is$ the probability for a given cognitive system of occupying a given state with energy E_i , is equivalent to $\widehat{H}_{CRT,\ i}$ —the value of the CRT Hamiltonian evaluated at a given state i state evaluated the same way as described in Section 6.2.3. Higher-energy states are exponentially suppressed, and the normalization constant Z_{CRT} known as the partition function, encodes the total energetic weight of all accessible cognitive states under CRT dynamics.

In CRT, the total Hamiltonian is constructed as a sum of its CRA and CRR components under the first law of thermodynamics

$$\widehat{H}_{CRT} = \widehat{H}_{CRA} + \widehat{H}_{CRR}.$$

This reflects the idea that the system's total energy includes both baseline allocation $\widehat{H}_{CRA}$ and dynamic reallocation $\widehat{H}_{CRR}$. Since these contributions are defined over the same set of possible cognitive states. This allows the partition function to be cleanly factorized into separate CRA and CRR terms as shown by

$$Z_{\mathrm{CRT}} = \sum_i \exp\left(-\beta H_{\mathrm{CRA},i}\right) \cdot \exp\left(-\beta H_{\mathrm{CRR},i}\right) = Z_{\mathrm{CRA}} \cdot Z_{\mathrm{CRR}}.$$

6.2.4.6 Thermodynamic Definition of Cognitive Entropy

CRT interprets this entropy not as a purely informational abstraction but as a physically embodied measure of thermodynamic inefficiency.

The Von Neumann entropy quantifies internal uncertainty or dispersion within a cognitive system, introduced in Section 6.2.4.1 as

$$S_{\mathrm{CRT}} = -\mathrm{Tr}(\rho_{CRT} \ln \rho_{CRT}) \ ,$$

where ρ_{CRT} is the system's density matrix, encoding the probabilistic distribution over cognitive states. The challenge, then, is to construct a physically plausible expression for ρ_{CRT} the system's density matrix. Two formulations are presented to address this. The first is a minimal

model in which both CRA and CRR are represented as paramagnets, resulting in a fully separable and computationally efficient system. The second is a more expressive model in which CRA remains a paramagnet, while CRR is modeled using an Ising-like interaction term to account for coupling and synchrony between cognitive units. In each case, the full CRT Hamiltonian is defined explicitly, followed by the corresponding expressions for the density matrix and partition function.

In the simplest possible case, CRA and CRR are each modeled as paramagnets—non-interacting systems in which cognitive regions behave independently. The CRA and the CRA and CRR Hamiltonians are assumed to commute, allowing the total entropyS_{CRT} to be additive, with each region contributing independently to the system's entropy.

Each region contributes a set of local energy terms, resulting in a fully diagonal Hamiltonian

$$H_{\mathrm{CRT}} = \sum_i \left(H_i^{\mathrm{CRA}} + H_i^{\mathrm{CRR}}\right) s_i,$$

where $s_i \in \{-1, +1\}$ represents whether cognitive region i is energetically active (+1) or inactive (–1), following conventions from spin-based models in physics.

For example, in the visuomotor decision network described in Chapter 3, the superior occipital gyrus (SOG) and superior parietal lobule (SPL) would each correspond to spin variables $s_{\mathrm{SOG}}$and s_{SPL}encoding their activation states during task engagement. The corresponding density matrix would then be given by

$$\rho_{CRT} = \frac{1}{Z_{CRT}} exp\left[-\beta \sum_i \left(H_i^{CRA} + H_i^{CRR}\right) s_i\right]$$

where $\beta = \frac{1}{k_B T_{\mathrm{CRT}}}$, with T_{CRT}denoting the cognitive temperature and k_B is the Boltzmann constant. Z_{CRT} is the CRT partition function described as

$$Z_{\mathrm{CRT}} = \sum_{\{s_i\}} \exp\left[-\beta \sum_i \left(H_i^{\mathrm{CRA}} + H_i^{\mathrm{CRR}}\right) s_i\right].$$

This formulation is computationally efficient and analytically separable. It is a physically plausible model of a density matrix that would yield CRT entropy, though it assumes regional independence and does not account for task-driven coordination or synchrony.

To incorporate empirically grounded features such as synchrony, phase-locking, and interregional coordination, CRR is instead modeled using an Ising-like structure. In this formulation, CRA remains diagonal, based on the assumption that baseline cognitive states are separable. Without separability, the cognitive system could not be described by a Hamiltonian, which would violate the first postulate of CRT, as defined in Section 6.2.1.1. Under this model, no assumption is made regarding the commutativity between the Hamiltonians of CRA and CRR.

To incorporate empirically grounded features such as synchrony, phase-locking, and interregional coordination, CRR is instead modeled using an Ising-like structure. In this formulation, CRA remains diagonal, based on the assumption that baseline cognitive states are separable. Without separability, the cognitive system could not be described by a Hamiltonian, which would violate the first postulate of CRT, as defined in Section 6.2.1.1. Under this model, no assumption is made regarding the commutativity between the Hamiltonians of CRA and CRR.

The Ising model was originally developed in statistical physics to explain ferromagnetism—specifically, how simple local interactions between neighboring atomic spins could give rise to large-scale, collective magnetic order (Brush, 1967). In the context of CRT, this same structure offers a principled way to model coordinated neural reallocation under energetic constraint. Just as the Ising model captures emergent global behavior from simple local

couplings between binary spin states, CRT must account for the emergence of coordinated, large-scale cognitive patterns from local interactions between distributed neural units. This same structure offers a principled way to model coordinated neural reallocation under energetic constraint, reflecting the parallel challenge CRT faces in formally describing emergent order within the brain.

Empirically, structured neural synchrony is observed across multiple scales—from spike-timing correlations in Hodgkin–Huxley dynamics, to long-term potentiation (LTP) in Hebbian plasticity, to mesoscopic neural field models such as the Wilson–Cowan framework. To reflect these interaction-based processes, CRR introduces coupling between cognitive units via pairwise terms—an abstraction that not only models but aligns with the empirically observed synchrony, coordination, and emergent dynamics that characterize real neural systems during episodes of cognitive strain and realignment. The corresponding Hamiltonian is expressed as

$$H_{\mathrm{CRT}} = \sum_i H_i^{\mathrm{CRA}} s_i - \sum_{i<j} H_{ij}^{\mathrm{CRR}} s_i s_j$$

where $s_i \in \{-1, +1\}$ as before. Here H_{ij}^{CRR} represents the pairwise interaction energy between cognitive units i and j, introduced by CRR during episodes of resource reallocation. Positive values of H_{ij}^{CRR}reflect energy-reducing co-activation (e.g., functional synchrony), while negative values reflect competitive or desynchronized dynamics. This term captures the structured dependencies that arise during resource reallocation. The beta parameter β is unchanged. The density matrix, under this model is expressed as

$$\rho_{CRT} = \frac{1}{Z_{CRT}} exp\left(-\beta \left[\sum_i H_i^{CRA} s_i - \sum_{i<j} H_{ij}^{CRR} s_i s_j \right] \right).$$

The partition function Z_{CRT} is now expressed as

$$Z_{\mathrm{CRT}} = \sum_{\{s_i\}} \exp\left(-\beta \left[\sum_i H_i^{\mathrm{CRA}} s_i - \sum_{i<j} H_{ij}^{\mathrm{CRR}} s_i s_j \right] \right).$$

This provides a physically grounded basis for computing cognitive entropy in CRT under an Ising model formulation of CRR.

6.2.5 CRT as a Physically Grounded Extension of The Free Energy Principle

The Free Energy Principle offers an information-theoretic account of inference in the brain, wherein cognition minimizes a variational free energy functional (Friston, 2010)

$$\mathcal{F} = D_{\mathrm{KL}}[q(s)|p(s \mid o)] - E_{q(s)}[\log p(o \mid s)].$$

Here, the first term $D_{\mathrm{KL}}[q(s)|p(s \mid o)]$ is the "Kullback–Leibler divergence", a measure of how far the brain's internal model $q(s)$ deviates from the ideal Bayesian posterior probability $p(s \mid o)$. The latent causes or hidden states of the environment that the brain attempts to infer is given by "s" represents latent causes and "o" represents sensory inputs or observed outcomes.

The KL divergence term is defined as

$$D_{\mathrm{KL}}[q(s)|p(s \mid o)] \equiv \sum_s q(s) \log \frac{q(s)}{p(s \mid o)}$$

which can be expanded to show its decomposition into entropy and cross-entropy terms given by

$$D_{\mathrm{KL}}[q(s)|p(s \mid o)] = -H[q(s)] - \sum_s q(s) \log p(s \mid o).$$

$H[q(s)] = -\sum_s q(s) \log q(s)$ is Shannon entropy of the brain's belief distribution denoted by $q(s)$. The second term of $\mathcal{F}$, $E_{q(s)}[\log p(o \mid s)]$ is the expected log-likelihood, or the expected causal evidence the brain assigns to the observation under its current beliefs of expected outcomes $E_{q(s)}$ regarding the likelihood of the observations o, given those causes. Minimizing

$\mathcal{F}$ aligns internal beliefs with external data, reducing surprise. As (Friston, 2010)notes, the free energy can also be expressed as the negative log "model evidence" minus the Shannon entropy of the "recognition density" which is given by

$$\mathcal{F} = -E_{q(s)}[\log p\,(o, s)] + E_{q(s)}[\log q\,(s)].$$

This form directly parallels the Helmholtz free energy identity where the first term corresponds to internal energy and the second to entropic cost. In CRT, the same trajectory can be followed by reformulating the cognitive dynamics in energy terms, ultimately arriving at a direct analog to the Helmholtz free energy identity $F = U - T\,S$.

6.2.5.1 CRT Parallels with the Free Energy Principle in the High-Resource Limit

Cognitive Resource Theory (CRT) was developed independently of the Free Energy Principle (FEP), with its foundations rooted in thermodynamics and physical systems modeling. It was only after the core structure of CRT had been established that connections to FEP were recognized, revealing convergent themes despite distinct theoretical origins. CRT was not constructed with the intent to incorporate the full Bayesian logic central to FEP, nor does it go out of its way to attempt to do so. FEP frames cognition as a process of variational inference under uncertainty, where surprise is minimized through continuous updating of internal beliefs (Friston, 2010). CRT, in contrast, focuses on how adaptive cognition is physically possible. It models cognition as a thermodynamically governed system, where available energy, entropy gradients, and structural constraints determine the feasibility and direction of resource reallocation. Recent work has emphasized the thermodynamic cost of belief updating under metabolic constraint (Fields *et al*., 2024), reinforcing the importance of frameworks that embed cognitive processes within physical systems. CRT addresses this need by explicitly incorporating

energy availability and entropy production into its governing equations, thus offering a thermodynamic foundation for adaptation and plasticity.

In the high-resource limit—where cognitive state distributions are fully separable and optimized—the reallocation function of CRR is effectively zero and the system's density matrix approaches a diagonal form captured by its entropy modeled as a paramagnet see Section 6.2.4.6. CRT and FEP align in their goals seeking minimal free energy states, albeit from different starting assumptions. FEP offers deep insight into probabilistic inference and model updating, while CRT focuses on the thermodynamic conditions that govern when and how such inference processes are energetically supported offering a physically grounded extension.

Together, these complementary frameworks offer a richer perspective of cognitive adaptation—unifying probabilistic reasoning and physical resource dynamics within a broader framework of physically grounded cognitive function. How CRT may further interface with FEP remains an exciting topic for further investigation.

6.2.6 Lagrangian and Path Integral Formulation of CRT

Physical systems tend to evolve along paths that minimize a quantity known as action—a measure of the system's total energetic expenditure over time. This principle, formally referred to as the principle of stationary action forms the 2nd postulate of CRT and is more commonly known as the principle of least action, both because minimization is the typical case and because the phrasing is more intuitive. The concept aligns with everyday metaphors like "following the path of least resistance" or "going with the flow"—expressions that echo nature's preference for efficient trajectories. In physics, this principle provides a powerful framework for understanding how dynamic systems behave under constraint. To capture this formally, CRT defines an action

functional, which quantifies how costly a given pattern of cognitive reallocation would be. The brain then follows the trajectory that minimizes this quantity, yielding the most energetically favorable path given current constraints.

To model cognitive processes as physically grounded dynamical systems, we define a Lagrangian for the evolution of cognitive state variables given by generalized coordinates q which correspond to the degrees of freedom a cognitive system can take while remaining physically lawful. The baseline dynamics are still governed by CRA which defines a minimal-energy trajectory. Deviations from this baseline—are mitigated by CRR which modulates energy flow across subsystems. The cognitive configuration space Q consists of all possible trajectories the brain can take through its set of physiological degrees of freedom including both functional activations and anatomical constraints. Each coordinate $q \in Q$ represents the activation state of a neural population actively engaged in a cognitive task at some given time, t —such as an ROI, a node in a functional network, or a localized circuit supporting perception, attention, or some other cognitive function. The rate of change $\dot{q}$ captures how quickly that activation shifts over time, and may correspond to observable dynamics such as fluctuations in the frequency content of a BOLD (blood oxygenation level dependent) or electrophysiological time series. Together, q and $\dot{q}$ describe the system's evolving trajectory through cognitive state space. This trajectory reflects both the brain's intrinsic dynamics (governed by CRA) and task-evoked adjustments (modulated by CRR), defining how cognitive systems reconfigure themselves to remain energetically viable and functionally effective. To formalize these dynamics, we define the CRT Lagrangian as the sum of a baseline term provided by CRA and a perturbation term introduced by CRR

$$\mathcal{L}_{CRT}(q, \dot{q}, t) = \mathcal{L}_{CRA}(q, \dot{q}) + \varepsilon R_{CRR}(q, \dot{q}, t),$$

where $\mathcal{L}_{CRA}(q, \dot{q}, t) = \frac{1}{2}\dot{q^2} - V(q(t))$ is the CRA Lagrangian. The function $V(q(t))$, represents the potential energy associated with the system's current configuration. Although it formally depends on time, it is standard practice to express this simply as $V(q)$ with the time dependence understood implicitly. $R_{CRR}(q, \dot{q}, t)$ is a perturbation term encoding task-induced reallocation demands, and ε is the perturbation coefficient, representing the strength of CRR influence. The Euler–Lagrange equation is simply how you derive the equations of motion from a Lagrangian. At its core, it's an upscaled, generalized version of Newton's second law $F = ma$ that applies not just to particles but to any dynamic system evolving over time. In Cognitive Resource Theory (CRT), it describes how a cognitive brain network evolves through its high-dimensional configuration space in a way that balances energetic cost, internal stability, and external task demands. Under real-world constraints, CRT models this evolution as a constrained dynamical system—one in which cognitive trajectories are shaped by limitations in energy availability and the brain's anatomical and physiological constraints. The Euler–Lagrange equation for CRT, under energetic constraints, takes the form of a constrained dynamical system

$$\left(\frac{\partial \mathcal{L}_{CRT}}{\partial \dot{q}}\right) - \frac{\partial \mathcal{L}_{CRT}}{\partial q} = \lambda \frac{\partial \phi(q, \dot{q}, t)}{\partial q}.$$

In CRT, cognitive friction ϕ quantifies the energetic mismatch between a system's current trajectory through cognitive configuration space and the baseline energetic capacity available for task performance. This means ϕ quantifies the energetic heat induced by some cognitive task straining the system and is formally defined as

$$\phi(q, \dot{q}, t) = \mathrm{D}(\dot{q^2}) - E_{\mathrm{CRA}}(t),$$

where $D(\dot{q})$ is the Rayleigh dissipation function, encoding anisotropic resistance across cognitive subsystems.

This dissipation function is denoted as

$$D(\dot{q}) = \frac{1}{2}\sum_{j=1}^{m}\sum_{k=1}^{m} C_{jk}\dot{q}_j\dot{q}_{k.}$$

The matrix C_{jk} are constants that are related to the damping coefficients governing the coupling strength or reconfiguration cost between cognitive components q_j and q_k in the system's configuration space. Cognitive friction is minimized when the system is operating efficiently — i.e., when dissipation matches available cognitive energy: $D = E_{CRA}$. The baseline $E_{CRA}(t)$ is energetic capacity available for cognitive action, as defined by the CRA at time t.

When $D > E_{CRA}$ the resulting cognitive friction induces a deviation from minimal-action trajectories in cognitive state space, which the system counteracts through CRR by realigning with a configuration better suited to mitigate the energetic costs of navigating tasks with high expected cognitive demands. More generally, λ(t) functions as a constraint multiplier that modulates cognitive reallocation in response to both cognitive load and thermodynamic conditions. This formulation unifies proactive energy allocation and reactive adaptation under a single mathematical framework.

The constraint multiplier $\lambda(t)$ is defined as a function that combines both energetic and entropic gradients in cognitive configuration space. It is shaped by gradients in the system's energy landscape and local entropy, capturing how internal dynamics respond to task demands and uncertainty. Specifically, it is given by the expression

$$\lambda(t) = \alpha \cdot \nabla_q E(q,t) + \beta \cdot \nabla_q S_{\mathrm{CRT}}(q,t).$$

The first term $\nabla_q E(q,t)$ captures how the gradient of cognitive energy varies with respect to this coordinate, reflecting the system's sensitivity to task-related energetic demands. The second term and $\nabla_q S_{\mathrm{CRT}}(q,t)$ quantifies the gradient of CRT-defined entropy, characterizing how internal

uncertainty or representational dispersion shifts across the configuration space. The coefficients α encodes energy-driven reallocation (task-load sensitivity), while β encodes sensitivity to entropy-driven demands, such as internal conflict or ambiguity.

6.2.6.1 Legendre Transformation from Lagrangian to Hamiltonian

To unify the Lagrangian and Hamiltonian formulations of CRT, we apply the Legendre transform, and we set the effective mass to unity, $m = 1$, to simplify the kinetic term. Starting from the total Lagrangian,

$$\mathcal{L}_{CRT}(q, \dot{q}, t) = \mathcal{L}_0(q, \dot{q}) + \varepsilon R_{CRR}(q, \dot{q}, t),$$

the canonical momentum is denoted as

$$p = \frac{\partial \mathcal{L}_{CRT}}{\partial \dot{q}} = \dot{q} + \varepsilon \frac{\partial R_{CRR}}{\partial \dot{q}}.$$

The Hamiltonian is then obtained by the Legendre transform given by

$$H_{CRT}(q, p, t) = p\dot{q} - \mathcal{L}_{CRT}(q, \dot{q}, t).$$

Substituting $q^{\cdot} = q^{\cdot}(p)$, we can then write the Hamiltonian as

$$H_{CRT}(q, p, t) = \frac{1}{2}p^2 + V(q) + \varepsilon R_{CRR}(q, p, t).$$

This confirms that the reallocation term R_{CRR}, while originally velocity-dependent, can be recast in terms of canonical coordinates, and validates its appearance in the Hamilton–Jacobi equation given by

$$\frac{\partial S_{CRT}}{\partial t} + \frac{1}{2}\left(\frac{\partial S_{CRT}}{\partial q}\right)^2 + V(q) + \varepsilon R_{CRR}(q, t) = 0.$$

Here, $S_{CRT} = S(q, t)$ is the action of the CRT system. The purpose of this exercise was to demonstrate that both the Lagrangian and Hamiltonian formulations of CRT represent the same physical system, and by deriving a clear expression for the Hamilton–Jacobi equation, we have achieved that objective.

6.2.6.2 Path Integral Representation of Cognitive Resource Dynamics

In the Lagrangian representation of CRT neural adaptation involved with some cognitive process can be modeled as a probabilistic trajectory through state space. These trajectories are governed not only by baseline energetics but also by transient reallocations induced by CRR. To capture this, we define a path integral over cognitive histories described by the generalized coordinate describing the degrees of freedom, q(t), incorporating both CRA and CRR components into the total action. This treats cognitive adaptation as a superposition of possible trajectories, each weighted by its energetic cost. In the classical limit, the dominant trajectory minimizes the action, producing efficient yet constrained cognitive responses. The path integral over $\mathrm{Dq(t)}$ sums over all cognitively plausible trajectories, with each trajectory weighted by an exponential kernel derived from the CRT action. This kernel reflects the energetic cost of the path, encoding the system's probabilistic preference for efficient reallocation. To describe such a path integral representation for possible paths a cognitive system might take and expectation of observable quantities based on this these possible paths, we must first describe the CRT partition function Z which is denoted by

$$Z(q) = \int Dq(t)\ e^{\frac{i}{\hbar}S_{CRT}[q(t)]},$$

where the CRT action $S_{CRT}[q(t)]$ is expressed as

$$S_{CRT}[q(t)] = \int dt\ \left(\mathcal{L}_0(q,\dot{q}) + \varepsilon R_{CRR}(q,\dot{q},t)\right).$$

While CRT adopts the formal machinery of action-based dynamics (*e.g.*, path integrals, partition functions), the CRT action $S_{CRT}[q(t)]$ has not yet been derived from fundamental fields. Instead, it is a phenomenological action defined over cognitive configuration space, encoding energetic, entropic, and relevant constraints. A full physical correspondence between

CRT and formal field-theoretic Lagrangians would require an explicit mapping of cognitive operators onto fundamental fields, a task that lies well beyond the scope of this dissertation.

In formalizing CRT, we adopt the convention of natural units by setting the reduced Planck's constant to unity ($\hbar = 1$). In this context, this reflects a move to natural units to simplify and generalize the structure of cognitive path weighting. By doing so, action and phase become dimensionless, allowing cognitive dynamics to be expressed more cleanly in terms of relative influence and path weights, rather than absolute units. This convention enables the partition function Z to take the form

$$Z = \int Dq(t)\ e^{iS_{CRT}[q(t)]},$$

which allows calculation of expected values of observables $\langle \mathcal{O}[q(t)] \rangle$ given by

$$\langle \mathcal{O}[q(t)] \rangle = \frac{1}{Z} \int Dq(t)\ \mathcal{O}[q(t)]\, e^{iS_{\mathrm{CRT}}[q(t)]}.$$

Examples of $\langle \mathcal{O}[q(t)] \rangle$ include $\mathcal{E}$ which is the expected energetic cost of a trajectory; maps to task difficulty or neural efficiency, ρ_{ij} which is a scalar measure of connection strength between brain regions i and j (*e.g.* FC, dFC, SC), T which is expected cognitive temperature across all trajectories and $J[q(t)] = S_{max} - S[q(t)]$ which describes "negentropy" or rather entropy reduction from a maximal baseline. Negentropy quantifies internal structure or representational precision gained along a trajectory. As an example how to calculated an expectation value under this formalism, consider the expected energetic cost $\mathcal{E}[q(t)]$ of executing some cognitive task. To do this, we write the energy functional as

$$\mathcal{E}[q(t)] = \int dt \left(\frac{1}{2} \dot{q^2} + V(q) + \epsilon R_{CRR}(q, \dot{q}, t) \right),$$

then the expression,

$$\langle \mathcal{E} \rangle = \frac{1}{Z} \int Dq(t) \left[\int dt \left(\frac{1}{2} \dot{q^2} + V(q) + \epsilon R_{CRR}(q, \dot{q}, t) \right) \right] e^{iS_{CRT}[q(t)]},$$

yields the expected energy which quantifies the average cost the system will expend across all feasible cognitive paths when engaging with a given task or decision. Other functionals, such as expected entropy, action complexity, or directional connectivity, can be similarly derived within this framework. Critically, the support of the path integral, which corresponds to trajectories that contribute to the value of an observable, $\langle O \rangle$, is shaped by the structure of $S_{CRT}[q(t)]$. From this foundation, the CRT partition function encodes not only optimal strategies but the full probability-weighted distribution of trajectories that a cognitive system could take under real-world constraints. In the absence of strenuous task demands, CRA governs minimal-effort cognitive dynamics along energy-efficient paths. In response to strain—such as increased task complexity, time pressure, or novelty—CRR reallocates energy to meet the system's expected energetic demands. This shifts the system's trajectory away from baseline and into a new region of state space, governed by the modified Lagrangian.

In traditional path integral formulations, any multiplicative constant c it is possible in future extensions to introduce a normalization constant c, analogous to a global scaling factor over the space of cognitive trajectories. In traditional path integral formulations, such constants are typically absorbed into the normalized partition function Z. However, within CRT, we allow for the possibility that such a scaling factor may carry theoretical or biological significance—potentially encoding baseline cognitive resolution, neuromodulatory tone, or inter-individual differences in resource sensitivity. While this constant is not explicitly modeled here, its inclusion could provide a future renormalization-parameter for individual variability in CRT dynamics.

6.2.7 Predictive Validity of CRT: Sleep–Wake Energetics and Neuroplasticity

To validate the empirical grounding of Cognitive Resource Theory (CRT) beyond the dataset investigated in this dissertation, a canonical neural contrast between the transition between sleep and wakefulness was examined.

In CRT, the Cognitive Resource Allocator (CRA) defines the brain's baseline internal energy configuration, shaped by metabolic efficiency, energetic stability, and homeostasis. When task demands or uncertainty strain this baseline capacity, the Cognitive Resource Reallocator (CRR) initiates adaptive reallocation, shifting energy toward relevant systems and downregulating inefficient processes as an investment to more effectively meet environmental demands and relieve internal cognitive friction. This reallocation incurs a thermodynamic cost, modeled as a deviation from the CRA-defined baseline.

The formal structure of CRT is captured by the expressions:

$$H_{CRT} = H_{\mathrm{CRA}} + \varepsilon R_{CRR}(T, E_{\mathrm{A}}), \qquad (1)$$

$$R_{CRR}(T, E_{\mathrm{A}}) = -\frac{\partial F_{CRR}}{\partial E_{\mathrm{A}}}, \qquad (2)$$

$$E_{\mathrm{A}} = E_{\mathrm{total}} - E_{\mathrm{CRA}} - E_{\mathrm{L}}. \qquad (3)$$

Equation (1) defines total cognitive energy expenditure as the sum of the baseline energetic load (CRA) and a context-sensitive reallocation cost (CRR). Equation (2) links the reallocation rate to the gradient of a free energy function F_{CRR} , introducing a thermodynamic cost landscape that governs reallocation efficiency. Equation (3) defines the energy pool available for CRR E_{A} after accounting for baseline and biologically locked energy (*e.g.,* maintenance of vital systems, homeostasis).

From these definitions, we derive

$$E_{\mathrm{CRR}} = \int_0^{E_{\mathrm{A}}} R_{\mathrm{CRR}}(T, E_{\mathrm{A}}) d\, E = -\int_0^{E_{\mathrm{A}}} \frac{dF_{\mathrm{CRR}}}{dE} dE,$$

$$\Rightarrow E_{\mathrm{CRR}} = F_{\mathrm{CRR}}(0) - F_{\mathrm{CRR}}(E_{\mathrm{A}}).$$

Therefore, if $E_{\mathrm{CRA}}^{\mathrm{wake}} > E_{\mathrm{CRA}}^{\mathrm{sleep}}$, then $E_{\mathrm{CRR}}^{\mathrm{sleep}} > E_{\mathrm{CRR}}^{\mathrm{wake}}$.

This result predicts that a lower baseline energy expenditure increases the energy available for dynamic reallocation, thereby enabling greater plasticity through CRR. Since the integral form expression for E_{CRR} holds for any allowable value of E_{A}, this result is general and does not depend on the specific value of R_{CRR}. Comparing this theoretical prediction to what is known in the literature, we note that empirical findings have reported that brain energy expenditure during non-rapid eye movement (NREM) sleep is known to decrease to approximately 85% of its waking value (DiNuzzo & Nedergaard, 2017).

This aligns precisely with $E_{\mathrm{CRA}}^{\mathrm{wake}} > E_{\mathrm{CRA}}^{\mathrm{sleep}}$, since E_{CRA} is defined by its construction as the brain's baseline internal cognitive energy. Therefore, a drop in the brain's internal energy expenditure maps to the subset of internal energy available for baseline cognitive function. Furthermore, the NREM sleep state has been consistently associated with enhanced neural plasticity relative to wakefulness (Nissen *et al*., 2021), which aligns precisely with CRT's prediction that a greater amount of energy should be available for CRR reconfiguration during sleep, $E_{\mathrm{CRR}}^{\mathrm{sleep}} > E_{\mathrm{CRR}}^{\mathrm{wake}}$, to facilitate neuroplastic adaptations that improve overall system configuration in response to cognitive friction induced by task-related strain under current baseline CRA support.

6.2.8 Summary of Cognitive Resource Theory

The Cognitive Resource Theory (CRT) framework unifies physical energetics, neural architecture, and cognition into a single, testable formalism. It models baseline and adaptive processes through Cognitive Resource Allocation (CRA) and Cognitive Resource Reallocation (CRR), and has empirical support in both observed neural adaptations associated with long-term action video game experience within the dataset investigated in this dissertation , and real-world phenomena outside this dataset, such as sleep–wake cycles.

From this perspective, the brain functions as a variational system constrained by thermodynamic costs, continuously navigating a dynamic cognitive resource landscape. Cognitive friction—arising from novelty, ambiguity, or task-induced strain —acts as a perturbation, displacing the system from its dynamic energetic equilibrium. The system's adaptive response reflects a shift toward reducing internal conflict and minimizing energetic inefficiency. This behavior aligns with the principle of stationary action in physics and offers a physically grounded extension of the Free Energy Principle within a framework of bounded cognitive resources.

Together, through theoretical consistency and empirical plausibility, establish CRT as a viable candidate for modeling adaptive cognition in real-world contexts. More empirical testing is of course required. As a current limitation here, CRT has not yet been validated with direct metabolic (*e.g.,* PET) measurements, and further refinements and modifications to the present framework may be necessary to ground this theory in known neural physiology.

Together, CRA and CRR define a resource-constrained cognitive manifold that evolves as a function of environmental pressure and internal resource availability. CRT formalizes this process using principles from gauge theory, statistical mechanics, and dynamical systems. CRT

unifies structure, function, and behavior associated with cognitive systems under a common physically plausible framework and provides the mathematical machinery to reason about cognitive thermodynamics; neuroplastic adaptation as a response to induced strain on neural systems; synaptic remodeling as an energetically costly reallocation effort that mitigates friction in response to strenuous task demands; experience-induced plasticity as a structured trajectory through constrained cognitive state space, shaped by task engagement and system limitations; cognitive fatigue as resource depletion over time without replenishment, formally modeled as an increased spread or divergence.

7 LIMITATIONS AND FUTURE CONSIDERATIONS

7.1 Strengths, Limitations of Analytical Modes

7.1.1 Brain Network Analysis: Dorsal and Ventral Visual Streams

This hypothesis-driven, anatomically grounded approach offered several advantages. By focusing on predefined inter-regional subnetworks—specifically the dorsal and ventral visual streams—we were able to constrain the analysis to functionally and topologically relevant areas implicated in visuomotor decision-making. This targeted strategy increased statistical power by maintaining a favorable N > number of ROIs ratio and reduced the risk of spurious group differences by narrowing the scope of comparisons.

This approach is especially effective when prior theory or empirical data, such as percent BOLD signal change, provides a principled basis for defining task-relevant circuits. As demonstrated in earlier work by Jordan (2021), using functional activation to guide anatomical ROI selection enables focused testing of mechanistic hypotheses while avoiding unnecessary statistical burden across unrelated brain regions.

However, this method comes with limitations. It may overlook broader network-level reorganizations or adaptations occurring outside of the predefined streams. Additionally, while functional ROI measures derived from fMRI provide robust summaries of regional co-activation, they lack the temporal resolution to capture finer-grained neural dynamics such as fast oscillatory coupling, cross-stream phase interactions, or transient signaling fluctuations. These limitations highlight the value of complementary modalities such as EEG or MEG, which offer

superior temporal precision and could reveal additional insight into dynamic reallocation patterns during decision-making.

The interpretability of anisotropy-based tractography also imposes constraints, particularly in regions affected by crossing fibers or partial volume effects. To mitigate these issues, we employed quantitative anisotropy (QA)-based tractography, which outperforms traditional FA methods in preserving directional specificity and resolving complex fiber orientations. QA, implemented via q-space diffeomorphic reconstruction (QSDR), enhances sensitivity to true axonal pathways and improves anatomical plausibility.

Despite these limitations, the results from Chapter 3 provide strong evidence for targeted neuroplasticity within the dorsal stream, a key network for visuomotor integration known to encode object trajectories(Cahill *et al*., 2024; Goodale & Milner, 1992; Tulloch & Pammer, 2019), and demonstrate how sustained action video game play may drive adaptive reallocation of cognitive resources. This work lays a mechanistic foundation for the broader whole-brain analyses and theoretical developments explored in the chapters that follow.

7.1.2 Whole Brain Analysis: SC-FC & SC-dFC

Clarifying the methodological strengths and constraints of our tractography constrained investigation of functional and directed connectivity is essential for interpreting our findings and informing future research. Below, we outline key strengths for future studies that would like to continue this line of inquiry put forth by this dissertation, examining behaviorally relevant neuroplastic refinements due to long-term experience with playing action video games.

Using white matter tractography to structurally constrain functional connectivity reduces false positives by limiting statistical comparisons to anatomically viable connections—i.e., those

supported by known white matter tracts. Unlike unconstrained full-brain FC analyses that test all possible pairwise combinations regardless of biological plausibility. Considering SC-FC and SC-dFC improves neurobiological interpretability and dramatically reduces the total number of comparisons.

Specifically, both SC-FC and SC-dFC analyses were computed across 13,818 valid statistical comparisons (excluding NaNs and self-connections). Under a null model with $\alpha = 0.05$, this would yield approximately 690 ± 26 false positives. In contrast, we observed substantially fewer: 498 for SC-FC ($Z = -7.38$, $p = 1.53 \times 10^{-13}$) and 592 for SC-dFC ($Z = -3.77$, $p = 0.00016$). The observed distributions deviate significantly from the null expectation, strongly indicating that these results reflect structured, behaviorally meaningful differences in connectivity rather than random noise.

The behavioral relevance of these results is further supported by consistent and interpretable violin plot distributions for node degree and local efficiency strengthens confidence in this framework. Our findings align with known neuroanatomical pathways and task-relevant brain systems, reinforcing the utility and validity of SC-based filtering for detecting meaningful group-level effects.

However, several limitations must be acknowledged. First, structural connectivity is inherently constrained by tractography's parameter bounds—minimum fiber length, angular thresholds, and model resolution. This may result in the omission of short-range, sharply turning, or multi-synaptic pathways, especially within complex relay hubs like the thalamus. Moreover, SC-based filtering excludes connections between regions that are functionally coordinated but lack a directly detected structural edge.

Tractography remains an indirect, model-based approximation of true anatomical architecture. While we mitigate some of its limitations by using quantitative anisotropy (QA)–based tractography, which outperforms traditional FA in resolving crossing fibers and preserving directional specificity, no tractography method offers absolute anatomical ground truth. QA, based on q-space diffeomorphic reconstruction (QSDR), improves sensitivity to true axonal trajectories and bolsters anatomical plausibility. Nonetheless, tractography fidelity ultimately constrains the scope of SC-based connectivity.

In parallel, functional ROI measures derived from fMRI are limited in temporal resolution and may fail to capture finer-grained dynamics such as fast oscillatory coupling or cross-network phase interactions. These limitations highlight the importance of complementary techniques, such as EEG or MEG, which offer the temporal precision necessary to characterize rapid reallocation events or state transitions that may underlie behaviorally relevant network adaptations.

Finally, while SC-FC and SC-dFC analyses offer anatomical grounding, they may miss distributed patterns of functional change that fall outside direct white matter pathways. Integrating this method with complementary data-driven approaches, such as the rcPCA-based ROI selection strategy introduced in Chapter 5, offers a promising way to recover signal that may be overlooked by strict structural constraints. In this sense, SC-based filtering and data-driven variance decomposition serve as synergistic tools for capturing both anatomically grounded and emergent features of neuroplastic adaptation.

7.1.3 Whole-Brain Analysis: rcPCA-Based ROI Selection

The rcPCA-based ROI selection framework provided a scalable, data-driven approach to identifying the most behaviorally informative brain regions without relying on predefined anatomical constraints. Unlike structurally constrained methods, PCA operates agnostically to prior anatomical assumptions, enabling detection of latent patterns of structured intersubject variability across the whole connectome.

By computing cumulative variance-weighted contributions across all components, the method reduces dimensionality while preserving interpretability. This significantly lowers the multiple comparisons burden that typically hinders full-brain ROI-wise testing, thereby improving both statistical power and the replicability of findings—especially in modestly sized samples where power and overfitting are major concerns.

This approach is particularly valuable in contexts like the present study, where the number of connectivity features far exceeds the sample size—an inherent challenge in high-dimensional neuroimaging data. By filtering ROIs based on structured variance, PCA mitigates this dimensionality mismatch, increasing statistical power and enhancing the robustness of downstream analyses.

The secondary hypothesis guiding this study was that the PCA-based variance model would reveal behaviorally relevant structure–function couplings and connectivity patterns that help explain the observed ~190 ms response time advantage in gamers. This hypothesis was supported across multiple modalities, with PCA-derived ROIs yielding reproducible group differences and brain–behavior correlations that aligned with CRR's predictions: a reallocation

of resources toward efficient visuomotor pathways and away from redundant or compensatory circuits. While these results are encouraging, the broader promise and potential for this method to generalize beyond the current study remain open for exploration. Given its statistical efficiency, adaptability, and interpretability, the PCA-based ROI selection framework may be especially useful for researchers navigating high-dimensional data with modest sample sizes, where structured variance filtering can sharpen signal, suppress noise, and reveal behaviorally meaningful patterns that might otherwise remain obscured.

Our validation efforts revealed that Spearman rank significance was lost when contributions were limited to only the top 20 ROIs per component for dFC receiver and SC metrics, but fully recovered when cumulative contributions across all ROIs were used—achieving machine-level precision across modalities once the number of included regions exceeded 90 (see Section 2.2.4.7 for details). This suggests that meaningful contributors may be more diffuse or non-monotonically distributed across components. While top-N truncation can highlight salient regions, it risks obscuring the global variance structure. Although PCA is linear, these discrepancies may indicate more complex or nonlinear variance patterns. Future work could apply nonlinear methods such as kernel PCA, manifold learning, or tensor decompositions to explore whether residual variance reflects interactions or features that escape linear separation. At a minimum, these findings underscore the importance of combining linear methods like PCA with downstream validation to ensure full coverage of relevant variance space.

Although PCA is a linear method, the observed discrepancies suggest that some relationships may be nonlinear. Future work may benefit from extending this framework through nonlinear dimensionality reduction approaches, such as kernel PCA, manifold learning, or tensor

decomposition, which may capture residual variance not separable by linear projection. Additionally, dynamic PCA or cross-modal tensor decomposition could track time-varying changes in variance structure, enabling applications in adaptive neurotechnology such as brain–computer interfaces (BCIs).

The PCA-derived ROI framework is also compatible with complementary techniques. For example, ICA (Independent Component Analysis) could uncover orthogonal, statistically independent signals that may corroborate or expand on PCA findings. Furthermore, PCA-derived ROIs can serve as informative priors for joint ICA (jICA) in multimodal fusion analyses. Such integration could strengthen robustness and facilitate comparison with more established ICA-based pipelines widely used in the neuroimaging community.

Another useful extension would involve calculating the directional skew of each ROI by taking the difference between sender and receiver contributions in dFC (i.e., sender minus receiver). To enable comparisons across subjects and modalities, this difference could be normalized by the total contribution (i.e., sender plus receiver) yielding a normalized score in the range [–1, 1].

Thus, a Directional Skew Index (DI) to capture asymmetries in directed connectivity (dFC) would be defined as

$$DI_i = \left(\frac{\text{Sender}_i \; - \; \text{\_Receiver}_\text{i}}{\text{Sender}_i \; + \; \text{Receiver}_\text{i}}\right).$$

A value near +1 would indicate a strong net sender (information source), –1 a strong net receiver (information sink), and 0 a balanced node with symmetrical inflow and outflow. This normalized skew metric could offer deeper insight into causal asymmetries and dynamic role

shifts in directed connectivity. By recovering the directional specificity otherwise collapsed in total influence measures, it enhances interpretability and enables a more nuanced characterization of regional dominance in information flow, particularly in the absence of strong priors.

This method offers ample room for future development. Incorporating demographic or clinical covariates (e.g., age, sex, IQ, education, symptom scores) and genetic markers such as single-nucleotide polymorphisms (SNPs) could help contextualize sources of variance and improve generalizability across populations. With further refinement, these tools could contribute to the development of diagnostic or prognostic frameworks in clinical neuroscience. Finally, benchmarking the PCA-derived ROI contributions against alternative feature selection strategies, including ICA, clustering algorithms, or model-derived importance scores from machine learning pipelines, may further clarify when and where this approach provides the most utility.

Evaluating robustness across large, multi-site datasets is also critical for assessing generalizability and translational potential. Taken together, the PCA-based ROI selection framework offers a scalable, mathematically principled approach to dimensionality reduction of brain regions to those most informative as measured by contribution to explained variance in neuroimaging analysis. Expanding the framework to include pairwise ROI coupling or grouping ROIs into resting-state or task-defined networks may enable richer interpretations at the level of functional systems rather than individual regions. While rooted in a linear decomposition, it opens the door to nonlinear and multimodal extensions and serves as a flexible foundation for developing future tools that can adapt to the complexity and diversity of modern brain data.

An initial attempt was also made to extend the PCA-based ROI selection framework to the SC-FC constrained dataset used in Chapter 4. Preliminary results showed successful validation of the method, suggesting that PCA can meaningfully extract informative ROIs even within anatomically restricted connectivity matrices. This reinforces the idea that structurally constrained and data-driven methods are not mutually exclusive, but rather complementary. When combined, they may provide a principled, high-resolution approach for identifying functionally relevant regions with robust anatomical plausibility. This hybrid strategy, anchored in white matter pathways yet guided by structured signal variance, has strong potential as a future pipeline for mapping neuroplastic adaptations, both within this dataset and more broadly beyond it.

7.1.4 CRT Limitations: Toward a Physiologically Grounded Framework

While Cognitive Resource Theory (CRT) offers a physically grounded and mathematically rigorous account of adaptive cognition, its current formulation remains limited by the absence of direct metabolic validation. To establish CRT as a fully viable model of brain function, future studies must empirically link its core constructs—such as cognitive temperature, available energy, and reallocation dynamics—to measurable physiological processes. Several promising research avenues are outlined below.

One critical next step is the use of metabolic imaging techniques such as FDG-PET and MR spectroscopy to quantify energy consumption during cognitive tasks. These methods offer a means to validate CRT's central variables, including the internally available energy for reallocation, $E_A(t)$, and dynamic shifts in metabolic demand predicted by CRR. Comparing task and rest states using PET could reveal how cognitive strain modulates regional energy uptake,

offering a way to track reallocation events in vivo. Over time, this could evolve into a framework for identifying neurophysiological biomarkers corresponding to CRT variables, linking theory directly to observable metabolic changes in the brain.

The study by Isomura *et al.* (2023), provided empirical support for the Free Energy Principle (FEP) spontaneous causal inference in cultured cortical networks, provides another rich opportunity for CRT-based reinterpretation. In that study, neural activity and plasticity evolved along a cost surface consistent with variational free energy minimization—demonstrating inference as a product of self-organized dynamics. CRT reframes this process in thermodynamic terms. Synaptic plasticity and firing threshold changes observed in vitro could be recast as energy reallocation processes over a constrained thermodynamic landscape. If successful, such modeling would offer a complementary account of inference grounded in measurable physical quantities like energy and entropy, and provide a clear bridge between CRT and FEP.

Several EEG metrics align naturally with CRT constructs. For example, EEG power can serve as a proxy for energetic investment, coherence reflects emergent network efficiency, spectral entropy indexes internal uncertainty, and Granger causality quantifies directional resource flow. Monitoring changes in these features over time may enable dynamic estimation of neuroplastic potential and track shifts in reallocation energy throughout learning or task engagement.

Using structural, functional, and perfusion MRI can also play a key role in further CRT validation. Applying tractography-constrained methods to training studies could reveal how connectivity reorganizes in response to repeated cognitive engagement. For example, increased

frontoparietal integration alongside reduced variance in visual regions may reflect energy-efficient network tuning, consistent with CRT's predictions.

Perfusion MRI, may offer a means of measuring regional energetic cost, providing spatially resolved insight into where reallocation is occurring using hemodynamics as proxy for resource reallocation. When combined with behavior or electrophysiology, such imaging could generate detailed maps of CRT dynamics across multiple timescales and modalities.

Altogether, these approaches support a multi-modal, multi-timescale strategy for empirical validation. They also point toward the future use of CRT in predictive modeling—for example, estimating when a system is likely to reallocate resources, when plasticity will peak, or how training protocols might be optimized. By integrating EEG, MRI, PET, and behavioral data, CRT could provide the foundation for principled, individualized models of cognitive function under constraint.

Finally, the tractography-constrained PCA method developed in this dissertation offers a natural pipeline for use in longitudinal designs. Its consistency across modalities suggests it could be a valuable tool for tracking structural-functional reallocation over time and grounding CRT predictions in real data. Taken together, these directions form a coherent empirical roadmap for CRT. By combining thermodynamic theory with real-world physiology and multimodal data, future work can continue to refine, validate, and apply CRT accordingly.

7.2 Participant Characteristics and Design Considerations

Our study recruited a sample of healthy young adults, allowing us to isolate the effects of long-term video game playing while minimizing confounds. However, this design choice also

imposes certain limitations. First, the dataset used in this dissertation captures a cross-sectional snapshot of individuals with long-term action video game experience. As such, it does not permit inferences about the rate of neuroplastic adaptation over time, limiting the ability to make direct causal claims. Determining how these changes evolve would require longitudinal studies and clinical training interventions. Additionally, our gender distribution was not balanced between gamers and non-gamers, limiting our ability to analyze gender-specific differences in brain and behavioral responses. While participants were recruited from university campuses with presumably similar educational backgrounds, we did not explicitly screen for education levels or cognitive ability, meaning we cannot establish direct correlations between baseline cognitive performance and task outcomes.

Nonetheless, a larger sample size would substantially benefit future research. Most importantly, greater statistical power would enable more sensitive testing of within-group brain–behavior correlations, making it possible to determine whether observed effects are driven primarily by gamers, non-gamers, or both. These distinctions could clarify group-specific visuomotor strategies and reveal potential subtypes of neural adaptation associated with different gaming subgenres. Additionally, larger cohorts would support a more granular analysis of individual differences and enable more robust comparisons across gaming subgenres (Bediou *et al*., 2023).

Another limitation is the absence of resting-state fMRI (rs-fMRI) data. Given the success of our PCA method in identifying behaviorally relevant ROIs, it would have been valuable to map these regions onto canonical resting-state networks and compare their connectivity profiles with rs-fMRI data.(Zhao *et al*., 2023) This could offer additional insight into how task-based

network dynamics relate to intrinsic functional organization. Unfortunately, resting-state scans were not collected as part of this study, limiting our ability to explore these relationships.

Furthermore, although our sample size was sufficient for statistical analysis, future studies should expand sample diversity to enhance generalizability. Another limitation is the absence of resting-state fMRI (rs-fMRI) data, which prevents us from assessing spontaneous functional connectivity and determining whether gaming-related neuroplasticity extends beyond task-driven effects to broader network-level adaptations. Moreover, action video games encompass a range of subgenres (e.g., FPS, RTS, MOBA, BR), and while participants in this study played a mix of these, we cannot differentiate the unique neural effects of specific game mechanics. Future research should investigate whether distinct gaming subgenres contribute to differential cognitive and neuroplastic adaptations.

Lastly, although prior research suggests that action video game experience may mitigate cognitive decline in older adults(Anguera JA; Basak *et al*., 2008), our study exclusively focused on young adults, leaving open the question of whether similar neuroplasticity effects extend across different age groups. Addressing these limitations in future studies will be crucial for fully characterizing the extent and generalizability of video game-induced cognitive and neural adaptations.

Furthermore, our task required a simple button-press motor response. We assumed that motor response times alone were not significantly different across groups, focusing instead on perceptual decision-making. However, future studies employing event-related fMRI, electroencephalography (EEG), or magnetoencephalography (MEG) could help distinguish decision-making processes from motor execution components.

7.3 Future Directions

This study establishes a foundation for understanding how long-term action video game (AVG) play shapes brain connectivity and supports more efficient visuomotor decision-making. Our findings—spanning structural, functional, and directed connectivity—demonstrate the power of theory-driven, multimodal neuroimaging analysis to uncover behaviorally relevant neural adaptations.

Building on these results, several promising directions emerge for extending the scientific and theoretical impact of this work. These include refining experimental designs, incorporating complementary modalities, expanding to broader populations, and advancing Cognitive Resource Theory (CRT) toward a general framework for adaptive dynamics. The following themes outline key opportunities for future research across methodological, psychological, and theoretical domains.

7.3.1 Advancing Video Game Research in Cognitive Neuroscience

The present study highlights how action video games (AVGs) can serve as a powerful model for investigating cognitive adaptation and neuroplasticity. Building on these findings, several promising research directions emerge for advancing the field of video game neuroscience. These directions focus not only on improving experimental design and generalizability, but also on deepening our mechanistic understanding of how gameplay shapes brain function across timescales, modalities, and populations. The following priorities represent key opportunities for future investigation:

Future studies should employ longitudinal designs to track neuroplastic changes over time and identify critical periods for skill transfer. Clinical training paradigms may further inform the

extent to which causal effects of AVG exposure can have on cognition and behavior. Direct cognitive assessments should be incorporated to evaluate whether observed neural adaptations translate into meaningful improvements in real-world behavior, enabling researchers to contextualize the extent and specificity of skill transfer.

As noted in our limitations (see Section 7.2), the absence of resting-state fMRI (rs-fMRI) data limited our ability to assess whether AVG-induced adaptations extend beyond task-based activity. We encourage future studies to incorporate rs-fMRI to examine how intrinsic network coherence aligns with the CRA's predicted dynamic equilibrium (see Section 6.2.2), and whether resting-state profiles retain signatures of prior CRR-driven plasticity.

This direction aligns with insights from Dr. Timothy Jordan's dissertation (Jordan, 2021) which emphasized the importance of rest-to-task transitions in shaping cognitive network dynamics. If CRA reflects a dynamic equilibrium, its structure may exhibit attractor-like properties—potentially evolving in response to sustained cognitive demands. Resting-state profiles could therefore offer a retrospective map of reallocation history. Methods such as attractor reconstruction from rs-fMRI or EEG time-series may provide a novel means of tracking how prior CRR events alter a control group's default resource configuration.

Increasing sample diversity—across age, gender, and educational background—will improve generalizability and reveal subgroup-specific effects. Larger cohorts will also enable more granular analysis of individual variability in neural plasticity and training outcomes.

Combining fMRI with EEG or MEG could help disambiguate perceptual, decisional, and motor components of task performance, as well as track fast-timescale reallocation events, attention shifts, or oscillatory dynamics relevant to CRR.

Video games—especially action video games, as investigated in this dissertation—should be recognized not only as tools for cognitive intervention or training, but as immersive environments capable of inducing experience-driven neuroplasticity that can be systematically measured and understood. When combined with theory-driven analysis and structurally constrained connectivity frameworks, they offer a powerful window into how the brain adapts to sustained periods of cognitive strain.

7.3.1.1 Comparative Cognitive Training Models

Action video game players exhibit cognitive adaptations comparable to those seen in other high-performance populations such as athletes, surgeons, or musicians—domains that also involve fast-paced decision-making, motor precision, and strategic flexibility. Unlike these traditional training environments, video games offer a uniquely accessible and experimentally tractable platform for studying sustained cognitive engagement under repeatable conditions. As such, AVGs may serve as a valuable benchmark for investigating experience-dependent neural optimization across domains. Comparative studies could clarify whether AVGs capture a generalizable class of resource reallocation strategies or represent a distinct model of performance optimization. This line of research may ultimately reveal common neural principles that underlie skill acquisition and expertise across cognitive domains.

7.3.1.2 Rethinking Game Categorization: A Mechanics-Based Approach

Recent studies in video game neuroimaging have increasingly attempted to parse cognitive effects by subgenre (e.g., FPS, RTS, MOBA, BR) (Bediou *et al*., 2023; Brilliant *et al*., 2019). While this genre-based classification aligns with industry norms and participant familiarity, it often obscures the specific gameplay elements driving neuroplasticity(Bavelier & Green, 2019). Given the convergence of mechanics across genres and growing freedom in player

experience, future research may benefit from adopting a mechanics-driven taxonomy—categorizing games based on core cognitive demands such as visuospatial tracking, rapid decision-making, working memory load, strategic planning, or emotional regulation.

While this may complicate recruitment and classification in cross-sectional studies like the one presented in this dissertation, the results here strongly support moving beyond descriptive approaches. Notably, we propose that a player's attitude toward gameplay—the degree to which they are actively engaged —may be a key moderator of neuroplastic outcomes which aligns with work suggesting a dependence on gamer style (Bavelier & Green, 2019). In line with CRT, when gameplay is experienced as *"fulfilling",* or a *' path toward mastery'*, the brain is more likely to allocate resources as an investment toward optimizing performance out of a optimizing performance out of an intrinsic desire to improve within a game state they genuinely enjoy playing , thereby reinforcing functional reorganization.

Since games even within a given genre may elicit a distribution of overlapping game mechanics, disentangling overlapping cognitive demands elicited by these mechanics, including higher-order processes like problem-solving, overcoming functional fixedness, or adaptive responses to survival scenarios—will help identify which neural systems are recruited by which gameplay features. A mechanics-based framework offers greater specificity and theoretical precision, enabling researchers to design more targeted interventions and trace causal links between gameplay features and cognitive outcomes. Even in open-ended environments like sandbox games, players often set internally generated goals(Blanco-Herrera *et al*., 2019) that demand sustained focus and skill acquisition, whether it's constructing complex architecture, mastering in-game physics, or optimizing resource flows

From the perspective of Cognitive Resource Theory (CRT), these self-imposed challenges(Blanco-Herrera *et al*., 2019) still invoke goal-directed engagement and incremental mastery, prompting dynamic reallocation of neural resources over time. Thus, CRT remains applicable not only to structured, feedback-rich action games but also to more exploratory gameplay formats, as long as the player is motivated to improve within a personally meaningful task space.

7.3.1.3 Psychological and Emotional Dimensions of Gameplay

Beyond enhancing response time speed or accuracy, video games may also promote meaningful psychological and emotional adaptations. These effects represent a promising dimension of neuroadaptive gaming, with potential applications across both clinical and non-clinical populations. Emerging research suggests that gameplay may influence emotional regulation, social cognition, resilience, and identity development. Specific game mechanics and genres may differentially support these outcomes. Narratively-rich games can scaffold emotional learning and recovery through exposure to challenge, loss, and moral decision-making (Martínez-Tejada *et al*., 2021). Games that simulate adversity and perseverance may offer therapeutic value for coping strategy development and psychological resilience (Colder Carras *et al*., 2018). Multiplayer and cooperative games can support the practice of social behaviors in low-stakes settings, potentially improving emotional expression, empathy, and interpersonal communication (Kral *et al*., 2018). Open-ended “sandbox” games that reward flexible thinking and exploration may facilitate cognitive flexibility and lateral thinking (Blanco-Herrera *et al*., 2019; Rahimi & Shute, 2021).

7.3.2 CRT-Informed Applications

The Cognitive Resource Reallocation (CRR) framework introduced in this work explains how neural resources are dynamically redirected under cognitive load, producing the neuroplastic refinements observed in long-term action video game players. Building on this foundation, several key directions emerge for future investigation, each offering a path toward deeper insight into how experience-driven demands shape adaptive brain function. Future research could use CRT to guide the design of real-time cognitive tasks—or even interactive video games—that deliberately induce or modulate cognitive friction in specific neural systems, optimizing neuroplastic refinement with quantitative precision.

Furthermore, using EEG, MEG, or dFC metrics to track task-based CRR signatures, including power-based proxies of cognitive energy, would enable real-time modulation of neural resource allocation, with potential applications in neuroadaptive interfaces, rehabilitation, or high-performance training. These principles could also be abstracted and potentially extended toward more adaptive artificial intelligence models by providing these systems with updates regarding internal inefficiency and resource reallocation, framed as physically grounded optimization strategies. Such systems could adjust how they process user queries in real time—pausing, redirecting effort, or seeking clarification based on internal friction—mirroring how human cognition adapts under uncertainty and load.

7.3.3 Towards Generalization of Cognitive Resource Theory

More broadly, Cognitive Resource Theory (CRT) represents a specific case within a larger theoretical framework developed by the author, which also includes Neural Resource Theory (NRT) and Dynamic Resource Theory (DRT). These generalizations extend CRT's

principles beyond cognition to broader neural and physical systems, but lie beyond the scope of the present work and are reserved for future investigation. As presented here, CRT anchors cognition in physical law and enables precise, testable predictions. Its broader scientific role will be defined through continued empirical testing, cross-disciplinary application, and integration within more generalized models of brain function and adaptive behavior. NRT formalizes resource dynamics across the entire nervous system, treating cognition as a partitioned subset of neural activity embedded within a broader field of structural and metabolic constraints. Building upon Cognitive Resource Theory (CRT), NRT extends the framework from functionally defined cognitive energy to encompass all measurable synaptic, glial, and neuromodulatory interactions across both central and peripheral nervous system domains. This theoretical shift not only grounds CRT in concrete biophysical substrates but also enables future simulations of system-level trade-offs with explicit thermodynamic structure—paving the way for a unified resource-based model of neural function and adaptation. DRT generalizes the principles of CRT and NRT into a thermodynamic, field-theoretic account of adaptation in emergent and self-organizing systems across domains and scales. While CRT and NRT focus on cognitive and neural domains, DRT extends to self-organizing systems more broadly exhibiting structured emergence, including biological, computational, and physical networks. It models adaptation as the interaction between a Resource Allocator (RA), which governs global energy distribution, and a Resource Reallocator (RR), which drives local, time-dependent reorganization in complex systems. By incorporating gauge symmetries, statistical mechanics, and free energy geometry, DRT formalizes how complex systems internally redistribute energy to maintain structure, adapt to perturbations, and support emergent behavior. This framework offers a physically grounded language for modeling adaptation and emergence across scales.

8 CONCLUSION

This dissertation has presented three complementary investigations into how long-term action video game (AVG) play reshapes brain connectivity through neuroplastic refinement, culminating in measurable enhancements in visuomotor decision-making. Each chapter applied a distinct methodological lens—regional brain network analysis of the visual streams, whole-brain tractography-constrained functional connectivity, and PCA-based data-driven filtering—unified by a shared goal: to understand how sustained cognitive demand shapes neural signaling through adaptive plasticity. Together, these studies offer converging evidence for a refinement process in gamers that optimizes cognitive resource deployment, reduces processing bottlenecks, and supports faster, more efficient action selection.

From a methodological standpoint, this work demonstrates the value of adopting a multimodal connectivity framework. Chapter 3 tested targeted hypotheses in the dorsal visual stream, using anatomically grounded ROIs and both structural and functional measures to validate task-relevant adaptations. Chapter 4 expanded this analysis to the whole brain, using tractography-constrained connectivity matrices to ensure biological plausibility while reducing statistical burden by focusing only on structurally viable pathways. Chapter 5 introduced a novel PCA-based filtering approach that enabled a fully data-driven sweep across connectivity space, identifying high-information regions without presupposed anatomical constraints and significantly enhancing statistical power. While each approach has its own strengths and limitations, their integration within a unified research program provides a comprehensive map of the neural adaptations underlying expert visuomotor performance.

Critically, the findings across all three studies align with the predictions of Cognitive Resource Reallocation (CRR), a hypothesis introduced in this dissertation to explain how behaviorally relevant brain networks become optimized through repeated exposure to high-demand cognitive conditions. The observed shift in gamers—from early sensory and feedback systems to more streamlined, anticipatory circuits—supports CRR's model of targeted energetic investment for efficient task execution. The convergence of structural, functional, and directed effects in key hubs (e.g., frontoparietal, cerebellar, and dopaminergic circuits) further reinforces the biological interpretability of CRR as a mechanistic framework for dynamic neural adaptation.

As the concept matured, CRR laid the foundation for a broader theoretical extension: Cognitive Resource Theory (CRT). In Chapter 6, CRT formalized the principles of CRR in terms of thermodynamic constraints, energy allocation, entropy production, and dynamic optimization—offering a physics-grounded model of cognition. It describes how energetic availability and system structure constrain the evolution of cognitive processes, making adaptive efficiency a core organizing principle. As with any theory, the ultimate measure of CRT will lie in its falsifiability and empirical precision—which the author looks forward to testing in future work.

This dissertation also proposes theoretical frameworks that generalize and extend CRT in Section 7.3.3. For example, although beyond the scope of this dissertation, Neural Resource Theory (NRT) extends beyond cognition to describe how energy and information are dynamically organized across all neural systems—including synaptic, glial, and metabolic components of the central and peripheral nervous system. Whereas CRT focuses on the functional organization of cognition, NRT offers a broader foundation for understanding neural

adaptation. Within this hierarchy, CRR can be understood as a specific instantiation of a more general principle that biological systems evolve by reallocating finite resources in response to environmental and internal constraints.

Finally, this trilogy of work reframes action video games not merely as tools for cognitive enhancement but as methodological platforms for studying experience-driven neuroplasticity under repeatable, ecologically valid conditions. When paired with theory-driven analysis and robust analytical tools, AVGs offer a powerful experimental testbed for modeling high-performance cognitive states—illuminating how the brain dynamically reallocates its internal resources in pursuit of mastery. In sum, this work contributes a suite of practical tools, validated methods, and foundational theory to the emerging science of cognitive optimization. It shows not only how to detect change—but how to understand it, and ultimately, how to shape it for the benefit of all.

REFERENCES

Adhikari, B. M., Jahanshad, N., Shukla, D., Glahn, D. C., Blangero, J., Fox, P. T., Reynolds, R. C., Cox, R. W., Fieremans, E., Veraart, J., Novikov, D. S., Nichols, T. E., Hong, L. E., Thompson, P. M., & Kochunov, P. (2018). Comparison of heritability estimates on resting state fMRI connectivity phenotypes using the ENIGMA analysis pipeline. *Human Brain Mapping*, *39*(12), 4893-4902. https://doi.org/10.1002/hbm.24331

Adhikari, B. M., Jahanshad, N., Shukla, D., Glahn, D. C., Blangero, J., Reynolds, R. C., Cox, R. W., Fieremans, E., Veraart, J., Novikov, D. S., Nichols, T. E., Hong, L. E., Thompson, P. M., & Kochunov, P. (2018). Heritability estimates on resting state fMRI data using ENIGMA analysis pipeline. *Pac Symp Biocomput*, *23*, 307-318.

Adhikari, B. M., Jahanshad, N., Shukla, D., Turner, J., Grotegerd, D., Dannlowski, U., Kugel, H., Engelen, J., Dietsche, B., Krug, A., Kircher, T., Fieremans, E., Veraart, J., Novikov, D. S., Boedhoe, P. S. W., van der Werf, Y. D., van den Heuvel, O. A., Ipser, J., Uhlmann, A.,Kochunov, P. (2019). A resting state fMRI analysis pipeline for pooling inference across diverse cohorts: an ENIGMA rs-fMRI protocol. *Brain Imaging and Behavior*, *13*(5), 1453-1467. https://doi.org/10.1007/s11682-018-9941-x

Ahn, S., & Lee, S.-K. (2011). Diffusion Tensor Imaging: Exploring the Motor Networks and Clinical Applications. *Korean journal of radiology : official journal of the Korean Radiological Society*, *12*, 651-661. https://doi.org/10.3348/kjr.2011.12.6.651

Andersen, R. A., & Cui, H. (2009). Intention, Action Planning, and Decision Making in Parietal-Frontal Circuits. *Neuron*, *63*(5), 568-583. https://doi.org/https://doi.org/10.1016/j.neuron.2009.08.028

Anguera JA, B. J., Rintoul JL, Al-Hashimi O, Faraji F, Janowich J, Kong E, Larraburo Y, Rolle C, Johnston E, Gazzaley A. Video game training enhances cognitive control in older adults. Nature. 2013 Sep 5;501(7465):97-101. doi: 10.1038/nature12486. PMID: 24005416; PMCID: PMC3983066.

American Psychological Association. (2018). *Cognition*. In *APA Dictionary of Psychology*. https://dictionary.apa.org/cognition

Aurelian, L., Warnock, K. T., Balan, I., Puche, A., & June, H. (2016). TLR4 signaling in VTA dopaminergic neurons regulates impulsivity through tyrosine hydroxylase modulation. *Translational Psychiatry*, *6*(5), e815-e815. https://doi.org/10.1038/tp.2016.72

Babaeeghazvini, P., Rueda-Delgado, L. M., Gooijers, J., Swinnen, S. P., & Daffertshofer, A. (2021). Brain Structural and Functional Connectivity: A Review of Combined Works of Diffusion Magnetic Resonance Imaging and Electro-Encephalography [Review]. *Frontiers in Human Neuroscience*, *15*. https://doi.org/10.3389/fnhum.2021.721206

Bajaj, S., Adhikari, B. M., Friston, K. J., & Dhamala, M. (2016). Bridging the Gap: Dynamic Causal Modeling and Granger Causality Analysis of Resting State Functional Magnetic Resonance Imaging. *Brain Connect*, *6*(8), 652-661. https://doi.org/10.1089/brain.2016.0422

Barbot, A., Park, W. J., Ng, C. J., Zhang, R. Y., Huxlin, K. R., Tadin, D., & Yoon, G. (2021). Functional reallocation of sensory processing resources caused by long-term neural adaptation to altered optics. *Elife*, *10*. https://doi.org/10.7554/eLife.58734

Basak, C., Boot, W. R., Voss, M. W., & Kramer, A. F. (2008). Can training in a real-time strategy video game attenuate cognitive decline in older adults? *Psychol Aging*, *23*(4), 765-777. https://doi.org/10.1037/a0013494

Basile, G. A., Quartu, M., Bertino, S., Serra, M. P., Boi, M., Bramanti, A., Anastasi, G. P., Milardi, D., & Cacciola, A. (2021). Red nucleus structure and function: from anatomy to clinical neurosciences. *Brain Struct Funct*, *226*(1), 69-91. https://doi.org/10.1007/s00429-020-02171-x

Bastos, A. M., & Schoffelen, J.-M. (2016). A Tutorial Review of Functional Connectivity Analysis Methods and Their Interpretational Pitfalls [Review]. *Frontiers in Systems Neuroscience*, *9*. https://doi.org/10.3389/fnsys.2015.00175

Bavelier, D., & Green, C. S. (2019). Enhancing Attentional Control: Lessons from Action Video Games. *Neuron*, *104*(1), 147-163. https://doi.org/10.1016/j.neuron.2019.09.031

Bavelier, D., & Green, C. S. (2025). Learning and Transfer: A Perspective From Action Video Game Play. *Current Directions in Psychological Science*, *34*(1), 43-50. https://doi.org/10.1177/09637214241287171

Bediou, B., Rodgers, M. A., Tipton, E., Mayer, R. E., Green, C. S., & Bavelier, D. (2023). Effects of action video game play on cognitive skills: A meta-analysis. *Technology, Mind, and Behavior*, *4*(1). https://doi.org/10.1037/tmb0000102

Beffara, B., Hadj-Bouziane, F., Hamed, S. B., Boehler, C. N., Chelazzi, L., Santandrea, E., & Macaluso, E. (2022). Dynamic causal interactions between occipital and parietal cortex explain how endogenous spatial attention and stimulus-driven salience jointly shape the distribution of processing priorities in 2D visual space. *Neuroimage*, *255*, 119206. https://doi.org/https://doi.org/10.1016/j.neuroimage.2022.119206

Benarroch, E. E. (2012). Chapter 2 - Central Autonomic Control. In D. Robertson, I. Biaggioni, G. Burnstock, P. A. Low, & J. F. R. Paton (Eds.), *Primer on the Autonomic Nervous System (Third Edition)* (pp. 9-12). Academic Press. https://doi.org/https://doi.org/10.1016/B978-0-12-386525-0.00002-0

Benjamini, Y., & Hochberg, Y. (1995). Controlling the False Discovery Rate: A Practical and Powerful Approach to Multiple Testing. *Journal of the Royal Statistical Society: Series B (Methodological)*, *57*(1), 289-300. https://doi.org/https://doi.org/10.1111/j.2517-6161.1995.tb02031.x

Bertoni, S., Franceschini, S., Mancarella, M., Puccio, G., Ronconi, L., Marsicano, G., Gori, S., Campana, G., & Facoetti, A. (2024). Action video games and posterior parietal cortex neuromodulation enhance both attention and reading in adults with developmental dyslexia. *Cerebral Cortex*, *34*(4), bhae152. https://doi.org/10.1093/cercor/bhae152

Blanco-Herrera, J., Gentile, D., & Rokkum, J. (2019). Video Games can Increase Creativity, but with Caveats. *Creativity Research Journal*, *31*, 119-131. https://doi.org/10.1080/10400419.2019.1594524

Blefari, M. L., Martuzzi, R., Salomon, R., Bello-Ruiz, J., Herbelin, B., Serino, A., & Blanke, O. (2017). Bilateral Rolandic operculum processing underlying heartbeat awareness reflects changes in bodily self-consciousness. *European Journal of Neuroscience*, *45*(10), 1300-1312. https://doi.org/https://doi.org/10.1111/ejn.13567

Blihar, D., Delgado, E., Buryak, M., Gonzalez, M., & Waechter, R. (2020). A systematic review of the neuroanatomy of dissociative identity disorder. *European Journal of Trauma & Dissociation*, *4*(3), 100148. https://doi.org/https://doi.org/10.1016/j.ejtd.2020.100148

Borodovitsyna, O., Duffy, B. C., Pickering, A. E., & Chandler, D. J. (2020). Anatomically and functionally distinct locus coeruleus efferents mediate opposing effects on anxiety-like behavior. *Neurobiology of Stress*, *13*, 100284. https://doi.org/https://doi.org/10.1016/j.ynstr.2020.100284

Brilliant, T. D., Nouchi, R., & Kawashima, R. (2019). Does Video Gaming Have Impacts on the Brain: Evidence from a Systematic Review. *Brain Sci*, *9*(10). https://doi.org/10.3390/brainsci9100251

Brockett, A. T., Hricz, N. W., Tennyson, S. S., Bryden, D. W., & Roesch, M. R. (2020). Neural Signals in Red Nucleus during Reactive and Proactive Adjustments in Behavior. *The Journal of Neuroscience*, *40*(24), 4715-4726. https://doi.org/10.1523/jneurosci.2775-19.2020

Brockett, A. T., & Roesch, M. R. (2021). Chapter Ten - Anterior cingulate cortex and adaptive control of brain and behavior. In A. T. Brockett, L. M. Amarante, M. Laubach, & M. R. Roesch (Eds.), *International Review of Neurobiology* (Vol. 158, pp. 283-309). Academic Press. https://doi.org/https://doi.org/10.1016/bs.irn.2020.11.013

Brush, S. G. (1967). History of the Lenz-Ising Model. *Reviews of Modern Physics*, *39*(4), 883-893. https://doi.org/10.1103/RevModPhys.39.883

Burgess, N., & O'Keefe, J. (2003). Neural representations in human spatial memory. *Trends in Cognitive Sciences*, *7*(12), 517-519. https://doi.org/https://doi.org/10.1016/j.tics.2003.10.014

Buhusi, C. V., & Meck, W. H. (2009). Relative time sharing: new findings and an extension of the resource allocation model of temporal processing. *Philos Trans R Soc Lond B Biol Sci*, *364*(1525), 1875-1885. https://doi.org/10.1098/rstb.2009.0022

Cahill, K., Jordan, T., & Dhamala, M. (2024). Connectivity in the Dorsal Visual Stream Is Enhanced in Action Video Game Players. *Brain Sciences*, *14*(12).

Caligiore, D., Pezzulo, G., Baldassarre, G., Bostan, A. C., Strick, P. L., Doya, K., Helmich, R. C., Dirkx, M., Houk, J., Jörntell, H., Lago-Rodriguez, A., Galea, J. M., Miall, R. C., Popa, T., Kishore, A., Verschure, P. F. M. J., Zucca, R., & Herreros, I. (2017). Consensus Paper: Towards a Systems-Level View of Cerebellar Function: the Interplay Between Cerebellum, Basal Ganglia, and Cortex. *The Cerebellum*, *16*(1), 203-229. https://doi.org/10.1007/s12311-016-0763-3

Cavanna, A. E., & Trimble, M. R. (2006). The precuneus: a review of its functional anatomy and behavioural correlates. *Brain*, *129*(Pt 3), 564-583. https://doi.org/10.1093/brain/awl004

Chen, L., Wang, Y., Niu, C., Zhong, S., Hu, H., Chen, P., Zhang, S., Chen, G., Deng, F., Lai, S., Wang, J., Huang, L., & Huang, R. (2018). Common and distinct abnormal frontal-limbic system structural and functional patterns in patients with major depression and bipolar disorder. *Neuroimage Clin*, *20*, 42-50. https://doi.org/10.1016/j.nicl.2018.07.002

Chen, W., Liang, J., Wu, Q., & Han, Y. (2024). Anterior cingulate cortex provides the neural substrates for feedback-driven iteration of decision and value representation. *Nature Communications*, *15*(1), 6020. https://doi.org/10.1038/s41467-024-50388-9

Churchland, M. M., Cunningham, J. P., Kaufman, M. T., Foster, J. D., Nuyujukian, P., Ryu, S. I., & Shenoy, K. V. (2012). Neural population dynamics during reaching. *Nature*, *487*(7405), 51-56. https://doi.org/10.1038/nature11129

Churchland, A. K., & Shadlen, M. N. (2009). Decision-Making and Vision. In L. R. Squire (Ed.), *Encyclopedia of Neuroscience* (pp. 329-338). Academic Press. https://doi.org/https://doi.org/10.1016/B978-008045046-9.00210-2

Cohen, R. A. (2011). Cuneus. In J. S. Kreutzer, J. DeLuca, & B. Caplan (Eds.), *Encyclopedia of Clinical Neuropsychology* (pp. 756-757). Springer New York. https://doi.org/10.1007/978-0-387-79948-3_1356

Conway, B. R. (2018). The Organization and Operation of Inferior Temporal Cortex. *Annu Rev Vis Sci*, *4*, 381-402. https://doi.org/10.1146/annurev-vision-091517-034202

Cox, R. W. (1996). AFNI: software for analysis and visualization of functional magnetic resonance neuroimages. *Comput Biomed Res*, *29*(3), 162-173. https://doi.org/10.1006/cbmr.1996.0014

Cox, R. W., & Hyde, J. S. (1997). Software tools for analysis and visualization of fMRI data. *NMR Biomed*, *10*(4-5), 171-178. https://doi.org/10.1002/(sici)1099-1492(199706/08)10:4/5<171::aid-nbm453>3.0.co;2-l

Dhamala, M., Liang, H., Bressler, S. L., & Ding, M. (2018). Granger-Geweke causality: Estimation and interpretation. *Neuroimage*, *175*, 460-463. https://doi.org/10.1016/j.neuroimage.2018.04.043

Dhamala, M., Rangarajan, G., & Ding, M. (2008). Analyzing information flow in brain networks with nonparametric Granger causality. *Neuroimage*, *41*(2), 354-362. https://doi.org/10.1016/j.neuroimage.2008.02.020

Dhamala, M., Rangarajan, G., & Ding, M. (2008). Estimating Granger Causality from Fourier and Wavelet Transforms of Time Series Data. *Physical Review Letters*, *100*(1), 018701. https://doi.org/10.1103/PhysRevLett.100.018701

DiNuzzo, M., & Nedergaard, M. (2017). Brain energetics during the sleep-wake cycle. *Curr Opin Neurobiol*, *47*, 65-72. https://doi.org/10.1016/j.conb.2017.09.010

Dziedzic, T. A., Bala, A., & Marchel, A. (2022). Anatomical aspects of the insula, opercula and peri-insular white matter for a transcortical approach to insular glioma resection. *Neurosurg Rev*, *45*(1), 793-806. https://doi.org/10.1007/s10143-021-01602-5

Drugowitsch, J., DeAngelis, G. C., Angelaki, D. E., & Pouget, A. (2015). Tuning the speed-accuracy trade-off to maximize reward rate in multisensory decision-making. *Elife*, *4*, e06678. https://doi.org/10.7554/eLife.06678

Drugowitsch, J., DeAngelis, G. C., Klier, E. M., Angelaki, D. E., & Pouget, A. (2014). Optimal multisensory decision-making in a reaction-time task. *Elife*, *3*. https://doi.org/10.7554/eLife.03005

Eickhoff, S. B., & Müller, V. I. (2015). Functional Connectivity. In A. W. Toga (Ed.), *Brain Mapping* (pp. 187-201). Academic Press. https://doi.org/https://doi.org/10.1016/B978-0-12-397025-1.00212-8

Fotiadis, P., Parkes, L., Davis, K. A., Satterthwaite, T. D., Shinohara, R. T., & Bassett, D. S. (2024). Structure–function coupling in macroscale human brain networks. *Nature Reviews Neuroscience*, *25*(10), 688-704. https://doi.org/10.1038/s41583-024-00846-6

Friston, K. (2010). The free-energy principle: a unified brain theory? *Nature Reviews Neuroscience*, *11*(2), 127-138. https://doi.org/10.1038/nrn2787

Friston, K., & Kiebel, S. (2009). Predictive coding under the free-energy principle. *Philos Trans R Soc Lond B Biol Sci*, *364*(1521), 1211-1221. https://doi.org/10.1098/rstb.2008.0300

Friston, K. J. (1994). Functional and effective connectivity in neuroimaging: A synthesis. *Human Brain Mapping*, *2*(1-2), 56-78. https://doi.org/https://doi.org/10.1002/hbm.460020107

Giacalone, M., Agata, Z., Cozzucoli, P. C., & Alibrandi, A. (2018). Bonferroni-Holm and permutation tests to compare health data: methodological and applicative issues. *BMC Medical Research Methodology*, *18*(1), 81. https://doi.org/10.1186/s12874-018-0540-8

Glass, B. D., Maddox, W. T., & Love, B. C. (2013). Real-time strategy game training: emergence of a cognitive flexibility trait. *PLoS One*, *8*(8), e70350. https://doi.org/10.1371/journal.pone.0070350

Gogolla, N. (2017). The insular cortex. *Current Biology*, *27*(12), R580-R586. https://doi.org/https://doi.org/10.1016/j.cub.2017.05.010

Gonzalez Alam, T. R. J., Cruz Arias, J., Jefferies, E., Smallwood, J., Leemans, A., & Marino Davolos, J. (2024). Ventral and dorsal aspects of the inferior frontal-occipital fasciculus support verbal semantic access and visually-guided behavioural control. *Brain Struct Funct*, *229*(1), 207-221. https://doi.org/10.1007/s00429-023-02729-5

Goodale, M. A., Milner, A. D., Jakobson, L. S., & Carey, D. P. (1991). A neurological dissociation between perceiving objects and grasping them. *Nature*, *349*(6305), 154-156. https://doi.org/10.1038/349154a0

Goodale, M. A., & Milner, A. D. (1992). Separate visual pathways for perception and action. *Trends Neurosci*, *15*(1), 20-25. https://doi.org/10.1016/0166-2236(92)90344-8

Green, C. S., & Bavelier, D. (2003). Action video game modifies visual selective attention. *Nature*, *423*(6939), 534-537. https://doi.org/10.1038/nature01647

Green, C. S., & Bavelier, D. (2007). Action-video-game experience alters the spatial resolution of vision. *Psychol Sci*, *18*(1), 88-94. https://doi.org/10.1111/j.1467-9280.2007.01853.x

Green, C. S., & Bavelier, D. (2015). Action video game training for cognitive enhancement. *Current Opinion in Behavioral Sciences*, *4*, 103-108.

Hahn, B., Ross, T. J., & Stein, E. A. (2006). Neuroanatomical dissociation between bottom–up and top–down processes of visuospatial selective attention. *Neuroimage*, *32*(2), 842-853. https://doi.org/https://doi.org/10.1016/j.neuroimage.2006.04.177

Herlin, B., Navarro, V., & Dupont, S. (2021). The temporal pole: From anatomy to function—A literature appraisal. *Journal of Chemical Neuroanatomy*, *113*, 101925. https://doi.org/https://doi.org/10.1016/j.jchemneu.2021.101925

Holdstock, J. S. (2005). The role of the human medial temporal lobe in object recognition and object discrimination. *Q J Exp Psychol B*, *58*(3-4), 326-339. https://doi.org/10.1080/02724990444000177

Holm, S. (1979). A simple sequentially rejective multiple test procedure. *Scandinavian journal of statistics*, 65-70.

Huff, T., Mahabadi, N., & Tadi, P. (2025). Neuroanatomy, Visual Cortex. In *StatPearls*. StatPearls Publishing

Hyun, G. J., Shin, Y. W., Kim, B. N., Cheong, J. H., Jin, S. N., & Han, D. H. (2013). Increased cortical thickness in professional on-line gamers. *Psychiatry Investig*, *10*(4), 388-392. https://doi.org/10.4306/pi.2013.10.4.388

Ide, J. S., & Li, C. S. (2011). A cerebellar thalamic cortical circuit for error-related cognitive control. *Neuroimage*, *54*(1), 455-464. https://doi.org/10.1016/j.neuroimage.2010.07.042

Jenkinson, M., Beckmann, C. F., Behrens, T. E., Woolrich, M. W., & Smith, S. M. (2012). FSL. *Neuroimage*, *62*(2), 782-790. https://doi.org/10.1016/j.neuroimage.2011.09.015

Jolliffe, I. T., & Cadima, J. (2016). Principal component analysis: a review and recent developments. *Philos Trans A Math Phys Eng Sci*, *374*(2065), 20150202. https://doi.org/10.1098/rsta.2015.0202

Jordan, T., & Dhamala, M. (2022a). Enhanced Dorsal Attention Network to Salience Network Interaction in Video Gamers During Sensorimotor Decision-Making Tasks. *Brain Connect*. https://doi.org/10.1089/brain.2021.0193

Jordan, T., & Dhamala, M. (2022b). Video game players have improved decision-making abilities and enhanced brain activities. *Neuroimage: Reports*, *2*(3), 100112. https://doi.org/https://doi.org/10.1016/j.ynirp.2022.100112

Jordan, T. J. (2021). *Effects of video game playing on sensorimotor decision-making abilities and brain network dynamics* Georgia State University]. Atlanta, GA.

Kakaei, E., Aleshin, S., & Braun, J. (2021). Visual object recognition is facilitated by temporal community structure. *Learn Mem*, *28*(5), 148-152. https://doi.org/10.1101/lm.053306.120

Kennerley, S. W., & Walton, M. E. (2011). Decision making and reward in frontal cortex: complementary evidence from neurophysiological and neuropsychological studies. *Behav Neurosci*, *125*(3), 297-317. https://doi.org/10.1037/a0023575

Kiyatkin, E. A. (2019). Brain temperature and its role in physiology and pathophysiology: Lessons from 20 years of thermorecording. *Temperature (Austin)*, *6*(4), 271-333. https://doi.org/10.1080/23328940.2019.1691896

Kravitz, D. J., Saleem, K. S., Baker, C. I., & Mishkin, M. (2011). A new neural framework for visuospatial processing. *Nature Reviews Neuroscience*, *12*(4), 217-230. https://doi.org/10.1038/nrn3008

Krimmel, S. R., Laumann, T. O., Chauvin, R. J., Hershey, T., Roland, J. L., Shimony, J. S., Willie, J. T., Norris, S. A., Marek, S., Van, A. N., Monk, J., Scheidter, K. M., Whiting, F., Ramirez-Perez, N., Metoki, A., Wang, A., Kay, B. P., Nahman-Averbuch, H., Fair, D. A.,…Dosenbach, N. U. F. (2024). The brainstem's red nucleus was evolutionarily upgraded to support goal-directed action. *bioRxiv*. https://doi.org/10.1101/2023.12.30.573730

Kucukboyaci, N. E., Kemmotsu, N., Leyden, K. M., Girard, H. M., Tecoma, E. S., Iragui, V. J., & McDonald, C. R. (2014). Integration of multimodal MRI data via PCA to explain language performance. *NeuroImage: Clinical*, *5*, 197-207. https://doi.org/https://doi.org/10.1016/j.nicl.2014.05.006

Kühn, S., & Gallinat, J. (2014). Amount of lifetime video gaming is positively associated with entorhinal, hippocampal and occipital volume. *Mol Psychiatry*, *19*(7), 842-847. https://doi.org/10.1038/mp.2013.100

Kühn, S., Gleich, T., Lorenz, R. C., Lindenberger, U., & Gallinat, J. (2014). Playing Super Mario induces structural brain plasticity: gray matter changes resulting from training with a commercial video game. *Molecular Psychiatry*, *19*(2), 265-271. https://doi.org/10.1038/mp.2013.120

Kühn, S., Lorenz, R., Banaschewski, T., Barker, G. J., Büchel, C., Conrod, P. J., Flor, H., Garavan, H., Ittermann, B., Loth, E., Mann, K., Nees, F., Artiges, E., Paus, T., Rietschel, M., Smolka, M. N., Ströhle, A., Walaszek, B., Schumann, G.,…Gallinat, J. (2014). Positive association of video game playing with left frontal cortical thickness in adolescents. *PLoS One*, *9*(3), e91506. https://doi.org/10.1371/journal.pone.0091506

Lamichhane, B., Adhikari, B. M., & Dhamala, M. (2016). Salience Network Activity in Perceptual Decisions. *Brain Connectivity*, *6*(7), 558-571. https://doi.org/10.1089/brain.2015.0392

Lee, M. H., Kim, N., Yoo, J., Kim, H.-K., Son, Y.-D., Kim, Y.-B., Oh, S. M., Kim, S., Lee, H., Jeon, J. E., & Lee, Y. J. (2021). Multitask fMRI and machine learning approach improve

prediction of differential brain activity pattern in patients with insomnia disorder. *Scientific Reports*, *11*(1), 9402. https://doi.org/10.1038/s41598-021-88845-w

Lewandowska, P., Jakubowska, N., Hryniewicz, N., Prusinowski, R., Kossowski, B., Brzezicka, A., & Kowalczyk-Grębska, N. (2022). Association between real-time strategy video game learning outcomes and pre-training brain white matter structure: preliminary study. *Scientific Reports*, *12*(1), 20741. https://doi.org/10.1038/s41598-022-25099-0

Lynn, C. W., & Bassett, D. S. (2019). The physics of brain network structure, function and control. *Nature Reviews Physics*, *1*(5), 318-332. https://doi.org/10.1038/s42254-019-0040-8

McKnight, P. E., & Najab, J. Mann-Whitney U Test. In *The Corsini Encyclopedia of Psychology* (pp. 1-1). https://doi.org/https://doi.org/10.1002/9780470479216.corpsy0524

Menon, V. (2015). Salience Network. *Brain Mapping: An Encyclopedic Reference*, *2*, 597-611. https://doi.org/10.1016/B978-0-12-397025-1.00052-X

Micheletti, S., Corbett, F., Atkinson, J., Braddick, O., Mattei, P., Galli, J., Calza, S., & Fazzi, E. (2021). Dorsal and Ventral Stream Function in Children With Developmental Coordination Disorder. *Front Hum Neurosci*, *15*, 703217. https://doi.org/10.3389/fnhum.2021.703217

Mishkin, M., & Ungerleider, L. G. (1982). Contribution of striate inputs to the visuospatial functions of parieto-preoccipital cortex in monkeys. *Behav Brain Res*, *6*(1), 57-77. https://doi.org/10.1016/0166-4328(82)90081-x

Mishkin, M., Ungerleider, L. G., & Macko, K. A. (1983). Object vision and spatial vision: two cortical pathways. *Trends in Neurosciences*, *6*, 414-417. https://doi.org/https://doi.org/10.1016/0166-2236(83)90190-X

Monosov, I. E. (2017). Anterior cingulate is a source of valence-specific information about value and uncertainty. *Nature Communications*, *8*(1), 134. https://doi.org/10.1038/s41467-017-00072-y

Monosov, I. E., Haber, S. N., Leuthardt, E. C., & Jezzini, A. (2020). Anterior Cingulate Cortex and the Control of Dynamic Behavior in Primates. *Curr Biol*, *30*(23), R1442-r1454. https://doi.org/10.1016/j.cub.2020.10.009

Mushtaq, F., Bland, A. R., & Schaefer, A. (2011). Uncertainty and cognitive control. *Front Psychol*, *2*, 249. https://doi.org/10.3389/fpsyg.2011.00249

Mwangi, B., Tian, T. S., & Soares, J. C. (2014). A review of feature reduction techniques in neuroimaging. *Neuroinformatics*, *12*(2), 229-244. https://doi.org/10.1007/s12021-013-9204-3

Nissen, C., Piosczyk, H., Holz, J., Maier, J. G., Frase, L., Sterr, A., Riemann, D., & Feige, B. (2021). Sleep is more than rest for plasticity in the human cortex. *Sleep*, *44*(3). https://doi.org/10.1093/sleep/zsaa216

Palaus, M., Marron, E. M., Viejo-Sobera, R., & Redolar-Ripoll, D. (2017). Neural Basis of Video Gaming: A Systematic Review [Review]. *Frontiers in Human Neuroscience*, *11*. https://doi.org/10.3389/fnhum.2017.00248

Pessoa, L. (2014). Understanding brain networks and brain organization. *Phys Life Rev*, *11*(3), 400-435. https://doi.org/10.1016/j.plrev.2014.03.005

Popa, L. S., & Ebner, T. J. (2019). Cerebellum, Predictions and Errors. *Frontiers in Cellular Neuroscience*, *12*. https://doi.org/10.3389/fncel.2018.00524

Purves D, A. G., Fitzpatrick D, et al. (2001). Projections to the Basal Ganglia. In A. G. Purves D, Fitzpatrick D, et al. (Ed.), *Neuroscience* (2nd ed.). Sinauer Associates. https://www.ncbi.nlm.nih.gov/books/NBK10988/

Renier, L. A., Anurova, I., De Volder, A. G., Carlson, S., VanMeter, J., & Rauschecker, J. P. (2010). Preserved functional specialization for spatial processing in the middle occipital gyrus of the early blind. *Neuron*, *68*(1), 138-148. https://doi.org/10.1016/j.neuron.2010.09.021

Revell, A. Y., Silva, A. B., Arnold, T. C., Stein, J. M., Das, S. R., Shinohara, R. T., Bassett, D. S., Litt, B., & Davis, K. A. (2022). A framework For brain atlases: Lessons from seizure dynamics. *Neuroimage*, *254*, 118986. https://doi.org/10.1016/j.neuroimage.2022.118986

Rolls, E. T. (2004). The functions of the orbitofrontal cortex. *Brain Cogn*, *55*(1), 11-29. https://doi.org/10.1016/s0278-2626(03)00277-x

Rolls, E. T. (2021). Chapter 1 - The neuroscience of emotional disorders. In K. M. Heilman & S. E. Nadeau (Eds.), *Handbook of Clinical Neurology* (Vol. 183, pp. 1-26). Elsevier. https://doi.org/https://doi.org/10.1016/B978-0-12-822290-4.00002-5

Rolls, E. T. (2023). Emotion, motivation, decision-making, the orbitofrontal cortex, anterior cingulate cortex, and the amygdala. *Brain Struct Funct*, *228*(5), 1201-1257. https://doi.org/10.1007/s00429-023-02644-9

Rolls, E. T., Huang, C.-C., Lin, C.-P., Feng, J., & Joliot, M. (2020). Automated anatomical labelling atlas 3. *Neuroimage*, *206*, 116189. https://doi.org/https://doi.org/10.1016/j.neuroimage.2019.116189

Rosch, K. S., & Mostofsky, S. (2019). Chapter 19 - Development of the frontal lobe. In M. D'Esposito & J. H. Grafman (Eds.), *Handbook of Clinical Neurology* (Vol. 163, pp. 351-367). Elsevier. https://doi.org/https://doi.org/10.1016/B978-0-12-804281-6.00019-7

Rubinov, M., & Sporns, O. (2010). Complex network measures of brain connectivity: Uses and interpretations. *Neuroimage*, *52*(3), 1059-1069. https://doi.org/https://doi.org/10.1016/j.neuroimage.2009.10.003

Rudebeck, P. H., & Rich, E. L. (2018). Orbitofrontal cortex. *Curr Biol*, *28*(18), R1083-r1088. https://doi.org/10.1016/j.cub.2018.07.018

Sammer, G., Neumann, E., Blecker, C., & Pedraz-Petrozzi, B. (2022). Fractional anisotropy and peripheral cytokine concentrations in outpatients with depressive episode: a diffusion tensor imaging observational study. *Scientific Reports*, *12*(1), 17450. https://doi.org/10.1038/s41598-022-22437-0

Scharnowski, F., Nicholson, A. A., Pichon, S., Rosa, M. J., Rey, G., Eickhoff, S. B., Van De Ville, D., Vuilleumier, P., & Koush, Y. (2020). The role of the subgenual anterior cingulate cortex in dorsomedial prefrontal-amygdala neural circuitry during positive-social emotion regulation. *Hum Brain Mapp*, *41*(11), 3100-3118. https://doi.org/10.1002/hbm.25001

Schlinger, H. D. (2015). Behavior analysis and behavioral neuroscience. *Front Hum Neurosci*, *9*, 210. https://doi.org/10.3389/fnhum.2015.00210

Seidler, R. D., Kwak, Y., Fling, B. W., & Bernard, J. A. (2013). Neurocognitive mechanisms of error-based motor learning. *Adv Exp Med Biol*, *782*, 39-60. https://doi.org/10.1007/978-1-4614-5465-6_3

Shi, J., Huang, H., Jiang, R., Mao, X., Huang, Q., & Li, A. (2022). The Right Inferior Frontal Gyrus Plays an Important Role in Unconscious Information Processing: Activation

Likelihood Estimation Analysis Based on Functional Magnetic Resonance Imaging. *Front Neurosci*, *16*, 781099. https://doi.org/10.3389/fnins.2022.781099

Shi, W., Meisner, O. C., Blackmore, S., Jadi, M. P., Nandy, A. S., & Chang, S. W. C. (2023). The orbitofrontal cortex: A goal-directed cognitive map framework for social and non-social behaviors. *Neurobiol Learn Mem*, *203*, 107793. https://doi.org/10.1016/j.nlm.2023.107793

Smith, S. M., Jenkinson, M., Woolrich, M. W., Beckmann, C. F., Behrens, T. E., Johansen-Berg, H., Bannister, P. R., De Luca, M., Drobnjak, I., Flitney, D. E., Niazy, R. K., Saunders, J., Vickers, J., Zhang, Y., De Stefano, N., Brady, J. M., & Matthews, P. M. (2004). Advances in functional and structural MR image analysis and implementation as FSL. *Neuroimage*, *23 Suppl 1*, S208-219. https://doi.org/10.1016/j.neuroimage.2004.07.051

Soares, J., Marques, P., Alves, V., & Sousa, N. (2013). A hitchhiker's guide to diffusion tensor imaging [Review]. *Frontiers in Neuroscience*, *7*. https://doi.org/10.3389/fnins.2013.00031

Sonne, J. R., V; Beato, MR. (2025). Neuroanatomy, Substantia Nigra. In S. Publishing (Ed.), *StatPearls [Internet]* (Updated 2024 Sep 10 ed.). StatPearls Publishing. https://www.ncbi.nlm.nih.gov/books/NBK536995/

Sporns, O. (2013). Structure and function of complex brain networks. *Dialogues Clin Neurosci*, *15*(3), 247-262. https://doi.org/10.31887/DCNS.2013.15.3/osporns

Stoodley, C. J., & Schmahmann, J. D. (2018). Chapter 4 - Functional topography of the human cerebellum. In M. Manto & T. A. G. M. Huisman (Eds.), *Handbook of Clinical Neurology* (Vol. 154, pp. 59-70). Elsevier. https://doi.org/https://doi.org/10.1016/B978-0-444-63956-1.00004-7

Storey, J. D., & Tibshirani, R. (2003). Statistical significance for genomewide studies. *Proc Natl Acad Sci U S A*, *100*(16), 9440-9445. https://doi.org/10.1073/pnas.1530509100

Sussillo, D., & Abbott, L. F. (2009). Generating Coherent Patterns of Activity from Chaotic Neural Networks. *Neuron*, *63*(4), 544-557. https://doi.org/10.1016/j.neuron.2009.07.018

Taylor, R., Tomić, I., Aagten-Murphy, D., & Bays, P. M. (2023). Working memory is updated by reallocation of resources from obsolete to new items. *Atten Percept Psychophys*, *85*(5), 1437-1451. https://doi.org/10.3758/s13414-022-02584-2

Tulloch, K., & Pammer, K. (2019). Tablet computer games to measure dorsal stream performance in good and poor readers. *Neuropsychologia*, *130*, 92-99. https://doi.org/https://doi.org/10.1016/j.neuropsychologia.2018.07.019

Wall, M. E., Rechtsteiner, Andreas, Rocha, Luis M. (2002). Singular Value Decomposition and Principal Component Analysis. *arXiv*.

Walter, B. L., & Shaikh, A. G. (2014). Midbrain. In M. J. Aminoff & R. B. Daroff (Eds.), *Encyclopedia of the Neurological Sciences (Second Edition)* (pp. 28-33). Academic Press. https://doi.org/https://doi.org/10.1016/B978-0-12-385157-4.01161-1

Wang, H., Wang, B., Normoyle, K. P., Jackson, K., Spitler, K., Sharrock, M. F., Miller, C. M., Best, C., Llano, D., & Du, R. (2014). Brain temperature and its fundamental properties: a review for clinical neuroscientists. *Front Neurosci*, *8*, 307. https://doi.org/10.3389/fnins.2014.00307

Wang, X.-J. (2002). Probabilistic Decision Making by Slow Reverberation in Cortical Circuits. *Neuron*, *36*(5), 955-968. https://doi.org/10.1016/S0896-6273(02)01092-9

Wong, W.-w., Rangaprakash, D., Diaz-Fong, J. P., Rotstein, N. M., Hellemann, G. S., & Feusner, J. D. (2021). Effects of visual attention modulation on dynamic effective

connectivity and visual fixation during own-face viewing in body dysmorphic disorder. *medRxiv*, 2021.2002.2015.21249769. https://doi.org/10.1101/2021.02.15.21249769

Woolrich, M. W., Jbabdi, S., Patenaude, B., Chappell, M., Makni, S., Behrens, T., Beckmann, C., Jenkinson, M., & Smith, S. M. (2009). Bayesian analysis of neuroimaging data in FSL. *Neuroimage*, *45*(1 Suppl), S173-186. https://doi.org/10.1016/j.neuroimage.2008.10.055

Xia M, W. J., He Y (2013) BrainNet Viewer: A Network Visualization Tool for Human Brain Connectomics. PLoS ONE 8(7): e68910. https://doi.org/10.1371/journal.pone.0068910.

Yeh, F.-C. (n.d-a). *DSI Studio*. Retrieved Aprill 11, 2025 from https://dsi-studio.labsolver.org/doc/how_to_interpret_dmri.html

Yeh, F.-C. (n.d.-b). *T3 whole brain connectometry: Quantitative anisotropy matrix*. Retrieved April from https://dsi-studio.labsolver.org/doc/gui_t3_whole_brain.html

Yeh, F. C. (2020). Shape analysis of the human association pathways. *Neuroimage*, *223*, 117329. https://doi.org/10.1016/j.neuroimage.2020.117329

Yeh FC, P. S. F. D. M. A., Yoshino M Fernandez-Miranda JC Vettel JM, Verstynen (2018). T. Population-averaged atlas of the macroscale human structural connectome and its network topology. *Neuroimage*. https://doi.org/doi: 10.1016/j.neuroimage.2018.05.027.

Yeh, F. C., & Tseng, W. Y. (2011). NTU-90: a high angular resolution brain atlas constructed by q-space diffeomorphic reconstruction. *Neuroimage*, *58*(1), 91-99. https://doi.org/10.1016/j.neuroimage.2011.06.021

Yeh, F. C., Verstynen, T. D., Wang, Y., Fernandez-Miranda, J. C., & Tseng, W. Y. (2013). Deterministic diffusion fiber tracking improved by quantitative anisotropy. *PLoS One*, *8*(11), e80713. https://doi.org/10.1371/journal.pone.0080713

Yeh, F. C., Wedeen, V. J., & Tseng, W. Y. (2010). Generalized q-sampling imaging. *IEEE Trans Med Imaging*, *29*(9), 1626-1635. https://doi.org/10.1109/tmi.2010.2045126

Yeo, B. T., Krienen, F. M., Sepulcre, J., Sabuncu, M. R., Lashkari, D., Hollinshead, M., Roffman, J. L., Smoller, J. W., Zöllei, L., Polimeni, J. R., Fischl, B., Liu, H., & Buckner, R. L. (2011). The organization of the human cerebral cortex estimated by intrinsic functional connectivity. *J Neurophysiol*, *106*(3), 1125-1165. https://doi.org/10.1152/jn.00338.2011

Zhang, C., Lee, T. M. C., Fu, Y., Ren, C., Chan, C. C. H., & Tao, Q. (2019). Properties of cross-modal occipital responses in early blindness: An ALE meta-analysis. *NeuroImage: Clinical*, *24*, 102041. https://doi.org/https://doi.org/10.1016/j.nicl.2019.102041

Zhao, W., Makowski, C., Hagler, D. J., Garavan, H. P., Thompson, W. K., Greene, D. J., Jernigan, T. L., & Dale, A. M. (2023). Task fMRI paradigms may capture more behaviorally relevant information than resting-state functional connectivity. *Neuroimage*, *270*, 119946. https://doi.org/https://doi.org/10.1016/j.neuroimage.2023.119946